

**Development of automated analysis methods for identifying
behavioral and neural plasticity in sleep and learning in *C. elegans***

By

Daniel Edward Lawler

A Dissertation

Submitted to Faculty of

Worcester Polytechnic Institute

In Partial Fulfillment
Of the Requirements for the Degree
Doctor of Philosophy in Biomedical Engineering

December 2019

Approved By:

Doctoral Advisor

Dirk Albrecht, PhD

Worcester Polytechnic Institute
Department of Biomedical
Engineering

Committee Chair

Songbai Ji, PhD

Worcester Polytechnic Institute
Department of Biomedical
Engineering

Kwonmoo Lee, PhD

Worcester Polytechnic Institute
Department of Biomedical
Engineering

Jagan Srinivasan, PhD

Worcester Polytechnic Institute
Department of Biology and
Biotechnology

William Schafer, PhD

MRC Laboratory of Molecular Biology
Neurobiology Division

Abstract

Neuropsychiatric disorders severely impact quality of life in millions of patients, contributing more Disease Affected Life Years (DALYs) than cancer or cardiovascular disease. The human brain is a complex system of 100 billion neurons connected by 100 trillion synapses, and human studies of neural disease focus on network-level circuit activity changes, rather than on cellular mechanisms. To probe for neural dynamics on the cellular level, animal models such as the nematode *C. elegans* have been used to investigate the biochemical and genetic factors contributing to neurological disease. *C. elegans* are ideal for neurophysiological studies due to their small nervous system, neurochemical homology to humans, and compatibility with non-invasive neural imaging. To better study the cellular mechanisms contributing to neurological disease, we developed automated analysis methods for characterizing the behaviors and associated neural activity during sleep and learning in *C. elegans*: two neural functions that involve a high degree of behavioral and neural plasticity.

We developed two methods to study previously uncharacterized spontaneous adult sleep in *C. elegans*. A large microfluidic device facilitates population-wide assessment of long-term sleep behavior over 12 hours including effects of fluid flow, oxygen, feeding, odors, and genetic perturbations. Smaller devices allow simultaneous recording of sleep behavior and neuronal activity. Since the onset of adult sleep is stochastically timed, we developed a closed-loop sleep detection system that delivers chemical stimuli to individual animals during sleep and awake states to assess state-dependent changes to neural responses. Sleep increased the arousal threshold to aversive chemical stimulation,

yet sensory neuron (ASH) and first-layer interneuron (AIB) responses were unchanged. This localizes adult sleep-dependent neuromodulation within interneurons presynaptic to the AVA premotor interneurons, rather than afferent sensory circuits.

Traditionally, the study of learning in *C. elegans* observes taxis on agar plates which present variable environmental conditions that can lead to a reduction in test-to-test reproducibility. We also translated the butanone enhancement learning assay such that animals can be trained and tested all within the controlled environment of a microfluidic device. Using this system, we demonstrated that *C. elegans* are capable of associative learning by observing stimulus evoked behavioral responses, rather than taxis. This system allows for more reproducible results and can be used to seamlessly study stimulus-evoked neural plasticity associated with learning. Together, these systems provide platforms for studying the connections between behavioral plasticity and neural circuit modulation in sleep and learning. We can use these systems to further our understanding of the mechanisms underlying neural regulation, function, and disorder using human disease models in *C. elegans*.

Acknowledgements

I'd like to thank the many people who have supported me during my journey over the past 5 years. First and foremost, I want to thank my advisor Dirk Albrecht, who has not just supported me with scientific discovery, but also shaped my passion for neuroscience and research. His knowledge and creative outlook on science helped drive me in my years at WPI. I'd also like to thank Bill Schafer, who graciously allowed me to train in his lab, gaining insight into the amazing work he and his group do. I'd like to thank my additional committee members Kwonmoo Lee, Songbai Ji, and Jagan Srinivasan for all the feedback, support, and constructive criticism they've given me as I developed my thesis project. I'd like to also thank all of the members of the Albrecht lab over the years: Ross Lagoy, Kyra Burnett, Hamilton White, Eric Larsen, Laura Innarelli especially who have all helped supported our lab grow and prosper while providing valuable insight and feedback.

I'd like to thank the WPI Biomedical Engineering and IGERT faculty and staff for creating an engaging and exciting environment for research and personal and professional development. I'd also like to thank the many collaborators I've worked with. Yee Lian Chew mentored me during my time in Dr. Schafer's lab and was instrumental in shaping the biological visions to go along with the engineering tools I worked on in my Ph.D. Doug Reilly, Mostafa Elfawal, Josh Hawk, Jeff Grant, and Karen Tran shared insight and helped develop valuable tools growing my project. Many undergraduate students including REU students Allison and Dina helped not just with developing my projects, but also helped me grow as a scientist through teaching others.

Finally, I'd like to thank my family and friends for supporting me throughout the ups and downs of graduate school. I'd especially like to thank my girlfriend Kelsea for always giving her unconditional support and encouragement and inspiring me to be the best I can be. And to my family, my brother Tim and my parents Jane and Dennis for always believing in me, motivating me, and making me the person I am today. I'm forever grateful for all you have done for me.

Table of Contents

ABSTRACT	II
ACKNOWLEDGEMENTS	IV
TABLE OF CONTENTS.....	VI
LIST OF FIGURES.....	XI
LIST OF TABLES	XII
LIST OF ABBREVIATIONS	XIII
CHAPTER 1: INTRODUCTION	1
<i>1.1: Neural plasticity: Background, methods of study, and impact</i>	<i>1</i>
1.1.1: Plasticity and adaptive function in neural networks.....	1
1.1.2: Neurological disorders and their impact.....	2
<i>1.2: Use and function of the model organism C. elegans.....</i>	<i>4</i>
1.2.1: C. elegans, and its advantages in use as an animal model for neurological disease.....	4
1.2.2: Sleep, sleep disorders, and sleep in model organisms including C. elegans	5
1.2.3: Learning and memory in C. elegans	9
<i>1.3: Quantifying neural activity and associated behavior in C. elegans.....</i>	<i>10</i>
1.3.1: Methods for studying C. elegans behavior and quiescence.....	10
1.3.2: Fluorescent proteins, calcium indicators, and measuring neural activity	12
<i>1.4: Project overview.....</i>	<i>13</i>
1.4.1: Long-term goal and specific aims.....	13
1.4.2: Chapter outline and overview.....	15
CHAPTER 2: COMPUTER VISION TOOLS FOR ANALYZING NEMATODE BEHAVIOR	18
ABSTRACT	19

INTRODUCTION.....	19
RESULTS.....	23
2.1: <i>Methods to analyze nematode odor preference</i>	23
2.1.1: Quantifying <i>C. elegans</i> attraction and aversion in stripe assays	23
2.1.2: Quantifying <i>C. elegans</i> attraction and aversion in gradient assays	25
2.1.3: Quantifying <i>C. elegans</i> attraction and aversion in pulse assays	27
2.1.4: Integration of multiple sensory inputs reveals behavioral preferences dictated by feeding state through use of a pulse assay	28
2.2: <i>Translation of behavioral assessment to neural imaging</i>	32
2.2.1: Pulse assays allow for seamless transition to neural imaging methods.....	32
2.3: <i>Tracking the lack of locomotion: Physiological relevance</i>	35
2.3.1: Image segmentation techniques to track behavioral quiescence and translate quiescence to sleep states	35
2.3.2: Development of high-throughput viability assessment for drug-screening application in parasitic nematodes..	41
DISCUSSION	47
METHODS AND MATERIALS	52
<i>Strains and C. elegans culture</i>	52
<i>Microfluidic device fabrication</i>	52
<i>Microfluidic stimulus preparation</i>	53
<i>Microfluidic device setup</i>	54
<i>Loading and experimentation with the Hamilton MVP Valve</i>	54
<i>Animal tracking systems</i>	55
<i>Culture of H. poly using mice</i>	56
<i>Sorting and loading of H. poly into 384-well plates</i>	56
<i>UMASS WormIR tracking</i>	57
<i>384-well plate movement tracking</i>	58
<i>Statistical analysis</i>	58
CHAPTER 3: SLEEP IN ADULT C. ELEGANS	60

ABSTRACT	61
INTRODUCTION.....	62
RESULTS.....	65
<i>3.1: What factors influence adult C. elegans sleep?</i>	65
3.1.1: Blue light disturbs adult C. elegans sleep.....	65
3.1.2: Presence of multiple animals, increased flow velocity, and increased arena size do not disturb C. elegans sleep	65
3.1.3: Exogenous melatonin does not increase sleep behavior in adult C. elegans	69
<i>3.2: Genetic effects on adult C. elegans sleep</i>	71
3.2.1: Investigation of melatonin synthesis and receptor mutations on sleep	71
3.2.2: Arousal deficient mutants show reduced sleep	73
3.2.3: Sensory processing mutants and their sleep implications	77
<i>3.3: Investigating the effects of sleep on stimulus-evoked response in sensory neurons</i>	80
3.3.1: ASH sensory neurons respond reliably despite delayed arousal.....	80
3.3.2: AWA sensory neuron shows modulated response during sleep state	83
3.3.3: Sensory processing differences arise between aversive and appetitive stimulation	86
DISCUSSION	89
METHODS AND MATERIALS	94
<i>Strains and C. elegans culture</i>	94
<i>Microfluidic device fabrication</i>	95
<i>Stimulus preparation</i>	96
<i>Microfluidic device setup</i>	96
<i>Population behavior imaging and identification of sleep events</i>	97
<i>Neural calcium imaging, sleep detection and data analysis in closed-loop system</i>	97
<i>Statistical analysis</i>	98
CHAPTER 4: AUTOMATED ANALYSIS OF SLEEP IN ADULT C. ELEGANS WITH CLOSED-LOOP ASSESSMENT OF STATE- DEPENDENT NEURAL ACTIVITY	100

ABSTRACT	101
INTRODUCTION.....	101
RESULTS.....	106
<i>High-throughput analysis of adult sleep</i>	106
<i>Environmental and sensory effects on sleep dynamics</i>	112
<i>Automatic sleep tracking, chemical stimulation, and neural imaging</i>	118
<i>Closed-loop stimulation and neural imaging of a reversal circuit</i>	122
DISCUSSION	126
METHODS AND MATERIALS	132
<i>Strains and C. elegans culture</i>	132
<i>Microfluidic device fabrication</i>	133
<i>Stimulus preparation</i>	133
<i>Microfluidic device setup</i>	134
<i>Population behavior imaging and identification of sleep events</i>	135
<i>Neural calcium imaging, sleep detection and data analysis in closed-loop system</i>	135
<i>Statistical analysis</i>	137
CHAPTER 5: ASSOCIATIVE LEARNING IN A MICROFLUIDIC FORMAT IN C. ELEGANS	138
ABSTRACT	139
INTRODUCTION.....	140
RESULTS.....	142
5.1: <i>Development of new associative learning assay</i>	142
5.1.1: Translation of the butanone enhancement assay into an all-microfluidic platform	142
5.2: <i>Learning assessment in pulse-based microfluidic butanone enhancement assay</i>	149
5.2.1: Quantifying attraction in an automated all-microfluidic pulse-based butanone enhancement assay	149
5.2.2: Young adults show association of the neutral butanone to food	151
DISCUSSION	154

METHODS AND MATERIALS	158
<i>Strains and C. elegans culture</i>	158
<i>Microfluidic device fabrication</i>	158
<i>Stimulus preparation</i>	159
<i>Microfluidic device setup</i>	159
<i>Animal tracking systems</i>	160
<i>Neural calcium imaging and data analysis</i>	160
<i>Statistical analysis</i>	161
CHAPTER 6: FUTURE DIRECTIONS AND CONCLUSIONS	162
6.1: <i>Furthering characterization and throughput of adult C. elegans sleep studies</i>	162
6.1.1: Further investigation of the disconnect between sensory response during sleep and premotor neuron response related to arousal delay	162
6.1.2: Use of optogenetic stimulation to further throughput of neural imaging during sleep and wake states	164
6.1.3: Characterize disease-related mutants to study sleep disorders impacting humans	167
6.2: <i>Future work investigating butanone enhancement neurally and across ages</i>	168
6.2.1: Investigation of butanone enhancement with older adults and L4s has so far been inconclusive	168
6.2.2: Study neural activity changes in associative learning assay	170
6.3: <i>Investigating functional properties of C. elegans sleep</i>	172
6.3.1: Combining sleep and learning assessment to study functional memory consolidation in C. elegans using optogenetics	172
6.4: <i>Summary and major conclusions</i>	174
CHAPTER 7: BIBLIOGRAPHY	176
CHAPTER 8: APPENDIX	192
APPENDIX 1	192
<i>Movement detection protocol for 384-well plate</i>	192
<i>Adult sleep project scripts</i>	197

List of Figures

FIGURE 1. CHAPTER STRUCTURE TO ACHIEVE SPECIFIC AIMS	17
FIGURE 2. SUMMARY AND DEMONSTRATION OF MICROFLUIDIC STRIPE ASSAYS.....	24
FIGURE 3. SUMMARY OF MICROFLUIDIC GRADIENT ASSAYS AND QUANTIFICATION METRICS	26
FIGURE 4. SUMMARY OF PULSE ASSAY FORMAT WITH ASSESSMENT OF CHEMOTAXIS IN MULTI-STIMULUS ASSAY .	30
FIGURE 5. PLOT SUMMARY OF MULTI-STIMULUS ASSAY FOR BEHAVIOR AND ASSOCIATED NEURAL ACTIVITY	34
FIGURE 6. TRACKING OF BEHAVIORAL QUIESCENCE AT HIGH MAGNIFICATION IN A MICROFLUIDIC DEVICE	39
FIGURE 7. TRANSLATION OF BEHAVIORAL QUIESCENCE MEASUREMENTS TO SLEEP METRIC	40
FIGURE 8. AUTOMATED VIABILITY 384-WELL PLATE SCREENING ASSAY	45
FIGURE 9. SCHEMATIC OF <i>H. POLY</i> CULTURE AND TEST PREP.....	59
FIGURE 10. ILLUMINATION STYLE IMPACTS SLEEP BEHAVIOR	67
FIGURE 11. ADULT <i>C. ELEGANS</i> EXHIBIT SIMILAR SLEEP PATTERNS WHEN ISOLATED OR IN LARGE MICROFLUIDIC DEVICES IN THE PRESENCE OF OTHER ANIMALS.....	68
FIGURE 12. MELATONIN DOES NOT INCREASE SLEEP BEHAVIOR IN ADULT <i>C. ELEGANS</i>	70
FIGURE 13. PUTATIVE MELATONIN RECEPTOR MUTANT SHOWS INCREASED SLEEP FRACTION	72
FIGURE 14. MUTANTS WITH DECREASED LOCOMOTOR AND SENSORY AROUSAL SHOW REDUCED SLEEP	75
FIGURE 15. SENSORY PROCESSING MUTANTS SHOW INCREASED SLEEP COMPARED TO WILDTYPE	79
FIGURE 16. ADULT <i>C. ELEGANS</i> SHOW INCREASED AROUSAL THRESHOLD DURING SLEEP BUT VARIED SENSORY RESPONSE.....	82
FIGURE 17: APPETITIVE SENSORY NEURON SHOWS ELONGATED NEURAL RESPONSE DURING SLEEP STATE.	85
FIGURE 18: SCHEMATIC OF NEURAL RESPONSES AND BEHAVIOR IN AVERSIVE AND APPETITIVE STIMULATION	88
FIGURE 19. YOUNG ADULT SLEEP IN WILD-TYPE <i>C. ELEGANS</i> IN “POPULATION BEHAVIOR” MICROFLUIDIC DEVICES	109
FIGURE 20. SPONTANEOUS ADULT SLEEP TRANSITIONS IN MICROFLUIDIC DEVICES	110
FIGURE 21. CHARACTERISTICS OF SPONTANEOUS WILD-TYPE ADULT SLEEP AND WAKE PERIODS	111

FIGURE 22. EFFECTS OF OXYGEN, FEEDING, FOOD SIGNALS, AND SENSORY INPUT ON YOUNG ADULT SLEEP DYNAMICS	116
FIGURE 23. COMPARISONS OF SLEEP FRACTION AMONG SPECIFIC GROUPS AND TIME RANGES.....	117
FIGURE 24. NEURAL ACTIVITY DURING SLEEP AND AWAKE STATES IN “NEURAL IMAGING” MICROFLUIDIC DEVICES	120
FIGURE 25. SLEEP DETECTION IN “NEURAL IMAGING” MICROFLUIDIC DEVICES	121
FIGURE 26. CLOSED-LOOP STIMULATION AND NEURAL RECORDING IN INDIVIDUAL FREE-BEHAVING ANIMALS	124
FIGURE 27. NEURAL IMAGING DURING CLOSED-LOOP EXPERIMENTS	125
FIGURE 28. DEVELOPMENT OF THE MICROFLUIDIC BUTANONE ENHANCEMENT ASSAY	146
FIGURE 29. ANALYSIS SCHEMATIC OF THE AUTOMATED PULSE-BASED BUTANONE ENHANCEMENT ASSAY	150
FIGURE 30. BUTANONE ENHANCEMENT ASSAY RESULTS IN PULSE-ASSAY FORMAT	153
FIGURE 31. CONTROL OF SLEEP NON-IDEAL WITH REACHR OPTOGENETIC LINE	166
FIGURE 32. ASSESSMENT OF ASSOCIATIVE LEARNING AS ANIMALS AGE	169
FIGURE 33. NEURAL IMAGING IN ASSOCIATIVE LEARNING ASSAY	171
FIGURE 34. MEMORY CONSOLIDATION SCHEMATIC	173

List of Tables

TABLE 1. COMPARISON OF ANIMAL MODELS FOR SLEEP	7
TABLE 2. SUMMARY ATTRACTION INDEX DATA.....	31
TABLE 3. SCORING OF AUTOMATED 384-WELL PLATE VIABILITY ASSESSMENT	46
TABLE 4: COMPARISON OF BUTANONE ENHANCEMENT ASSAY FORMATS	148

List of Abbreviations

AA	Acetic Acid
AI	Attraction Index
ALS	Amyotrophic Lateral Sclerosis
ATR	All Trans Retinal
CAD	Computer Aided Design
CGC	<i>C. elegans</i> Genetic Center
CI	Chemotaxis Index
CNS	Central Nervous System
CS	Conditioned Stimulus
DA	Diacetyl
DMSO	Dimethyl Sulfoxide
DTS	Developmentally Timed Sleep
EEG	Electroencephalography
F	Fluorescence
GECI	Genetically Encoded Calcium Indicator
HCl	Hydrochloric Acid
MCI	Mild Cognitive Impairment
MP	Megapixels
MRI	Magnetic Resonance Imaging
MVP	Modular Valve Positioner
NA	Numerical Aperture
NGM	Nematode Growth Medium
PD	Parkinson's Disease
PDMS	Polydimethylsiloxane
RLS	Restless Leg Syndrome
SIS	Stress Induced Sleep
US	Unconditioned Stimulus

Chapter 1: Introduction

1.1: Neural plasticity: Background, methods of study, and impact

1.1.1: Plasticity and adaptive function in neural networks

From infancy to old age our brains are constantly adapting and changing, adapting the structure and function of the components and connections that create the complex and powerful organ of the human brain. This reaction is called neuroplasticity. Often neural plasticity has direct links to neural excitability. For example, in cases of injury to the CNS or inflammation of tissues, neural plasticity occurs due to increased nociceptive afferent input (i.e. in the case of chronic injury and inflammation) or decreased nociceptive afferent input (i.e. from nerve damage) that are reflected in changes to the excitability of the afferent nociceptive circuit involved (Sessle, 2016).

Several techniques have been used to study and quantify changes to neural excitability in the human brain. These include positron emission tomography (PET), magnetic resonance imaging (MRI), functional MRI (fMRI), magneto (MEG) and electro (EEG) encephalography, and transcranial magnetic stimulation (TMS), each providing non-invasive insight onto neuroplastic processes (Sharma et al., 2013). And while there are many mechanisms and a lot of work studying the dynamics of neural networks, little is known about the cellular changes that underly functional neural plasticity.

One of the most evident examples of function of neural plasticity is learning and the formation of memories. It should be expected, as neural plasticity is essentially the brain's internal mechanism for integrating new information into the vast neural networks that dictate human experience and behavior (Galván, 2010). It is widely accepted that during learning there are reversible physiological changes in synaptic transmission that need to be consolidated to form long-term memories (Lamprecht and LeDoux, 2004; McGaugh, 2000). Sleep also plays an important role in neural plasticity. In fact, it is thought that neural plasticity and memory consolidation is one of the key reasons why we sleep (Albouy et al., 2008; Frank and Benington, 2006; Gorgoni et al., 2013; Rauchs et al., 2008; Walker and Stickgold, 2006; Walker et al., 2005). Our brain's plasticity has aided humans in developing levels of function and cognition unrivaled by other species, however the complexity of the human brain makes understanding and developing treatments for neuropsychiatric disorders all the more challenging.

1.1.2: Neurological disorders and their impact

Neuropsychiatric disorders severely impact quality of life in millions of patients, contributing more Disease Affected Life Years (DALYs) than cancer or cardiovascular disease (NIMH). This includes mental and behavioral disorders such as Alzheimer's disease (AD), which affects over 5.5 million Americans (Alzheimer's Association, 2013), and neurological disorders affecting basic daily functions, like sleep. Sleep disorders alone affect an estimated 50-70 million adults in the US (Institute of Medicine (US) Committee on Sleep Medicine and Research, 2006).

The public view of neurological disorders has experienced a transformation in recent years in acceptance and urgency to address the debilitating effects caused by these disorders. Formerly, AD would be confused for an older relative having “their mind fail them”, and the dramatic and debilitating mental trauma from PTSD were dismissed, left untreated as a culturally normal result of war or other trauma. In large part, neurological issues were overlooked as often patients do not present outward symptoms and understanding of the complex human brain was in its infancy. As the average age of the global population rises, the prevalence of neurodegenerative diseases is ever-increasing. In the early 2000’s there was a push towards understanding the early signs of neurodegenerative diseases like AD, defining early signs of dementia as Mild Cognitive Impairment (MCI). Publications on MCI rose from the tens to nearly 1000 per year by the end of the 2000s (Petersen et al., 2009) Many neurodegenerative disorders like AD, Parkinson’s Disease (PD), and Amyotrophic Lateral Sclerosis (ALS) are particularly devastating because there are very little treatment options, and the disease has a drastic effect on loved ones, care givers, and all social connections to the patient (Coon and Edgerly, 1999). Only in the last decade have treatment strategies been developed that can even slow neurodegeneration caused from AD, PD, ALS, but still, many have no cure for their ailments.

Repairing disease that effects the central nervous system (CNS) will require not just transplantation of cells, but repair of the widespread neural network damage generated by diseases affecting the CNS (Xu et al., 2011). Neurodegenerative diseases such as AD and PD can trigger regional and widespread apoptosis in neurons, using endogenous

pathways (Bredesen et al., 2006). With changes happening across the brain, the brain has adapted to become highly dynamic, altering structure and neural pathways in a process known as brain plasticity. Sometimes this plasticity can be of benefit, strengthening functional performance, learning new tasks, and expanding the possibilities of the mind. Other times like in AD networks become disturbed due to buildup of proteins, plaques, or other forms of extracellular deposition like amyloid- β , causing progressive neuronal loss and functional connectivity changes (Viscomi and D'Amelio, 2012). Treatment of AD and other neurodegenerative disorders require an understanding of how neural plasticity (especially destructive) arises, and how these factors can be prevented early as signs of MCI arise. Researchers have turned to the use of simpler model organisms with sufficient homology to develop understanding of the neurochemical origins of neurodegenerative disorders.

1.2: Use and function of the model organism *C. elegans*

1.2.1: *C. elegans*, and its advantages in use as an animal model for neurological disease

C. elegans provide a simple but robust model to study neurological disorders and development. Sydney Brenner and colleagues first discovered the usefulness of the organism for biological application (Brenner, 1974). It possesses a number of useful features for neurological research. *C. elegans* are the first organism to have a fully mapped neural connectome, consisting of only 302 neurons which form about 7000 chemical synapses (White et al., 1986). They are transparent, which allows for easy imaging to internal features like neurons relevant for study. They are extremely small, growing to about 1 mm in length, which allows for cultivation of many animals without

consuming vast resources. They share many genetic features with mammals, including important classes of neurotransmitters such as GABA, Dopamine, Glutamate, Acetylcholine, Serotonin, Tyramine, Octopamine, and many more. They have quick generational times (3 days) and self-reproduce hundreds of isogenetic progeny allowing for rapid generation of many synchronized animals for study. There are also a number of genetic tools for generation of mutant strains for studying the effects of specific genes on behavior and beyond (Antoshechkin and Sternberg, 2007; Boulin and Hobert, 2012; Friedland et al., 2013), and their genome is fully mapped (Consortium*, 1998). In addition to the useful characteristics of *C. elegans* which make them easy to study, they share a number of neurological functions that are implicated in neurological disorders, including sleep and learning.

1.2.2: Sleep, sleep disorders, and sleep in model organisms including C. elegans

Despite consuming nearly a third of our lives, the function of sleep remains a mystery. Reduction in the amount and quality of our sleep affects our productivity and leads to serious health concerns such as cardiovascular issues (Liu et al., 2002; Newman et al., 2000; Schwartz et al., 1998; Shamsuzzaman AM et al., 2003), diabetes (Gottlieb et al., 2005), and obesity (Hasler et al., 2004). Sleep disorders affect an estimated 50-70 million adults in the United States alone and often are poorly diagnosed (Institute of Medicine (US) Committee on Sleep Medicine and Research, 2006). Additionally, sleep deprivation is shown to affect our alertness in performing daily functions (Banks and Dinges, 2007) as well as our learning and memory (Kreutzmann et al., 2015). There have been a number of proposed core functions of sleep including controlling energy usage (Benington and

Craig Heller, 1995), metabolic control of macromolecule biosynthesis (Mackiewicz et al., 2007), and memory consolidation and neural plasticity (Frank and Benington, 2006; Karni et al., 1994) however there is no consensus as to why we sleep. It is now understood that sleep is observed across species and similarities in functionality can be drawn to establish an evolutionary basis for sleep (Campbell and Tobler, 1984).

Human sleep studies are common for diagnosing issues of an individual, however, animal models have long been used to uncover physiological and molecular mechanisms of sleep in a more rapid fashion (Toth and Bhargava, 2013). An ideal animal model to study human sleep disorders shares characteristics of sleep with humans, has access to genetic tools necessary for modeling human disease, and is capable of high-throughput study. **Table 1** demonstrates pros and cons of common animal models used to study sleep. Animals such as rats, dogs, and birds (Vorster and Born, 2015) are used to model sleep because they are physiologically similar to humans and allow for the use of electroencephalogram (EEG) to study the electrical activity in the brain as is used in humans to diagnose sleep abnormalities. Use of these model organisms typically is costly both in terms of time and money, and they lack the tools necessary for high-throughput genetic control. This deficiency suggests that there is a need for a model organism of higher genetic control (Crocker and Sehgal, 2010; Sehgal and Mignot, 2011), significant genetic homology (Lai et al., 2000), and capability of high-throughput study such as the nematode *Caenorhabditis elegans* (*C. elegans*) (Antoshechkin and Sternberg, 2007) to model sleep disorders.

Table 1. Comparison of animal models for sleep

Animal	Pros	Cons
Mammals (humans, dogs, mice, rats, cats, etc.)	<ul style="list-style-type: none"> -Similarity to humans -Use of EEG -More extensively researched 	<ul style="list-style-type: none"> -Lack high-throughput capability
Birds	<ul style="list-style-type: none"> -Use of EEG -Link to putative sleep function 	<ul style="list-style-type: none"> -Morphological differences in brain
Other invertebrates (bees, <i>Drosophila</i>)	<ul style="list-style-type: none"> -Easy to maintain, use in high throughput -Genetic tools 	<ul style="list-style-type: none"> -Link to human sleep functions still unclear

Periods of feeding and locomotion arrest in *C. elegans* has long been observed (Cassada and Russell, 1975) during lethargus stages. Over the past decade, research on *C. elegans* behavior has drawn links between periods of behavioral quiescence to sleep in humans. Observations of sleep-like characteristics of *C. elegans* began in 2008 (Raizen et al., 2008a) when Raizen et al. demonstrated that states of lethargus in *C. elegans* showed sleep-like properties. This form of quiescence is shown during molting periods between the four larval stages of *C. elegans* and is termed developmentally timed quiescence. Quiescence has also been shown during periods of high stress (Hill et al., 2014) including heat, cold, hypertonicity, and tissue damage, and most recently food deprivation (Skora et al., 2018) and hypoxia (Nichols et al., 2017). This form of quiescence has been termed SIS. These quiescent states have been shown to share human sleep functions such as synaptic plasticity (Dabbish and Raizen, 2011) and metabolic control (Driver et al., 2013). Additionally, these states demonstrate behavioral characteristics of sleep seen in humans such as rapid reversibility (Raizen et al., 2008a; Trojanowski et al., 2015), increased arousal threshold (Cho and Sternberg, 2014; Raizen et al., 2008a), stereotypical posture (Iwanir et al., 2013; Schwarz et al., 2012; Tramm et al., 2014), and homeostatic response to sleep deprivation (Driver et al., 2013; Nagy et al., 2014a; Raizen et al., 2008a).

1.2.3: Learning and memory in *C. elegans*

Well prior to the discovery of sleep-like states in *C. elegans* researchers knew that the simple model organism was capable of plastic neurological behaviors through their evident capability to adapt and learn in their environments. Rankin et al. (Rankin et al., 1990) were the first to demonstrate non-associative learning and memory in *C. elegans*. They showed that *C. elegans* was capable of learning in response to a mechanical stimulus. They demonstrated this habituation style learning was both short-term and long-term lasting over 24 hours. The first study demonstrating learned behavior in *C. elegans* came from Hedgecock and Russell (Hedgecock and Russell, 1975) who demonstrated that *C. elegans* had associative learning based on thermotaxis to temperatures they were grown at. Since these first studies, a number of associative learning paradigms have been tested including pairing 1-propanol with HCl in an aversive olfactory learning experiment (Amano and Maruyama, 2011) as well as pairing butanone with food in a positive learning assay (Torayama et al., 2007).

C. elegans also demonstrate adaptive learning (Colbert and Bargmann, 1995; Hilliard et al., 2005; L'Etoile et al., 2002; Schafer and Kenyon, 1995), regulating their responsiveness to repetitive odors and adapting responsiveness in mechanisms to better survive their environment. These adaptations can be sensitive to specific receptors or general across entire networks. Despite their simple nervous system, *C. elegans* are able to navigate towards desirable locations based on environmental cues such as water soluble attractants/repellents, temperature, pH, and oxygen levels (Bono and Maricq, 2005; Troemel, 1999), providing baselines to assess learning and behavior.

1.3: Quantifying neural activity and associated behavior in *C. elegans*

1.3.1: Methods for studying *C. elegans* behavior and quiescence

Methods to track *C. elegans* behavior (Dusenbery, 1985; Waggoner et al., 1998; Bono and Bargmann, 1998; Ritu Dhawan, 1999; Pierce-Shimomura et al., 1999) have been developed over the past few decades to be used in plate based assays and in recent years in a more environmentally controlled manner in microfluidic devices (Albrecht and Bargmann, 2011). Sleep assessment utilizes the machine vision tools developed for general behavioral assessment but focuses on recognizing quiescence, a behavioral feature of sleep. Centroid tracking (Van Buskirk and Sternberg, 2007) and frame subtraction (Raizen et al., 2008a) were the first image analysis methods used to quantify behavioral quiescence in *C. elegans* and more recently posture analysis (Nagy et al., 2014b) methods have been developed sensitive to characteristics of *C. elegans* quiescence for a more thorough approach. Each of these methods however have limitations preventing high-throughput assessment of *C. elegans* sleep. Frame subtraction is only applicable to single animals (Raizen et al., 2008a) at a time because of potential animal overlap between frames, centroid tracking alone is inefficient at capturing small movements or shape changes sensitive to quiescence (Nagy et al., 2014b), and posture analysis is computationally intensive limiting throughput to 3-5 animals per day (Nagy et al., 2014a). In order to increase sleep assessment throughput to 100 or more animals per experiment we propose to adapt a centroid tracking method with body morphology assessment (Albrecht and Bargmann, 2011) to track many

behavior in many worms in a manner more sensitive to short movements that are necessary for capturing sleep bouts.

In recent years the use of microfluidics (Meldrum and Holl, 2002; Mitchell, 2001; Sia and Whitesides, 2003) for environmental control and delivery of spatially and temporally controlled stimuli (Taylor and Jeon, 2010) has become popular with *C. elegans*. These devices have also been termed “artificial dirt” for their ability to mimic the natural soil dwelling conditions of *C. elegans* through the use of micro-posts, channels, and chambers that match the size of the worms allowing for roaming behavior (Lockery et al., 2008). Most commonly, devices are fabricated using polydimethylsiloxane (PDMS) which is a biocompatible and transparent polymer. PDMS is also gas permeable, which keeps the animals viable while allowing for the device to absorb bubbles that may get introduced into the microfluidic arena during set up. Devices are fabricated using soft lithography (Sia and Whitesides, 2003) techniques to create a “master” to be used as a template for molding devices in PDMS. The PDMS mold is made, inlet and outlet holes are punched into the device, and fluid flow can then be established across the microfluidic arena in a laminar fashion. All *C. elegans* behaviors are ultimately dictated by their neural circuit, and researchers have developed tools to directly measure how activity in the neural circuit associates with particular behaviors. Microfluidics are especially useful as they provide a small fixed area for imaging on the scale of individual neurons.

1.3.2: Fluorescent proteins, calcium indicators, and measuring neural activity

The gold-standard technique for electrophysiological measurement of electrical properties of cells is known as patch-clamp (Veitinger, 2011). Patch-clamp and other electrophysiological measurement techniques were developed in the past centuries to measure the excitability of cell membranes, and measuring action potentials. In patch-clamping, researchers can measure directly the changes in membrane currents or potential using glass micropipettes placed in living or excised tissue. These techniques however are invasive, damaging the cell of interest, and therefore only provide a temporary measurement of neural activity. Because of this, researchers sought to develop techniques more suitable for measuring neural activity in living organisms.

The use of genetically encoded calcium indicators (GECIs) such as GCaMP (Nakai et al., 2001) has become widespread to assess calcium activity in cells and living organisms. GCaMP was created from the fusion of green fluorescent protein (GFP) with calmodulin and M13, creating a dynamic sensor of calcium levels. GCaMP belongs to a family of GECIs that provide functional measurements of neural activity in a non-invasive optical manner, *C. elegans* can be easily genetically modified by injecting plasmids of interest into their gonads to be delivered to future generations. Using this technique, progeny can express plasmids containing genes for calcium sensors like GCaMP, expressing them selectively across the cellular system. Researchers can then make use of *C. elegans*' transparent body to image directly to neurons, both in single neuron and multi-neuron whole brain imaging techniques.

Published work (Larsch et al., 2013) that our lab has developed has demonstrated capability of measuring the changes to neural activity that happen in response to stimulus cues. The technology utilizes microfluidic arenas to deliver stimuli in a precise spatial and temporal fashion. It has full control of the microfluidic environment through use of timing valves, controlling the inlets, and controlling outlet flow. Software to track neurons and integrate fluorescent measurement is used to automate the process of assessing neural activity in freely moving *C. elegans* regardless of what neuron is fluorescently tagged.

1.4: Project overview

1.4.1: Long-term goal and specific aims

Our long-term goal is to use *C. elegans* to understand the molecular and neural circuitry changes that underlie neurological disorders. The objective of this project is to develop high-throughput analysis systems to automate the assessment of behavioral plasticity associated with sleep and learning. Further, to translate these assessment tools towards neural imaging systems to functionally measure changes in neural plasticity in *C. elegans*. I hypothesize that systems capable of studying behavioral and neural plasticity in *C. elegans* will be able to elucidate cellular mechanisms that underlie neurological disease using human neurological disease models in *C. elegans*. It is expected that by achieving these three specific aims, this thesis will contribute systems useful for understanding the underlying cellular mechanisms underlying neurological disorders involved with learning and sleep.

1. Develop high throughput behavioral assays to assess adult sleep behavior in microfluidic devices

Currently we are able to analyze *C. elegans* behavior of 100 animals with 4 separate genotypes simultaneously in microfluidic devices (Albrecht and Bargmann, 2011). We have found that adult *C. elegans* exhibit sleep states when in the microfluidic environment that differs from previously reported *C. elegans* sleep states. To assess the sensitivity of the system in measuring sleep bouts, we will investigate sensory modulation of sleep behavior by subjecting animals to odorant pulses and measure changes to sleep dynamics. Additionally, we will assess how sensory deficient mutants sleep and how they are affected by odorant conditions.

2. Automate neural imaging methods to create a closed-loop assessment system of sleep and wake neural recordings to assess neural plasticity during sleep.

C. elegans show an increase in arousal threshold (Cho and Sternberg, 2014; Raizen et al., 2008a) during sleep suggesting modulation in the neural circuit during sleep-like states. To assess state-dependent modulation of the neural circuit, we will utilize a sleep assessment system to track sleep states of *C. elegans* and deliver stimulus during sleep and awake states. We will assess where in the neural circuit modulation of neural activity occurs. We expect modulation of neural activity to occur at the interneuron level rather than the sensory neuron level.

3. Improve the reproducibility and translatability of associative learning assays by developing assessment systems in microfluidic devices.

We will develop behavior-based assessments of associative learning in a butanone enhancement assay to increase throughput of measurements of learning and allow for investigation of learning across various lifecycle stages. Adapting from plate-based chemotaxis assays, we will develop systems to study attraction to conditioned stimuli using instantaneous behavioral metrics rather than taxis location based metrics, allowing for future translation of methods across ages and to neural imaging assessment. These assays will be developed using microfluidic devices for higher reproducibility of stimulus conditions.

1.4.2: Chapter outline and overview

The 3 specific aims detailed above will be accomplished in **Chapters 2-5** of this thesis document (**Fig. 1**). In **Chapter 2** I will detail methods to study behavioral plasticity in nematodes, a crucial component of understanding how to apply behavioral understanding to functional state assessment. Sleep and learning are complicated phenomena, requiring precise behavioral patterns to be understood to make confident determinations of changes within the state. Information contained in **Chapter 2** contributed both to **Aim 1** and **Aim 3**.

In **Chapter 3** I will investigate the effects of neuromodulators on sleep, establish that sleep phenotypes can be recovered using rescue lines, and begin to study closed-loop

automation of sensory neuron evoked response during sleep. The work in this chapter will contribute towards both **Aim 1** and **Aim 2**

In **Chapter 4** I will detail in depth studies that demonstrate high-throughput behavioral assessment of sleep in microfluidic devices exposed to a number of odorant and genetic perturbations. I will also demonstrate the use of an automated closed-loop state assessment system used to stimulate animals during sleep and wake states. Work in this chapter follows work from **Chapters 2 and 3** and contributes to both **Aim 1** and **Aim 2**.

In **Chapter 5** I will demonstrate translation of the butanone enhancement assay into an all microfluidic format, providing a platform to study associative learning that minimizes issues of test-to-test reproducibility, animal handling agitation, and translatability of findings to neural activity. Work in this chapter contributes to **Aim 3**.

Finally, in **Chapter 6** I will introduce the future directions of this project, and ideas for advancing what has been discovered in **Chapters 2-5**.

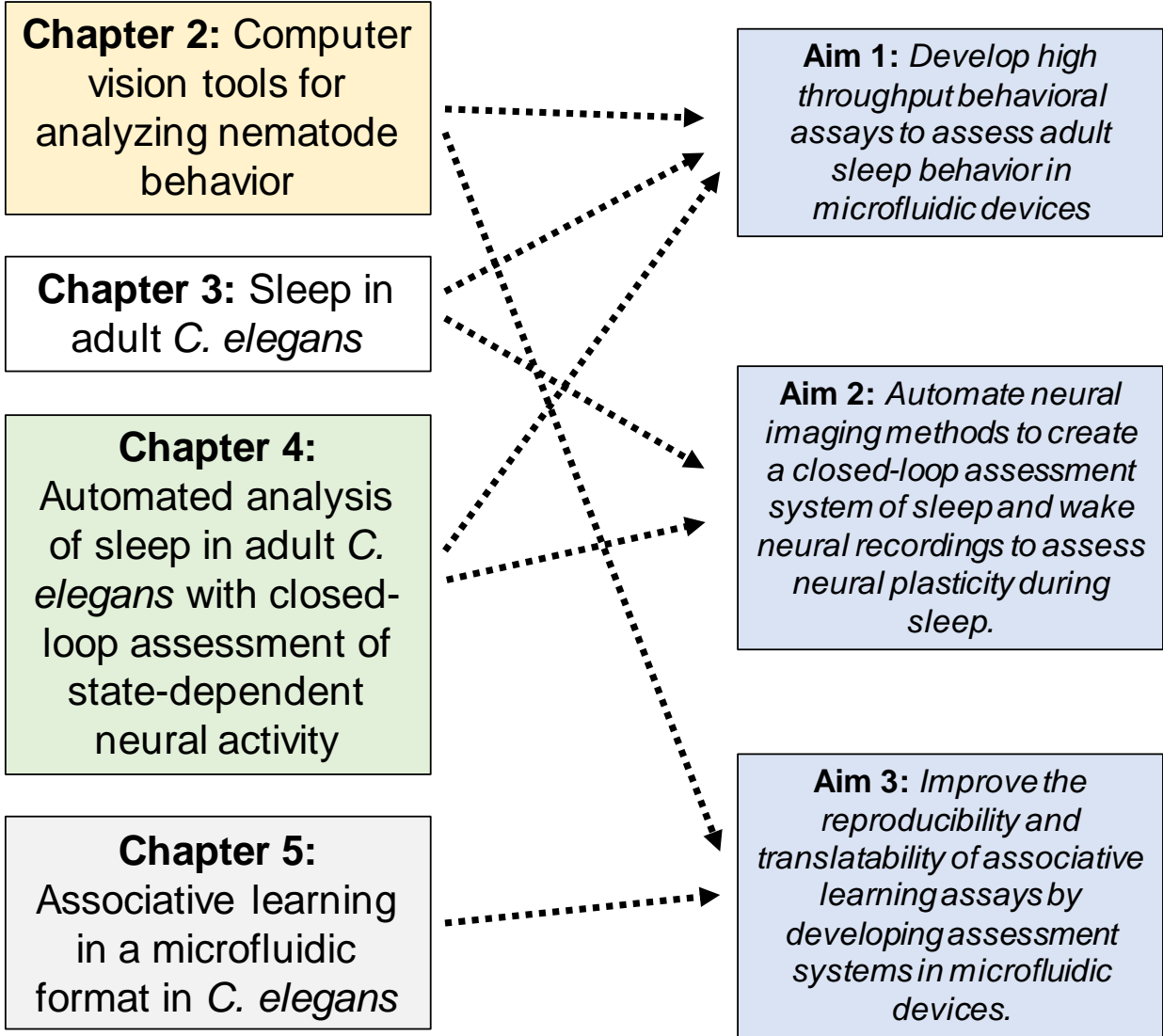


Figure 1. Chapter structure to achieve specific aims

Chapter 2: Computer vision tools for analyzing nematode behavior

Work in this chapter has been aided by several collaborators. Experiments with acids and *C. elegans* were conducted Jeff Grant of the Alkema lab. Gradient assay systems were demonstrated and shared with me by Karen Tran a former MS student in the Albrecht lab. The initial development of work studying behavioral quiescence in adult *C. elegans* began during the summer of 2015 with help from Allison Marley, an undergraduate student participating in the Research Exchange for Undergraduates (REU) program here at WPI. Finally, I formed a collaboration with Dr. Mostafa Elfawal of the Aroian lab working on vitality assessment systems for parasitic nematodes. Dr. Elfawal developed the parasitic nematode culture protocols, prepared the 384-well plates for testing, and imaged the plates. I worked on assessing the videos and developing automated systems of classification to score living and dead animals for drug screening applications. This work was supported in part by an NSF IGERT award (DGE 1144804) and by the Burroughs Wellcome Fund Career Award at the Scientific Interface, and the National Science Foundation NSF CBET 1605679 and EF 1724026, NIH R01DC016058.

Abstract

Ever since the establishment of *C. elegans* as a model organism for studying human disease, researchers have aimed to characterize the behaviors of the nematode to establish connections to higher level organisms up to humans. Behaviors come in all shapes and forms, from complex to nuanced. Manual tracking of animals is possible, but cumbersome. Development of automated behavioral tracking and classification systems has allowed researchers to more confidently establish trends in *C. elegans* behavior, and increase throughput of assessment. Tracking *C. elegans* behavior has also benefited from the use of structured assay environments, such as those provided by microfluidic devices. Here, we demonstrate the use of stripe, gradient, and pulse microfluidic assays for assessing chemoattraction, necessary for the study of learned association to odorants. Additionally, we demonstrate image segmentation techniques to track the lack of motion, relevant for studying sleep. These image segmentation techniques have broader application, as we used these techniques to develop an automated viability assessment system for development of a high-throughput anthelmintic drug screening system for parasitic nematodes.

Introduction

The use of animal models in biological research has increased dramatically over the past decades. Animal models allow researchers to take a more rigorous look into how a disease presents itself from the molecular level all the way up to visible behavioral changes, in the hopes of developing an understanding of how to treat disease. In general animal models are stereotyped to apply to specific areas of biological research due to

varying homology, attractive features for particular research formats, and functional factors such as ease of use and cost (Ankeny and Leonelli, 2011). There are a number of common animal models, each with characteristics that provide advantages from their translatability to human function to capabilities in high-throughput study. Each animal model presents unique challenges in how to assess their behavior, accounting for functional differences, expectations of how their behavior will translate to human disease, and the methods of capturing behavior. Understanding the subtle nuances that differentiate healthy function from disfunction and disease require understanding of how disease or disorder manifests itself in that individual animal. These shifts in behavior can be fairly obvious such as changes in appearance or viability or indistinct such as a modulated ability to perform a task, shifts in preference of behavior, or a change in frequency of success in how a behavior is commonly performed.

C. elegans provide several distinct advantages that make them an ideal model system for studying the connections between behavior and neurological function. They have quick generational times (3 days) and self-reproduce hundreds of isogenetic progeny allowing for rapid generation of many synchronized animals for study. There are also a number of genetic tools for generation of mutant strains for studying the effects of specific genes on behavior and beyond. Their nervous system is compact, and their behaviors are most often organized in forms of taxis towards attractants or away from repellants. In a laboratory setting animals are often housed on agar dishes with bacterial food. They exhibit sinusoidal crawling behavior, most often crawling forward as they roam to explore their environment seeking food and optimal environmental conditions (Albrecht and

Bargmann, 2011; Gray et al., 2005). Occasionally animals will exhibit long reversals that are coupled with reorientation from an “omega” turn to escape or change their search path, or shorter reversals pulling their nose away from less desired locations. Additionally, they will pause momentarily often to feed if bacterial food is present (Flavell et al., 2013), or to probe the local area when encountering objects or other animals.

Although it is possible to track animals manually, automated systems using computer vision techniques provide a great advantage in the throughput of behavioral data capture and the reliability of behavioral assessment. A number of “worm trackers” have been developed for studying these behaviors most commonly tracking animals on an agar dish. Methods to track *C. elegans* behavior (Dusenbery, 1985; Waggoner et al., 1998; Bono and Bargmann, 1998; Ritu Dhawan, 1999; Pierce-Shimomura et al., 1999) have been developed over the past few decades to be used in plate based assays and in recent years in a more environmentally controlled manner in microfluidic devices (Albrecht and Bargmann, 2011).

The major drawback to tracking animals on a plate comes from a lack of environmental control and chemical stimulus reliability. It becomes a great an additional hurdle to control for humidity and temperature while also probing for behavioral response to chemical stimulation. To combat these issues, microfluidic devices are used to create a consistent fluid environment with the ability precisely deliver chemical stimulus and monitor natural *C. elegans* behavior (Albrecht and Bargmann, 2011). These microfluidic devices have a

hexagonal array of microposts, facilitating sinusoidal crawling. Tracking systems have also been developed for use accounting for the micropost structure of the microfluidic device, allowing users to study behavior in a controlled liquid environment, probing for changes relevant to neurological function and disease states.

In this Chapter, I aim to demonstrate methods of behavioral analysis primarily in *C. elegans* but also in the parasitic nematode *Heligmosomoides polygyrus* (*H. poly*), highlighting computer vision techniques for analyzing nematode behavior. The chapter will cover methods for studying chemotaxis in *C. elegans* and their applications in studying learning, memory, and adaptation. I will introduce three microfluidic assay formats and discuss their pros and cons, and how they can best be used to understand *C. elegans* behavioral plasticity. It will also cover methods to study movement to study quiescence both in association to sleep and in viability assessment. We expect that these methods will provide the assessment platforms to develop automated analysis systems to track behavioral plasticity involved in sleep and learning in *C. elegans*.

Results

2.1: Methods to analyze nematode odor preference

2.1.1: Quantifying *C. elegans* attraction and aversion in stripe assays

There are three primary microfluidic device formats that we use to assess behavioral preference: stripe, gradient, and pulse. Each method is unique in its pros and cons in the breadth of behavioral information and reliability of assessment. The simplest format is a stripe of odor. Flow in the microfluidic environment is laminar, so devices can be designed (Albrecht and Bargmann, 2011) to create spatially separated odor stripes with consistent widths to study how animals interact with a stripe of odor over time (**Fig. 2a**). Commonly, an odorant is presented in the middle third of the arena with dye to distinguish its location, with buffer surrounding the stripe (**Fig. 2b**). As in plate-based chemotaxis assays (Ward, 1973), quantification of attraction to a stripe is found by calculating a chemotaxis index based on preferential residency inside or outside of the stripe (**Fig. 2c**). This results in a -1 (pure aversion) to +1 (pure attraction) scale to assess an animal's attraction to the stripe. You can also assess animal behavior at the edge of the stripe to gain more information about how animals perceive the shift in odor profile. As expected, animals show an immediate strong attraction to a stripe of NA22 *E. coli* (**Fig. 2d**), with chemotaxis index reaching +1, and strong aversion to a stripe of pH 2.5 hydrochloric acid (HCl) (**Fig. 2e**), with chemotaxis index stabilizing between -0.6 to -0.8. However, when presented with a more neutral stimulus that is typically aversive (Amano and Maruyama, 2011; Sambongi et al., 2000) in pH 4.0 acetic acid (AA), animals exhibit a neutral or even positive chemotaxis (**Fig. 2f**) contradicting the expectation of aversion.

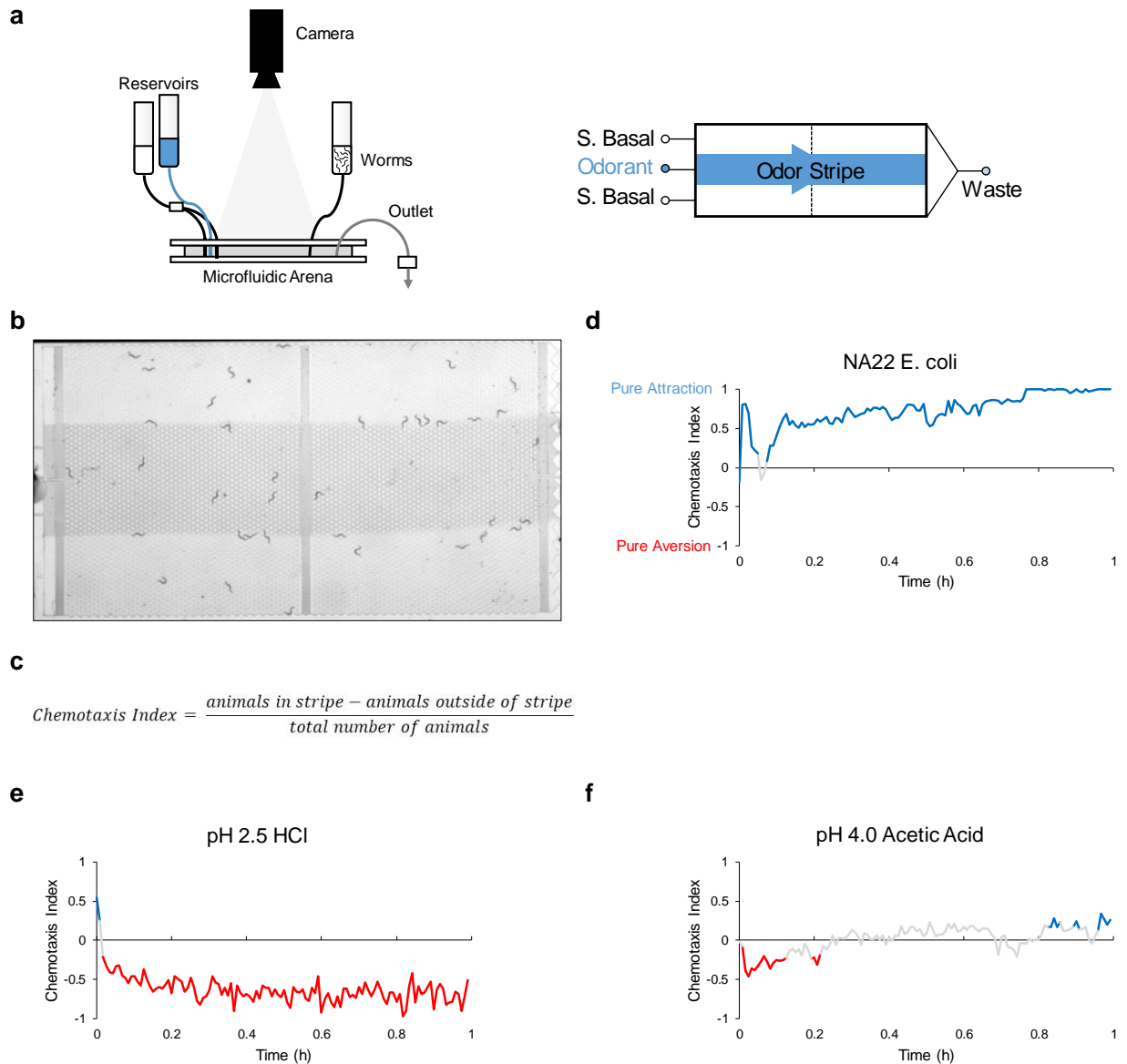


Figure 2. Summary and demonstration of microfluidic stripe assays

(a) Schematic side-view of the microfluidic system on the left with two reservoir inlets (one for *S. Basal* buffer split with a 2-way splitter, and one for the odorant), and a device odorant profile with the center odor stripe in birds eye view on the right. (b) Image of a microfluidic device with an active odorant stripe flowing in the middle with dye to visualize. (c) Formula for calculating Chemotaxis Index in the stripe microfluidic assay format. (d) Chemotaxis index over a one-hour assay of wildtype animals to a stripe of NA22 *E. coli* ($n = 28$ animals). (e) Chemotaxis index over a one-hour assay of wildtype animals to a stripe of pH 2.5 HCl ($n = 24$ animals). (f) Chemotaxis index over a one-hour assay of wildtype animals to a stripe of pH 4.0 AA ($n = 36$ animals). Chemotaxis index plots in d-f are colored blue for positive index values indicating attraction, grey for neutral values, and red for negative values indicating aversion.

2.1.2: Quantifying C. elegans attraction and aversion in gradient assays

Like the previously described stripe device, gradient devices are designed to present animals with a variable odorant environment to study chemotaxis behavior. As their name suggests, the devices are designed with distributed mixing channels to mix an odorant with buffer creating a linear gradient from the center of the arena towards the edges (**Fig. 3a,b,c**). This gradient of odor concentration creates a more realistic odorant profile for animals to navigate, removing edge effects seen with stripe devices. The primary quantifiable measure of the gradient device is Y-position residency over time, as animals will navigate up and down the gradient until they find a preferred location, often traversing in the X direction once they find their desired location. Based on this taxis profile, a similar chemotaxis index can still be applied by calculating the worm density in the Y-axis (**Fig. 3d**) and measuring the difference of animals residing in a given ratio of the middle (highest odorant concentration) regions and outside (lowest odorant concentration) regions (**Fig. 3e**). Chemotaxis indices follow similar patterns to the stripe device, however gradient devices also give a chance to study balance between odorant preferences that a stripe device cannot.

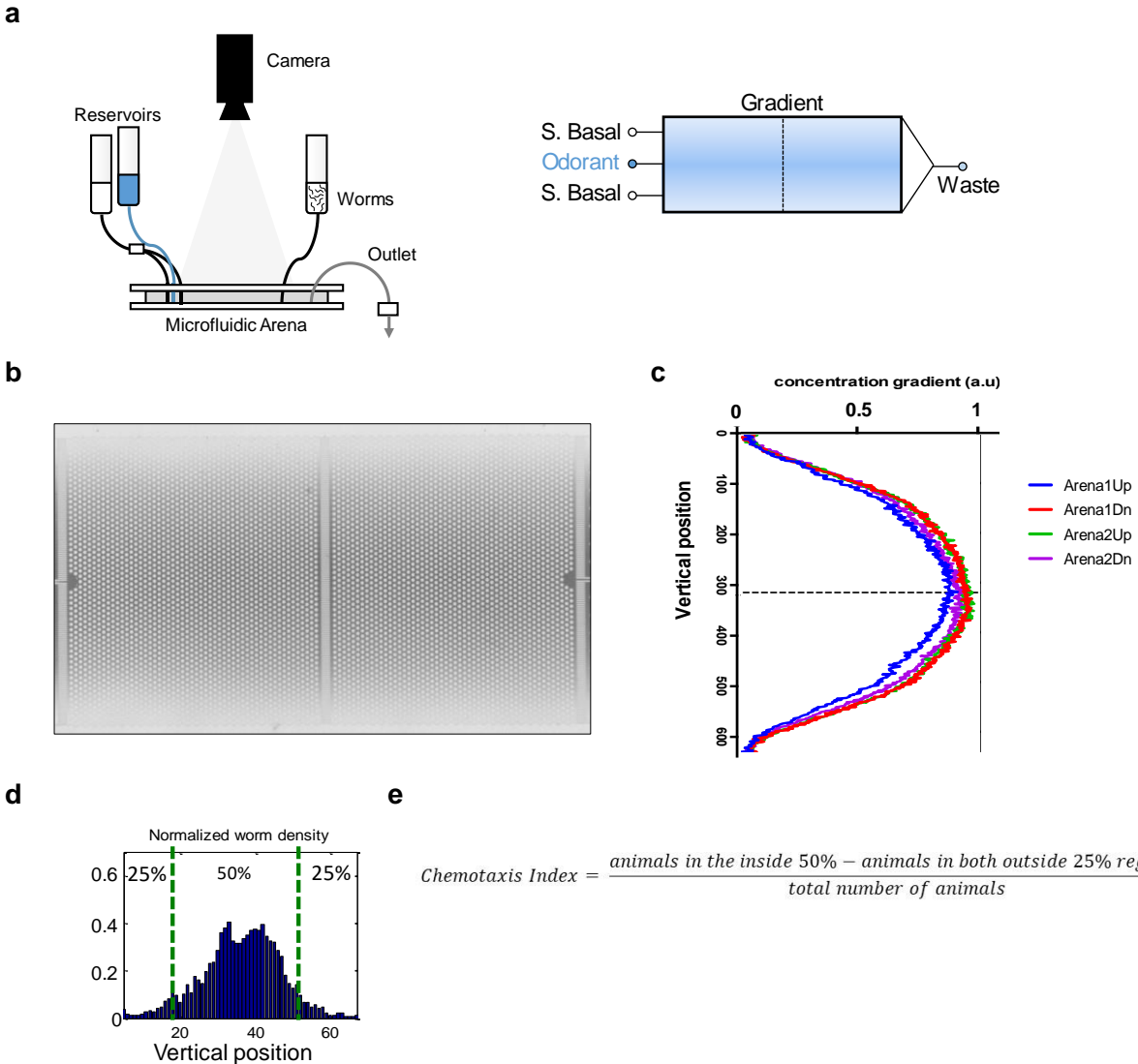


Figure 3. Summary of microfluidic gradient assays and quantification metrics

(a) Schematic side-view of the microfluidic system on the left with two reservoir inlets (one for S. Basal buffer split with a 2-way splitter, and one for the odorant), and a device odorant profile of a linear gradient in birds eye view on the right. (b) Image of a microfluidic device with an active linear gradient flowing with dye to visualize odor. (c) Concentration profile in normalized absorbance across the vertical axis of the microfluidic device, taken in points in arena 1 and 2 in upstream and downstream locations. Arena 1 being the left behavioral arena in a 2-arena microfluidic device and arena 2 being the right behavioral arena (Karen Tran, 2015). (d) Example of normalized density plot for animals in the gradient device, with vertical position used to calculate chemotaxis index (Karen Tran, 2015). (e) Formula for calculating Chemotaxis Index in the gradient microfluidic assay format.

*2.1.3: Quantifying *C. elegans* attraction and aversion in pulse assays*

The third microfluidic format for assessing behavioral dynamics is the pulse assay. Pulse assays provide several advantages over stripe and gradient style assays, but also have some drawbacks. The pulse format allows for precise timing of stimulus application, with devices designed to balance flow such that odorant or buffer can be presented in a “wall” of odor across the arena reaching all animals. Using a 3-way valve, a single control buffer reservoir loads one of two potential upstream channels at a time, directing flow such that the arena fills with only buffer or odorant with given user activation (**Fig. 4a**). Control of this valve allows the user to pre-program timing patterns to be applied, and dye is included in the odorant to visualize the switching between buffer and odorant (**Fig. 4b**). Rather than relying on animal behavior to dictate what odor they experience, pulse timing is in complete user control, allowing the user to pre-determine the exact temporal dynamics of odorant exposure for their experiment. Pulse formats also allow for flexible measurement of behavioral preference: studies can look at instantaneous behavioral reactions, or more extended ones, giving a breadth of behavioral information to dissect.

The major drawback of pulse assays is they do not provide the same taxis information that a continuous odorant profile of a stripe or gradient assay, requiring a deeper look at behavior to quantify preference. In general, when a population of animals exhibits more forward-biased taxis when attracted to a stimulant and will turn or reverse away from a stimulant they are averse to (Pierce-Shimomura et al., 1999). Likewise, upon odor removal you will see animals turn in attempt to re-enter an attractive odor, or speed forward to escape from an aversive odor. An example of preference quantification we

have used uses probability of forward movement to determine an “Attraction Index” that closely mimics the standard chemotaxis index used in stripes and gradients. This attraction index is calculated by dividing the probability of forward motion during odorant exposure, divided by the probability of forward motion outside of exposure (**Fig. 4c**). To balance the index to match the easy to understand scoring of a chemotaxis index (negative = aversive, 0 = neutral, positive = attractive) we also subtract 1 from the index. By doing so, if animals cease forward motion during an odorant in an attempt to turn and initiate an avoidance response, their Attraction Index would approach -1. If there is no difference between motion during and outside of odorant simulation the Attraction Index would read 0. If the animals exhibit more attraction-characteristic forward motion during the pulse and show decreased forward motion due to turning and avoidance response upon stimulus removal the index will be positive.

2.1.4: Integration of multiple sensory inputs reveals behavioral preferences dictated by feeding state through use of a pulse assay

To assess this quantification method, we designed a pulse assay to dissect how *C. elegans* behavioral preferences shift with multiple sensory inputs depending on their feeding state. In the wild, *C. elegans* need to navigate environments with a plethora of sensory input (Hart and Chao, 2010) and make decisions of what areas are safe for egg laying, plentiful for feeding and growth, or dangerous because of harsh conditions or predators. We presented groups of well-fed and 2 h starved animals with mixed odorant cues to assess how feeding state shifts their behavioral preference. Each pulse of odorant contained 1.1 μ M Diacetyl, a moderate concentration of a behaviorally attractive food

odor (Chuang and Collins, 1968), but a varying concentration of Glycerol, an osmolyte that creates unfavorable hyperosmotic conditions which stress *C. elegans* (Lamitina et al., 2004). Groups of three 30s pulses of odorant with 30s rest times were given every 4 min, with each group increasing the Glycerol concentration from a baseline of 0 mM up to 500 mM in 100 mM increments (**Fig. 4d**).

Each device contained four 16 mm x 15 mm arenas housing four independent populations of ~25 freely crawling animals that share the same fluidic environment. For each test, two arenas contained well-fed animals and two arenas contained 2 h starved animals. We quantified the Attraction Index for each group of 3 pulses ($n = \sim 100$ animals each group). With no glycerol, both groups showed attraction to the pulse of diacetyl with well fed animals exhibiting an Attraction Index of 0.43 ± 0.2 s.e.m. and starved animals exhibiting an Attraction Index of 0.35 ± 0.07 . Although differences between groups are not significant ($p > 0.05$), as the concentration of Glycerol increased, starved animals on average showed a higher Attraction Index to the mixed odorant solution at every concentration, including positive attraction at 200 mM Glycerol when well-fed animals showed aversion (**Fig. 4e**). Data summarized in **Table 2** below.

Table 2. Summary Attraction Index data.

Data from multi-stimulus assay in **Fig. 4e**. Error bars signify s.e.m.

Glycerol Concentration	<u>Well-fed</u> animals	<u>Starved</u> animals
	Attraction Index	Attraction Index
0 mM	0.43 ± 0.2	0.35 ± 0.07
100 mM	0.39 ± 0.36	0.65 ± 0.42
200 mM	-0.02 ± 0.14	0.07 ± 0.17
300 mM	-0.15 ± 0.08	-0.04 ± 0.09
400 mM	-0.25 ± 0.04	-0.11 ± 0.09
500 mM	-0.22 ± 0.04	0 ± 0.07

2.2: Translation of behavioral assessment to neural imaging

2.2.1: Pulse assays allow for seamless transition to neural imaging methods

A primary advantage of the pulse microfluidic device format is its ease in use for neural imaging applications. Neural imaging devices can be designed to mimic any of the three behavioral stimulation types but are sized to fit the entire field of view at higher magnification objectives on an epifluorescence microscope, such that the neuron(s) of interest are clearly visible. They are designed with 3 mm x 3 mm arenas as opposed to the 16 mm x 15 mm arenas used in behavior devices previously mentioned. While possible (Larsch et al., 2015), it is more difficult to observe translatable neural activity measurements to their respective behavioral measurements in both the stripe and gradient system. Forming direct comparisons requires animals to mimic behavior and/or timing in both systems, but the user has no direct way to control for how animals will behave. In contrast, pulse devices observe temporal changes that can be mimicked and synced between larger behavior monitoring devices and their smaller neural imaging focused counterparts. This allows the user to collect all relevant behavioral information in large populations for higher throughput and collect neural activity data without needing to match behavior output. Additionally because the neural imaging assay can be streamlined to focus solely on neural activity, animals can be paralyzed with tetramisole, an anthelmintic drug that paralyzes body wall muscles in *C. elegans* (Lewis et al., 1980), to facilitate neural imaging data with less movement-artifact generated noise.

Using the multi-stimulus assay format described above, we demonstrated how the pulse assay system can be used to study changes in neural activity as well as behavior. We

mimicked the same pulse format as in **Fig. 4d**, however we also performed the reverse Glycerol steps after the stepwise climb up in concentration, climbing down until again reaching 0 mM Glycerol. In (**Fig. 5**) we show plots of behavioral probability averaged for each pulse, and below the associated neural activity in the AWA and ASH sensory neurons. This odor-neuron pair was chosen since the g-protein coupled receptor (GPCR) *odr-10* is expressed in AWA that detects the odorant Diacetyl for chemosensation (Sengupta et al., 1994), and hyperosmotic solutions such as those caused by high Glycerol concentrations, are detected by ASH (Hilliard et al., 2005).

After a characteristically high naïve response in AWA (peak $\Delta F/F_0 = 1.32 \pm 0.16$ s.e.m.), AWA responded reliably regardless of Glycerol concentration, remaining consistent to the consistent stimulation of 1.1 μ M Diacetyl. On the other hand, ASH activity varied greatly depending on Glycerol as expected, but also varied based on experience. For low Glycerol concentrations (0 and 100 mM) ASH saw no response, which matched a lack of change in behavioral effects. Once Glycerol concentrations were upped to 200 mM, ASH started showing response (peak $\Delta F/F_0 = 0.55 \pm 0.28$), however peak ASH response happened at 400 mM (peak $\Delta F/F_0 = 1.74 \pm 0.50$) rather than at 500 mM (peak $\Delta F/F_0 = 1.57 \pm 0.37$). Additionally, when Glycerol was ramped down, ASH response dropped dramatically at 400 mM to almost no response (peak $\Delta F/F_0 = 0.04 \pm 0.04$), suggesting adaptation to the prior Glycerol stimulus. Behavior mimicked this interesting “relief” neural phenomenon, as animals showed much higher aversion during ramped-up Glycerol stimulation rather than ramped-down.

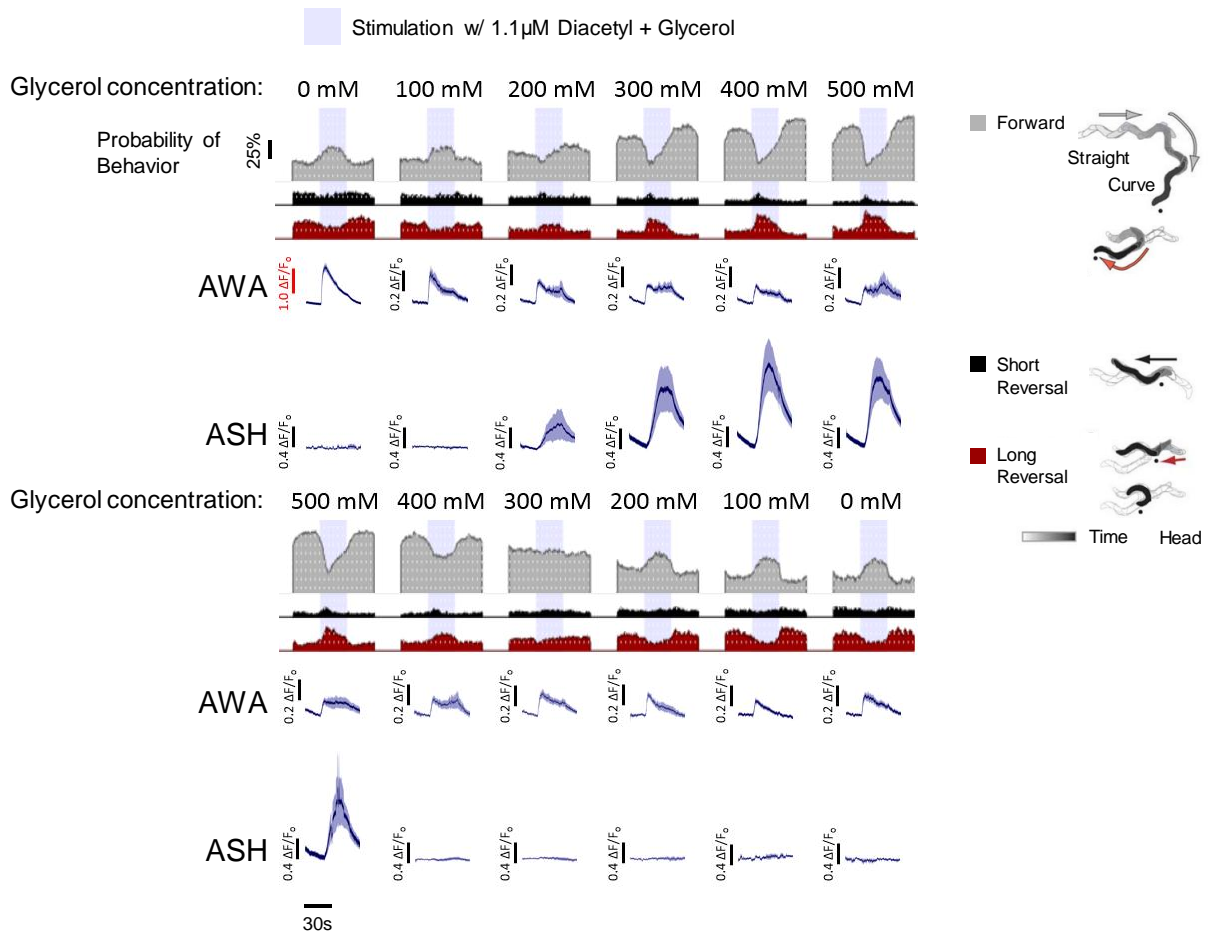


Figure 5. Plot summary of multi-stimulus assay for behavior and associated neural activity

Data summarized in two groups with up-ramping glycerol concentration on top, and down-ramping glycerol concentration on bottom. For each concentration of glycerol, the average 90 second profile from 3 pulses summarized with (from top to bottom): probability over time of forward motion, probability over time of short reversals, probability over time of long reversals, neural activity in AWA sensory neuron (shading represents \pm s.e.m.), neural activity in ASH sensory neuron (shading represents \pm s.e.m.). Stimulus applied in middle 30 s (from 30s-60s) and shaded in light blue. Horizontal white dashed lines represent 10% probability.

Behavioral schematic on the right side of the figure adapted by permission from Springer Nature Customer Service Centre GmbH: Albrecht DR and Bargmann CI. High-content behavioral analysis of *Caenorhabditis elegans* in precise spatiotemporal chemical environments. *Nature Methods* **8**(7):599-605 (2011). License Number 4725421152425

2.3: Tracking the lack of locomotion: Physiological relevance

2.3.1: Image segmentation techniques to track behavioral quiescence and translate quiescence to sleep states

In addition to tracking locomotion, there are many neurophysiological phenomena that results in a lack of locomotion. These include dwelling states associated with feeding (Flavell et al., 2013), paralysis by agents like tetramisole (Lewis et al., 1980), and behavioral quiescence associated with sleep (Raizen et al., 2008a). Tracking of the lack of motion often involves similar image segmentation techniques to those with motion, but major differences in metrics of importance.

Sleep assessment utilizes the machine vision tools developed for general behavioral assessment but focuses on recognizing quiescence, a behavioral feature of sleep. Centroid tracking (Van Buskirk and Sternberg, 2007) and frame subtraction (Raizen et al., 2008a) were the first image analysis methods used to quantify behavioral quiescence in *C. elegans* and more recently posture analysis (Nagy et al., 2014b) methods have been developed sensitive to characteristics of *C. elegans* quiescence for a more thorough approach. Each of these methods however have limitations preventing high-throughput assessment of *C. elegans* sleep. Frame subtraction is only applicable to single animals (Raizen et al., 2008a) at a time because of potential animal overlap between frames, centroid tracking alone is inefficient at capturing small movements or shape changes sensitive to quiescence (Nagy et al., 2014b), and posture analysis is computationally intensive limiting throughput to 3-5 animals per day (Nagy et al., 2014a).

To develop systems to characterize behavioral quiescence, we first need expectations of what will be observable during tracking. We used animals tagged with GCaMP in body wall muscles expressing the muscle-type specific myosin heavy chain isoform *myo-3* (Ardizzi and Epstein, 1987). This generates animals whose body wall muscles illuminate upon movement/activation, allowing us to track periods of high body wall activity and low activity. We observed that *myo-3:GCaMP* animals showed clear high activity during active movement, but much lower activity during bouts of behavioral quiescence (**Fig. 6a**). Tracking the highest 0.1% of pixels in the field of view, moments of activity and quiescence were easily distinguishable (**Fig. 6b**).

This demonstrated to us that behavioral quiescence was clearly quantifiable through observing periods of muscle relaxation, however, tracking quiescence in this manner would limit experimental throughput so we sought to replicate these quantifiable measures through less invasive techniques. In developing a system with the highest degree of per-animal accuracy, we chose to mimic frame-subtraction based algorithms previously described (Raizen et al., 2008a) due to their algorithmic simplicity and accuracy for total body motion. Centroid based methods are useful for larger populations especially when tracking many animals, but they present false quiescent scenarios when animals are moving but staying located in a single space, causing their centroid to not change even though their body is moving. This can happen when animals center their movement around a single circular post, which is accessible within the microfluidic arena environment. The first step of frame subtraction involves body segmentation (**Fig. 6c**),

where a binary image is created based on thresholding of the image to locate objects of the appropriate size to be a worm. The segmented animal can then be calculated for each frame (**Fig. 6d**) and consecutive frames are subtracted from one another resulting in another binary image where pixels that only belonged to one of the two images in question will be present (**Fig. 6e**). The absolute value of the subtracted frame-to-frame difference represents the moved pixels of the animals' body from frame to frame and can be normalized to represent a fraction of the body displaced (**Fig. 6f**). In the example shown, blue bars represent frames where $<1/8^{\text{th}}$ of the animals' body moved from the previous frame. An additional issue that becomes apparent is that to determine the functional state (such as sleep) and not just temporary behavioral quiescence. For tracking whether the animal is in a sleep state and not just temporarily pausing, an expert in the field would look for temporal clues as well, to suggest that the animal is relaxing into a quiescent state and remains quiescent for an elongated period. Thus, to come up with sleep assessment metrics we needed to optimize both movement, and temporal parameters to fit user expectations of sleep state.

We tracked an individual animal manually through 12 hours of locomotion, taking frames once every 10 seconds. For each frame multiple observers independently marked whether they thought the animal was awake or asleep, and data was compared to come up with a consensus sleep or wake determination based on the gold standard available of user observation. To optimize our sleep assessment parameters, we calculated for each frame how our computer vision techniques would score each frame based on the amount of movement (as a fraction of the body displaced) and the number of frames to

take a frame subtraction from. We found the optimal accuracy of sleep assessment to occur when less than 1/8th of the body was displaced, and 3 consecutive frames were considered for assessment (**Fig. 7a**).

With this sleep assessment system, we can now assess how genetic and environmental perturbations effect sleep in the microfluidic device with a completely automated analysis system. For example, a moderate 1.1 μ M Diacetyl concentration suppresses quiescence over 3 hours (**Fig. 7b**) compared to buffer alone, with animals consistently roaming the arena in search of the attractive bacterial byproduct odor. In translating this to sleep, animals showed significantly less sleep (**Fig. 7c**) in the presence of diacetyl ($0.2\% \pm 0.4\%$) compared to tests with only S. Basal buffer ($15.1\% \pm 6.6\%$, $*p < 0.01$, **Fig. 7d**).

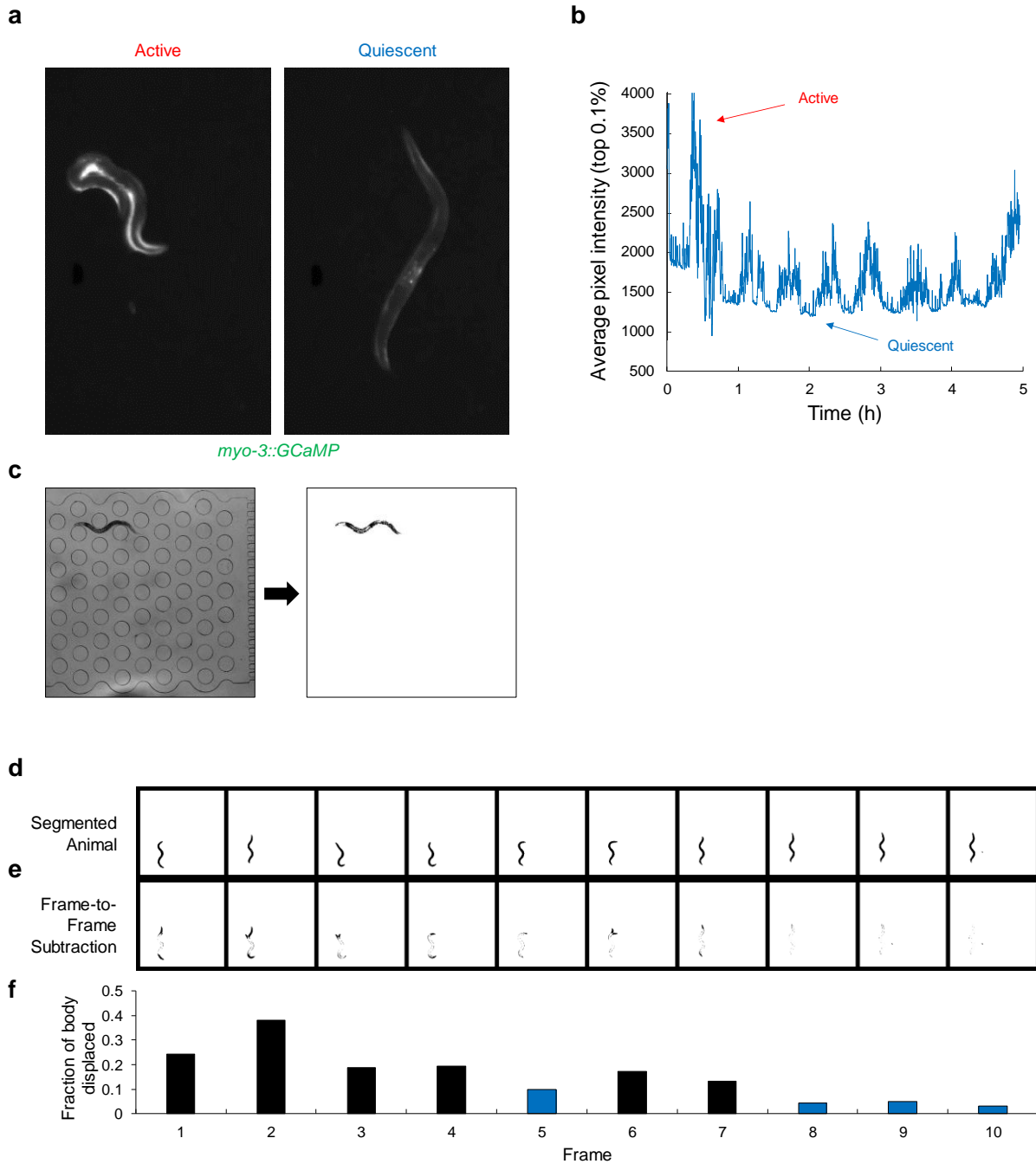


Figure 6. Tracking of behavioral quiescence at high magnification in a microfluidic device

(a) Images of an active and quiescent frames from an animal expressing GCaMP in body wall muscles under the *myo-3* promoter. (b) Plot of average pixel intensity of the top 0.1% of pixels in frames captured from a plotted over 5 hours. Periods of quiescence show low activity compared to periods of activity. (c) Image of animal in a microfluidic device before and after segmentation. (d) 10 segmented animal frames taken at 1 frame every 10 s. Binary image where dark pixels show animal body. (e) Frame-to-frame subtraction of consecutive frames from the above segmentation. Binary image where black pixels designate movement between frames. (f) Quantified displacement normalized to body size in 10 frames from d and e. Blue bars represent displacement less than $1/8^{\text{th}}$ of the animal's body size.

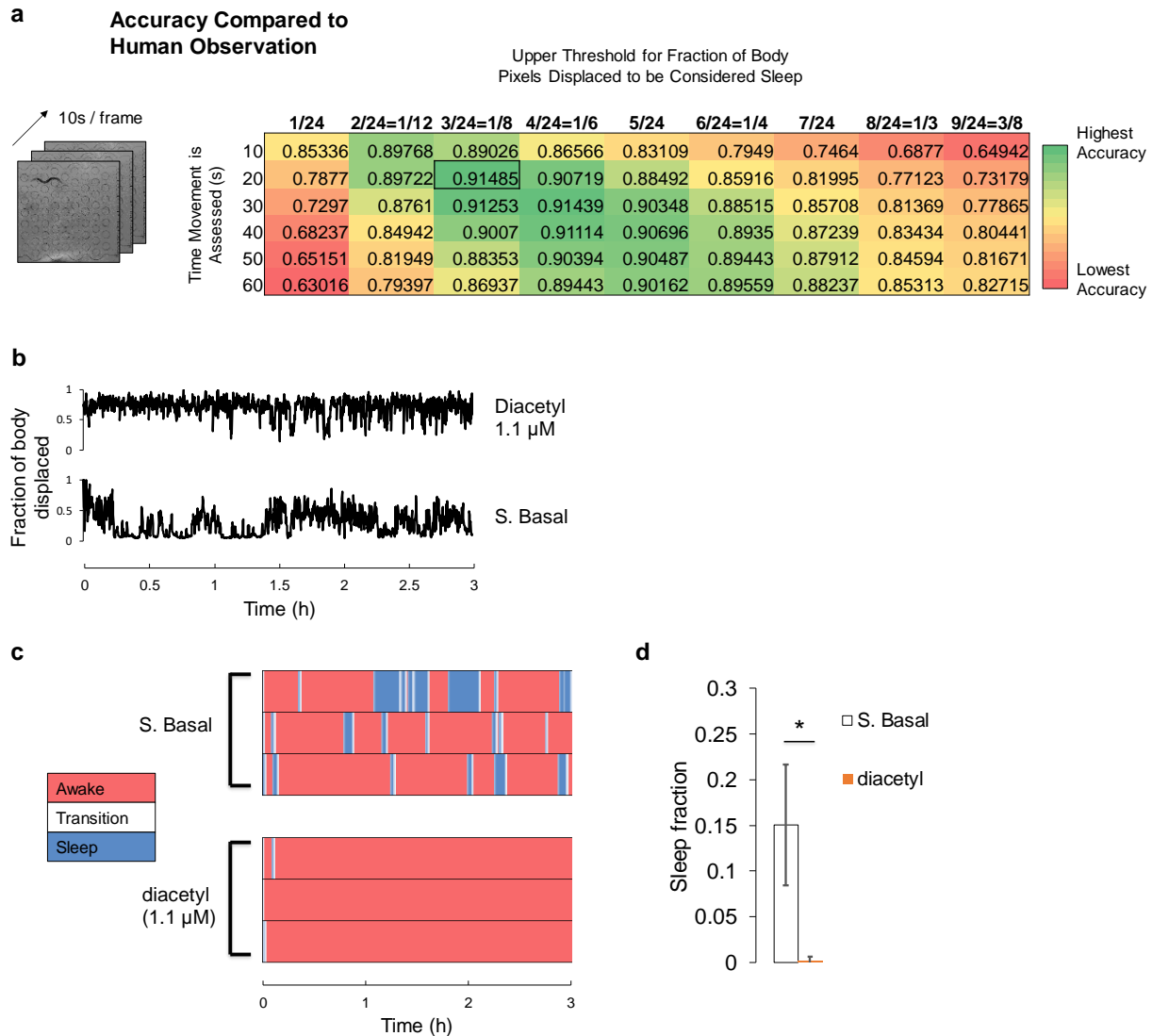


Figure 7. Translation of behavioral quiescence measurements to sleep metric

(a) Accuracy optimization table comparing gold standard of human observation to computer determined sleep states. 12 h of animal behavior taken at 1 frame every 10 s were classified by multiple observers to find a consensus sleep or awake state for each frame. Frame subtraction accuracy is assessed in the table with varying frames considered for frame subtraction algorithm, and movement index thresholds determined by the fraction of body size used as a cut off for movement designating sleep/wake. Green shows high accuracy, red shows low accuracy. (b) Movement index through fraction of body displaced frame-to-frame plotted for 1.1 μM Diacetyl and S. Basal buffer over 3 h experiment. Individual animal each per odor. (c) Classified sleep/awake states and transitions plotted over 3 h experiments with 1.1 μM Diacetyl and S. Basal buffer. (n=3 animals each condition). (d) Average sleep fraction for data in c. Statistics for d performed using an unpaired two-tailed t-test. *P<0.01. Error bars signify s.d.

2.3.2: Development of high-throughput viability assessment for drug-screening application in parasitic nematodes

Viability is a biological metric that requires assessment of the lack of animal locomotion, rather than assessment of locomotion style, similar to that of sleep. In some biological applications, the sought outcome is a lack of mobility, rather than a measurement of mobility type, such as in development of anthelmintic drugs. We applied a similar algorithm to tackle the issue of assessing parasitic nematode viability following drug treatment, with the goal of developing a high-throughput drug-screening platform for the discovery of anthelmintic drugs.

Nearly 1.5 billion people worldwide are infected with a species of soil transmitted nematode (STN) according to the World Health Organization (WHO). This includes roundworms such as *Ascaris lubricoides*, whipworms such as *Trichuris trichura*, and hookworms such as *Ancylostoma duodenale* and *Necator americanus*. Morbidity associated with heavier infection of STNs include malnutrition, anemia and cognitive and physical impairment (Crompton and Nesheim, 2002; Hotez et al., 2008). Anthelmintic drugs have been developed to treat these infections, however there is a rising emergence of drug resistance amongst these nematode populations (Boelaert and Consortium, 2016; Kaminsky et al., 2008; Penchovsky and Traykovska, 2015), thus there is a need for discovery of new alternative and effective drugs to treat infection diseases caused by parasitic nematodes. *C. elegans* are commonly used for anthelmintic drug discovery (Burns et al., 2015; Partridge et al., 2017; Weeks et al., 2016), however a lack of

homology with parasitic nematode species can often lead to variable drug effectiveness between species.

Phenotypic screening systems are most commonly used in drug discovery, but they can lack translational effectiveness in treating the target organism. Thus, methods used to test viability using animal models directly provide a translatable advantage in determining potential effectiveness of screening hits, however culture of STNs to adulthood require a mammalian host system, so drug screening platforms are difficult to develop. Thus, to test the effectiveness of potentially new anthelmintic drugs, we developed a screening method using adult parasites cultured from laboratory animals, but assayed in a high-throughput 384-well plate format. Using COPAS worm sorting technology, we were able to develop a protocol for sorting the adult stage of *H. poly* parasites into a 384-well format for parallel drug screening.

Once sorted in 384-well plates, animals are imaged using the UMASS WormIR system (**Fig. 8a**) to create continuous behavior videos across the entire 384-well plate (**Fig. 8b**). Because the source image comes from one center-mounted camera, and there are slight movement-artifacts, the initial images are auto-rotated and corrected using a simple image registration method (**Appendix 1**) to create stable wells to image. The visible center of the well is then isolated as it varies depending on the x-y position of the well on the 384-well plate (**Fig. 8c**) and all other pixels are ignored. Images are segmented and subsequently consecutive frames are subtracted across the entire video, creating a

fraction of body displaced in a binary image (**Fig. 8d**). The density of pixels displaced represents the amount of movement in the well, and can be scored frame by frame to determine what fraction of the video animals were moving over a given threshold (**Fig. 8e**).

To assess the method for accuracy, manual scoring was performed on each well, rating movement on a scale of 0 (no movement) to 3 (viable active movement). More difficult cases with only occasional movement (scored 1) or movement with non-regular pausing (scored 2) occur, and were also assessed in the algorithm. **Table 3** shows scoring averages for the fraction of moving wells classified based on our 384-well plate assessment algorithm with an optimized threshold of 3.5% movement to designate activity on a given frame. Animals were either treated with 100 μ M of the anthelmintic drug pyrantel, or given a comparable control solution of the solvent DMSO (0.5%).

A “Z-Factor” score is often used to characterize the effectiveness of a high-throughput screening assay (Zhang et al., 1999). Scores above 0.5 are considered excellent assays, as 0.5 would represent 12 standard deviations difference between sample means. Our algorithm does an excellent job in scoring the difference between viable and active animals when humans are also able to, registering a Z-factor score of 0.76, however the system is still not ideal for marginal cases, where animals show partial activity.

$$Z' = 1 - \frac{3(\sigma_p + \sigma_n)}{|\mu_p - \mu_n|}$$

Where μ_p and σ_p are the mean and standard deviation values of the positive control (or alternately, the treated samples) and μ_n and σ_n are those of the negative control (Bray et al., 2004).

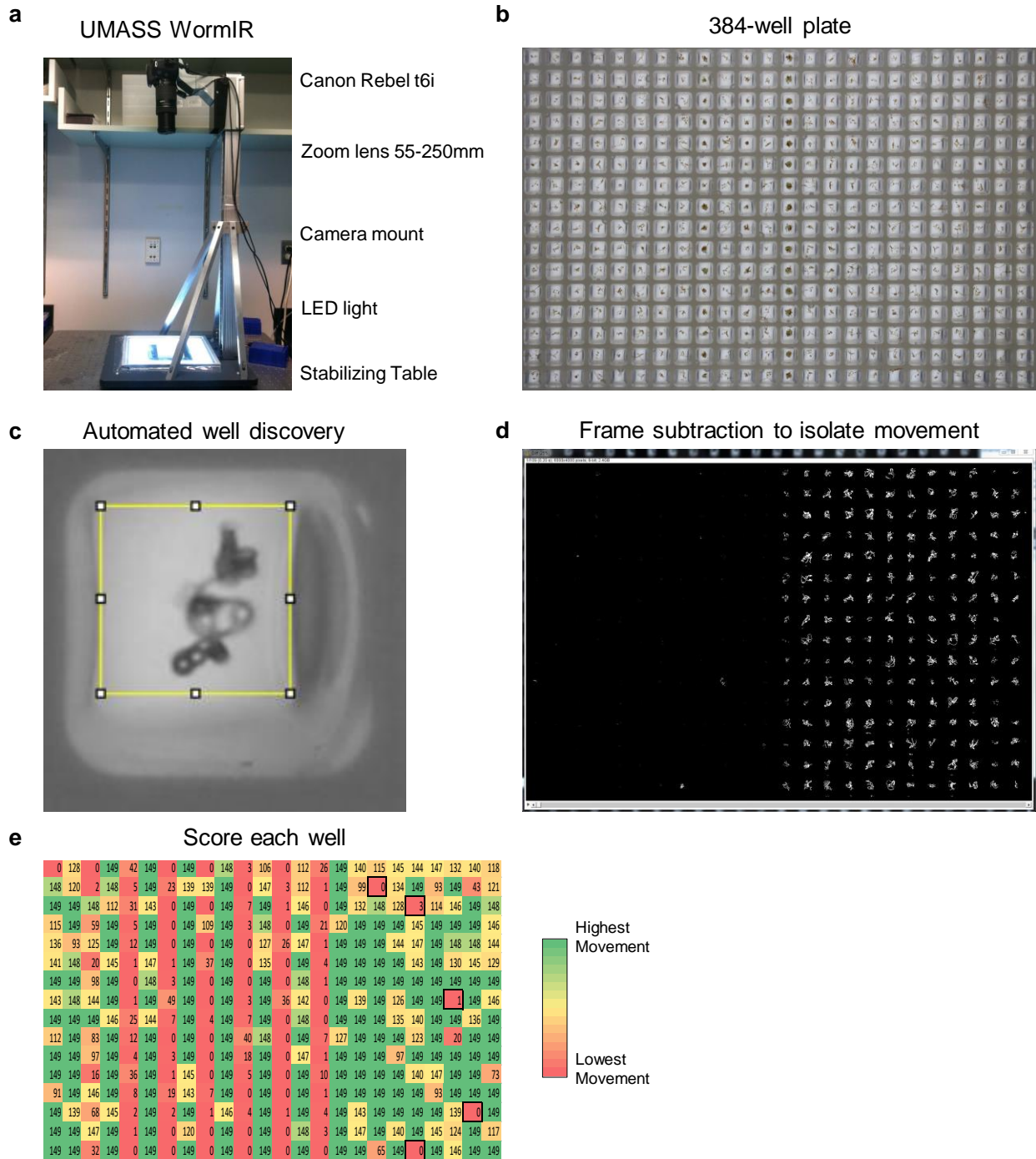


Figure 8. Automated viability 384-well plate screening assay

(a) Image of the UMass WormIR system developed by Mostafa Elfawal in the Aroian lab at UMass Medical School. (b) Birds eye view image of a loaded 384 well plate with *H. poly* animals in each well. (c) Mid-script well discovery image showing the automated outline of one well. (d) Segmented image of frame-to-frame movement within the 384-well plate automated assessment script. (e) Scoring of each of the 384 wells for the number of frames with suprathreshold movement scores. Red shows low movement while green shows high movement frames.

Table 3. Scoring of automated 384-well plate viability assessment

Scored group	Mean	SD	Z factor 3 to 0	Z Factor (3,2) to (1,0)	Z Factor treated to untreated
3	0.99	0.04	0.76	-0.03	-0.90
2	0.73	0.24			
1	0.18	0.16			
0	0.01	0.04			
3's and 2's	0.91	0.18			
1's and 0's	0.06	0.11			
Treated	0.08	0.19			
Untreated	0.84	0.29			

Discussion

In this chapter, we established microfluidic methods for tracking behavioral plasticity in the nematode *C. elegans* and demonstrated the broad impact of these tracking tools in development of a high-throughput viability assessment system in for drug treatment of the parasitic nematode *H. poly*. Standard chemotaxis assays have been used with *C. elegans* for decades (Bargmann and Horvitz, 1991; Tajima et al., 2001; Torayama et al., 2007; Ward, 1973) to establish behavioral patterns, linking observably simple behavior to more complex behavioral paradigms. There is a balance between simplicity and reproducibility however, because if systems to study behavior do not exhibit proper control the resulting findings lose credibility. Step-response type chemotaxis assays have been used in agar plate systems as well (Jansen et al., 2002; Miller et al., 2005), however it becomes very difficult to investigate true border effects due to diffusion of odorant through the agar and through the open air environment. If you were to imagine the immediate environment of any animal crawling on an agar dish, their nose is not going to be buried in the agar, rather rotating and moving above and around the liquid and air environment above the agar, constantly in flux. Steep changes in concentration can create a step-like response, but these step-like responses are inexact and difficult to replicate.

Instead of conforming this style of assay to the agar dish, adapting the assay to the microfluidic format opens the door to more precise and reliable odorant distribution. Flow within microfluidic devices are laminar, allowing loading channels to distribute different odorants without mixing in the device. This naturally creates odorant step presentation,

as seen in (**Fig. 2b**). When animals navigate within the pulse microfluidic assay they will find themselves encountering the pulse boarder at some point of the experiment, usually both giving an opportunity to enter or exit the stripe of odorant in the middle. Using centroid tracking we can identify where the head of each animal is at all times, allowing us to find every instance when the nose encounters one of the two odorant edges. This allows us to determine on average how animals behave at the odor edge, potentially identifying mutants who do not demonstrate likewise odorant decisions to their wildtype counterparts. Additionally, the stripe assay lends itself readily to chemotaxis assessment (**Fig. 2c**) although with interesting results. Data collected in our lab has suggested that animals tend to be curious about odors, often shifting chemotaxis towards odors they are traditionally considered averse to. In an example like NA22 *E. coli* it is clear and obvious that they have an unconditional attraction (**Fig. 2d**). In the assay shown, once an animal entered the stripe of food they almost always remained. In the first few minutes of the assay, animals did some exploration of the microfluidic environment, but quickly discover the odorant stripe of food and remain in the food for the duration of the experiment. Conversely, to a strong HCl stripe shown in (**Fig. 2e**) animals very readily exited the stripe, seeking the neutral environment of *S. Basal* in the outer flow environments. This was expected to be observed as well with a moderate AA stripe, but animals seemed fairly neutral to the aversive stimulus, making decisions to remain, enter, and exit the stripe in nearly even proportions. An interesting phenomenon, though it suggests chemotaxis assessment in the microfluidic device may be best studied using other formats such as the gradient device.

Gradient style microfluidic devices (**Fig 3a**) allow users to mimic the odor distribution most similarly seen in plate based chemotaxis assays (Ward, 1973). Animals show the expected tendency of climbing an attractive gradient and descending an aversive gradient while seeking the most suitable conditions present in their environment (Karen Tran, 2015; Larsch et al., 2015). It has been shown that intricate analysis methods can dissect the neural circuits involved gradient traversing animals (Larsch et al., 2015), however undoubtably experiential limitations of the method make assessment of neural plasticity more challenging. Translating the neural activity as animals climb or descend a gradient makes comparisons in subtle changes in plasticity much more difficult to assess. For that reason, pulsed based microfluidic assays are the preferred method for assessment of spontaneous neural activity. A number of device types have been fabricated to assess odor-evoked neural response including trips that trap the head of the animal, exposing the nose to chemosensory stimulants that can be flowed past (Chronis et al., 2007; Reilly et al., 2017), or arena style devices that allow for freely moving animals to be neurally imaged (Larsch et al., 2013). Translating chemotaxis behavior in larger population assessment devices in this system presents additional challenges though (**Fig. 4a**). With exposure to a temporal shift in odor, navigation can not be the behavioral assessment tool, so instantaneous behavior must be classified into aversive and attractive phenotypes. We demonstrated one instance of this in assessing animal preference to multiple conflicting stimuli (**Fig. 4e**), showing that starved animals are able to withstand more aversive stimulation if more attractive odorant cues are available. We also demonstrated how this system can be directly translated to neural imaging systems,

showing how neural activity in two sensory neurons, AWA and ASH, are modulated during this temporal odor multi-stimulus assay (**Fig. 5**).

While taxis is often the studied manifestation of behavior plasticity in *C. elegans*, the simple model organism also demonstrates several important behavioral markers that do not involve specific study of movement, but rather the measure of inactivity. Animals will exhibit periods of behavioral quiescence either momentarily when making decisions, when they want to remain situated to feed or probe their surrounding area, when they cannot move due to paralytics, or in sleep-like behavior that researchers have established as having connections to sleep in higher level organisms (Trojanowski and Raizen, 2015). We showed how sleep-like states can be more readily identified with computationally simple image segmentation techniques, that avoid potential pitfalls of centroid tracking or more complex behavioral analysis methods (**Fig 6,7**). Establishment of behavioral quiescence metrics allow for more thorough investigation of the timing, regulation, and modulation of sleep behavior and eventually through associated neural activity.

Additionally, behavioral quiescence presents itself through measurements of vitality. While *C. elegans* are commonly used as a platform to assess development of anthelmintic drugs, they lack homology with many parasitic nematodes reducing the efficacy of drug discovery. With collaboration formed with Mostafa Elfawal from the Aroian lab, we developed a high-throughput drug screening platform for parasitic nematodes using 384-well plates. To assess vitality of *H. poly* parasitic nematodes, I used similar image

segmentation techniques that assess sleep behavior in *C. elegans* and showed how this system can be used to monitor the vitality as parasitic nematodes are screened for drugs that can cause lethality.

Altogether, these methods provide the tools to assess *C. elegans* behavior necessary for developing high-throughput tools to assess how nematodes like *C. elegans* behave, allowing us to make direct connections to behavioral paradigms that are implicated in neurological disease. This chapter represents the basis of how measurements in all subsequent chapters in this thesis are defined.

Methods and Materials

Strains and *C. elegans* culture

All *C. elegans* strains were maintained under standard conditions on NGM plates and fed OP50 *E. coli* bacteria seeded onto each plate. Wild-type animals were Bristol strain (N2). Neural imaging strains expressing GCaMP in specific neurons were: (ASH (Larsch et al., 2013)) **CX10979**, *kyEx2865* [*Psra-6::GCaMP3*; *Pofm-1p::GFP*]; (AWA (Larsch et al., 2013)) **CX14887**, *kyls598* [*Pgpa-6::GCaMP2.2b* 50 ng/ μ L, *unc-122p::dsRed*] expressing GCaMP integrated in AWA neurons. An imaging strain expressing GCaMP in body wall muscles was: (*myo-3*) **AQ2953**, *ljls131* [*Pmyo-3::GCaMP3-URSL-RFP*]. To synchronize for age, we picked L4 larval stage animals one day prior to experimentation such that all animals tested were at the young adult stage.

To prepare for an experiment, animals were isolated by genotype and/or arena placement and then transferred to an unseeded NGM plate immediately prior to experimentation. The plates were then flooded with S. Basal buffer (100 mM NaCl, 50 mM KPO₄; pH 6.0) prior to their experiment. Animals were then collected into loading tubing using a 1 mL syringe prior to injection into the microfluidic arena.

Microfluidic device fabrication

All microfluidic devices were fabricated as previously described (Lagoy and Albrecht, 2015). Briefly, transparency photomasks were printed at 25,000 dpi from designs sketched using DraftSight CAD software. SU-8 mold masters were prepared on silicon wafers using standard photolithography techniques, and microfluidic devices were fabricated by pouring degassed PDMS (Sylgard 184, Dow Corning) onto the mold and

heat curing. Individual devices were then cut out and punched to provide inlet and outlet flow. A hydrophobic glass substrate was created by vapor deposition of tridecafluoro-1,1,2,2-tetrahydrooctyl trichlorosilane (TFOCS, Gelest) and then sealed reversibly to the microfluidic channels. An upper glass slide, with holes drilled over inlet and outlet ports with a diamond-coated drill bit, was sealed above the device, which was then placed into a metal clamp.

Microfluidic stimulus preparation

All odor dilutions were freshly prepared on the day of experimentation. NA22 *E. coli* stock solutions were prepared using previously described methods (Keil et al., 2017). Briefly, NA22 *E. coli* was cultured, concentrated into pellet form, and suspended in S. medium buffer. A stock solution was diluted to an OD600 of 7.0, and 50 µg/ml of kanamycin was added to prevent bacteria from growing. Chemical solutions were prepared at a 1:20 dilution of stock solution and filtered through a 5 µm filter. Hydrochloric acid (HCl) and Acetic acid (AA) solutions were prepared by slowly titrating stock solution into a stirring beaker of S. Basal while a pH meter was submerged in the solution. Samples were removed at the respective 2.5 and 4.0 pH readings. Glycerol (Sigma) was dissolved to a 1M stock solution in S. Basal, and diluted to the appropriate concentration for the multi-stimulus assay. Diacetyl (1.1 µM) was prepared from a 10⁻³ dilution (11 mM) stock solution immediately prior to experimentation. Visualization of the stripe, gradient, and pulse was aided using xylene cyanol 1X dye.

Microfluidic device setup

Microfluidic devices were cleaned, assembled, and degassed in a vacuum desiccator for 30–60 min prior to experimentation. Degassing devices accelerates the absorption of air bubbles within the device. For behavioral experiments, devices were filled with 5% (w/v) Pluronic F127 through the outlet port to prevent bacterial and molecular absorption by passivation of the microfluidic surfaces and to minimize bubble entrapment via its surfactant properties. Neural imaging devices used for behavioral quiescence measurements were filled with control buffer alone. Reservoirs of loading solutions were prepared as previously described (Lagoy and Albrecht, 2015), purging the reservoir system of bubbles and connecting the tubing into the inlets of the device. Once flow was properly established, animals were gently loaded into their respective arenas and allowed to roam for 15–20 min prior to experimentation. For neural imaging experiments, a control valve is used to switch between stimulus and control buffer conditions within 0.5 s.

Loading and experimentation with the Hamilton MVP Valve

The Hamilton MVP (Modular Valve Positioner) Valve comes equipped with a chemically inert Polytetrafluoroethylene (PTFE) flow path and rotational valve allowing for 8-valve tubing connections to be automatically controlled to be dispensed from one outlet. For experimentation purposes, one valve is dedicated to a buffer syringe for purging the line with S. Basal. The remaining 7 connections were used to load a series of stimulus conditions. Each of the 7 solutions is prepared in a 2 mL Eppendorf tube, and the top is perforated such that rigid tubing can be inserted and held in place. The purge valve is

used to create a reverse pressure to fill the tubing from the Eppendorf tube, loading the MVP valve for fast switching. The MVP valve interfaces directly with custom MATLAB software which controls the waste and control valves through the ValveLink 8.2 (AutoMate Scientific) controller as well as the MVP valve position. After switching, fluid takes about 30 s to reach the tip of the single outlet to the MVP valve, so valve positioning occurs a minute prior to stimulation.

Animal tracking systems

Videos of behavior in stripe and pulse assays were captured using a 6.6 MP PixelLink FireWire Camera at 2 fps for 1 h with an image resolution of ~30 pixels/mm. Videos were processed after experimentation as previously described using MATLAB to extract behavioral data (Albrecht and Bargmann, 2011). Behavioral quiescence (sleep) videos were acquired at 5x magnification (NA=0.25) with a Hamamatsu Orca-Flash 4.0 sCMOS camera using MicroManager/ImageJ software. The system has a Lumencor SOLA-LE solid-state lamp pulsed to excite GCaMP during fluorescence calcium imaging and to record the natural autofluorescence of *C. elegans* for tracking body movement as well. To achieve autonomous experimentation, custom Arduino and MicroManager scripts work together to control illumination timing and image acquisition. An Arduino Uno microcontroller was programmed to control fluidic valves through a ValveLink 8.2 (AutoMate Scientific) controller. A MicroManager script allows the user to configure all camera and illumination settings prior to experimentation.

A custom ImageJ script was written for image segmentation and movement index calculations in behavioral quiescence measurements post-acquisition. Briefly, the image

is cropped and then a binary mask is created using thresholding to find the animal body. Objects of the appropriate pixel size for a single young adult are segmented, and consecutive frames are subtracted. The resulting binary image is calculated and the fraction of body displaced is calculated based on the original animal segmentation size.

Culture of *H. poly* using mice

H. poly parasites were maintained in Swiss Webster mice following standard protocols (Johnston et al., 2015). Briefly, 5 weeks old mice (both genders) were infected with 600 infective third stage larvae. To harvest adult parasites, infected animals were sacrificed to collect small intestines where adults reside. Longitudinally open intestines were incubated for two hours in Hanks buffer in a tea strainer over a collecting beaker, allowing worms to detach from the intestinal tissues and migrate through the strainer to be collected at the bottom of the beaker and form a ball of tangled worms. Tangled worms were picked with worm picker and transferred into a petri dish containing Culture Medium (RPMI1640, 100U penicillin, 100ug/ml streptomycin, 10ug/ml amphotericin) and incubated overnight at 37°C and 5% CO₂ to allow worms to untangle before sorting.

Sorting and loading of *H. poly* into 384-well plates

Plates containing singled worms were removed from the incubation and allow them to cool down to room temperature and form tight spring like shape (**Fig. 9**). Worms were transferred into the sample cup of the COPAS bio sorter. Using the manufacturer protocols, two worms were sorted into each well of the 384-plate format in 25 µL of culture medium (RPMI1640, 100U penicillin, 100ug/ml streptomycin, 10ug/ml amphotericin).

Sorted plates were incubated over night at 37°C and 5% CO₂ to allow worms to rest after sorting. The next day sorted plates were subjected to manual sorting correction, where dead worms due to sorting condition were removed using a worm picker and replaced with healthy and motile worms. Also, wells with single worms were enriched by adding a second worms and wells with > two worms were corrected by removing all worms and replacing them with two healthy worms. Using epMotion liquid handler another 25µL of culture medium were added to give a final assay volume of 50µL. Selected wells were treated with pyrantel dissolved in DMSO giving a final concentration of 100 µM and 0.5% DMSO. Negative control was also included (0.5% DMSO). Assay plates were incubated for 48 hours at 37°C and 5% CO₂. Due to unknown reasons some healthy worms form into a tight spring-like shape with very low motility making it harder to differentiate between healthy silent worm and dead or intoxicated worms. To address such issue, parasites were stimulated with ~1 µL of 20% sodium hypochlorite, using a 384-pin replicator that allows worms to be stimulated in all wells at same time. Such stimulation induces vigorous motility in living worms, but not in dead or intoxicated ones, allowing for clear determination of animal viability pre-assay. This stimulation is terminal however, but animals last for at least 10 min, long enough to take images of the entire plate for 1 min.

UMASS WormIR tracking

UMASS WormIR was developed by Mostafa Elfawal to allow imaging all wells in the 38- well plate at single still images. The system is composed of Canon Rebel T6i camera with 55-250 mM zoom lens, mounted on sturdy camera mount fixed to wide base housing LED light source that located on the top of an air stabilizing table. Assay plates

were placed in gated chamber above the LED light allowing the camera to automatically take 120 still images at 2 fps. Using ImageJ, the still images were stitched together to generate 1 min long videos for analysis.

384-well plate movement tracking

Detailed ImageJ script and walkthrough included in **Appendix 1**.

Statistical analysis

Statistics were performed using one-way ANOVA with Bonferroni's correction for multiple comparisons or an unpaired two-tailed t-test when specified for 2 sample comparison, using the Statistics and Machine Learning Toolbox in MATLAB. Data represented as mean \pm s.e.m. or mean \pm s.d. and are consistent for each experiment. For accuracy assessment, accuracy was determined by the fraction of correct sleep and wake decisions divided by the total number of consensus sleep/wake observations. In neural recordings, the top and bottom 1% of instantaneous fluorescent intensity was removed to reduce noise in peak fluorescence calculations.

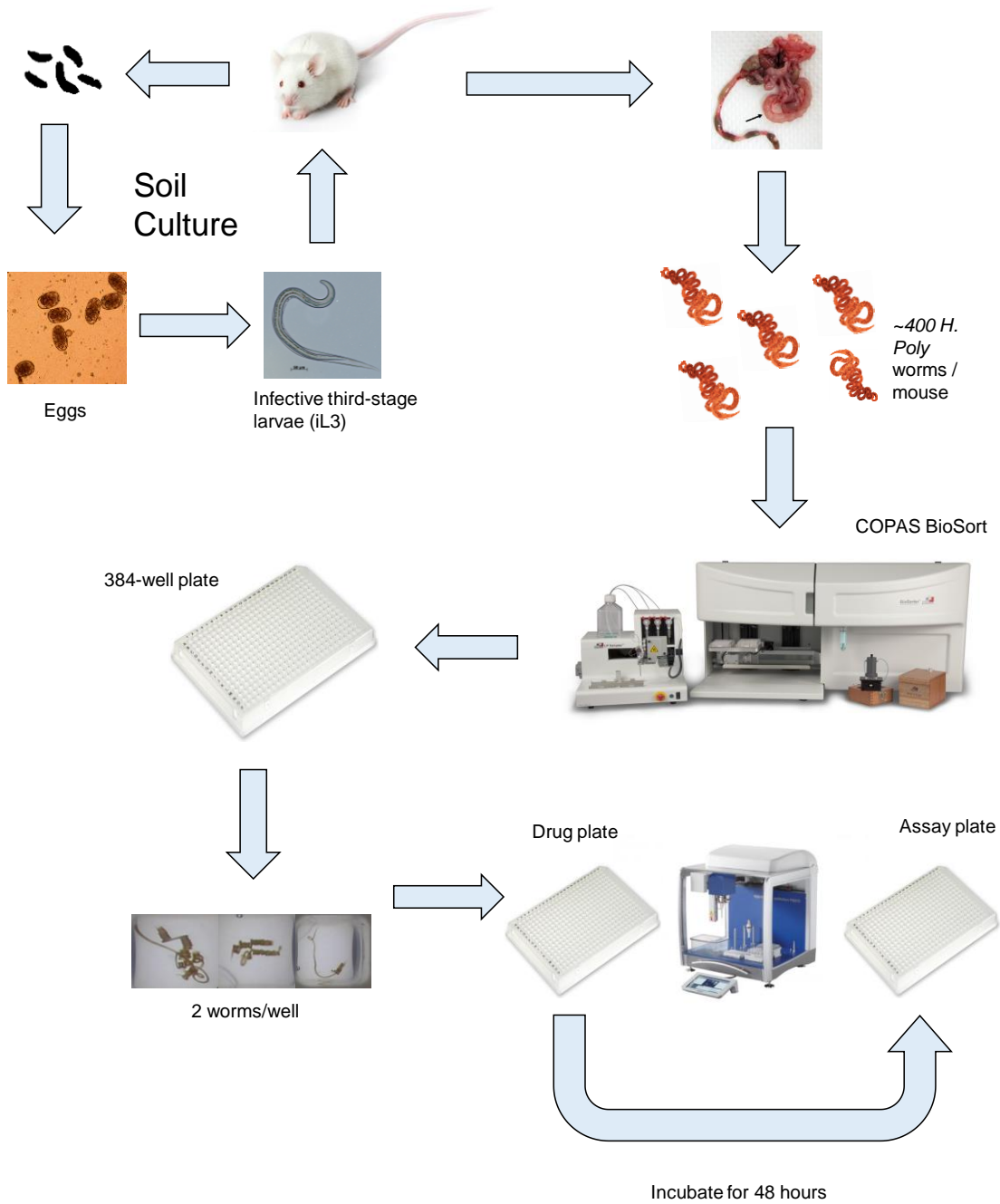


Figure 9. Schematic of *H. poly* culture and test prep

Schematic shows a step-by-step process of cultivation, culture, sorting, and drug screen preparation. Image adapted from Mostafa Elfawal.

Chapter 3: Sleep in adult *C. elegans*

The initial development of the upcoming systems to study sleep in adult *C. elegans* began during the summer of 2015 with help from Allison Marley, an undergraduate student participating in the Research Exchange for Undergraduates (REU) program here at WPI. A collaboration was formed with Dr. William Schafer's lab at the MRC Laboratory of Molecular Biology, and I worked alongside a Post-Doc Dr. Yee Lian Chew in Dr. Schafer's lab. Dr. Chew provided and developed many of the mutant animals tested in this chapter. This work was supported in part by an NSF IGERT award (DGE 1144804) and by the Burroughs Wellcome Fund Career Award at the Scientific Interface, and the National Science Foundation NSF CBET 1605679 and EF 1724026, NIH R01DC016058.

Abstract

Using fundamental behavioral characteristics observed across species, researchers in recent years have established periods of behavioral quiescence observed in the model organism *C. elegans* as true sleep states. Primarily, study of sleep in *C. elegans* has focused on behavioral quiescence observed during lethargus known as developmentally timed sleep (DTS) and quiescence observed after exposure to stressors termed stress induced sleep (SIS). We have observed that young adult *C. elegans* exhibit similar behaviorally quiescent periods in microfluidic devices free of induced stressors, providing a flexible platform for assessment of how genetics and stimulants can affect sleep behavior in *C. elegans*. We assessed the effects of blue light, presence and collision with other animals, melatonin, sensory stimulants, and arousal and sensory deficient mutations on sleep. We found that aversive blue light led to decreased sleep, while the presence of multiple animals had no effect on sleep rates. Young adult animals were observed to have an increased arousal threshold however sensory responses were reliable regardless of sleep state. A putative melatonin receptor knockout led to increased sleep that was recovered with re-expression under an endogenous promoter. Additionally, we observed that arousal deficient mutants exhibited less sleep during adults, providing possible links between sleep and arousal in *C. elegans*.

Introduction

C. elegans have been shown to demonstrate states of quiescence during lethargus (Raizen et al., 2008a), periods of high stress (Hill et al., 2014), and satiety (Gallagher and You, 2014) that have been shown to share fundamental characteristics with sleep in other species (Singh et al., 2013). These quiescent states have been shown to share human sleep functions such as synaptic plasticity (Dabbish and Raizen, 2011) and metabolic control (Driver et al., 2013). Additionally, these states demonstrate behavioral characteristics of sleep such as rapid reversibility (Raizen et al., 2008a; Trojanowski et al., 2015), increased arousal threshold (Cho and Sternberg, 2014; Raizen et al., 2008a), stereotypical posture (Iwanir et al., 2013; Schwarz et al., 2012; Tramm et al., 2014), and homeostatic response to sleep deprivation (Driver et al., 2013; Nagy et al., 2014a; Raizen et al., 2008a). With the plethora of similarities of this state to sleep in other organisms, the field has made a push to define this quiescent state as simply “sleep” (Trojanowski and Raizen, 2015). Preliminary data shown in **Chapter 2** demonstrates that young adult *C. elegans* exhibit bouts of behavioral quiescence when contained in microfluidic devices in S. Basal devoid of other chemical stimulus that share similarities with other sleep-like states in *C. elegans*.

C. elegans is an organism capable of high-throughput behavioral analysis (Albrecht and Bargmann, 2011; Cronin et al., 2005; Dusenbery, 1985; Husson, 2012; Moy et al., 2015; Ramot et al., 2008) however methods to quantify sleep (Nagy et al., 2014b; Raizen et al., 2008a; Van Buskirk and Sternberg, 2007) in *C. elegans* have yet to be developed to the same standards. Because studies of *C. elegans* sleep to this point have focused on

Developmentally Timed Sleep (DTS) and Stress Induced Sleep (SIS) to define mechanisms involved in sleep in *C. elegans* (Trojanowski et al., 2015), these definitions yield limitations in translation to higher level organisms. DTS only occurs during the molting periods between larval stages in development and does not occur during adulthood of *C. elegans*, limiting when assessment of sleep can occur. Molecular conservation of sleep regulation has been shown in multiple cases with both DTS and SIS (Trojanowski and Raizen, 2015). Links have been made to the rhythm of DTS being regulated by homologous timing genes (Monsalve et al., 2011), however their rhythms are not circadian. Epidermal growth factor signaling, which has been shown to regulate sleep in humans (Kramer et al., 2001), also has been shown to promote SIS in *C. elegans* (Van Buskirk and Sternberg, 2007). SIS has been shown using highly aversive stimuli, however, these stimuli often produce a behavioral response that will interfere with behavior generally associated with sleep and the modeling of human sleep disorders. Satiety also leads to sleep; however, it also is coupled with a specific behavioral response, limiting its association as a general sleep model.

Studying spontaneous adult sleep in the microfluidic environment allows us to assess a wide array of genetic and chemical perturbations without changing the core sleep assessment principals. Additionally, the ability to use young adult *C. elegans* to study sleep will yield more significant behavioral data because the animal has reached full cellular and neurological development, providing for a more translatable model to study behavioral and neural plasticity associated with sleep that may apply to humans. Irregularities in sleep that are associated with sleep disorders can involve either a

behavioral or sensory phenotype or both, thus in this Chapter we sought to assess two systems to measure how stimulation can affect *C. elegans* behavior and neural activity associated with sleep. To do so, we utilize microfluidic devices designed to facilitate the natural sinusoidal crawling motion of *C. elegans*, while also providing a structure for rapid chemical stimulation (Albrecht and Bargmann, 2011). Smaller versions of this device mimic the same basic design, but also allow for the animal to be contained in a field-of-view suitable for calcium imaging to assess neural activity spontaneously and from sensory-evoked response (Larsch et al., 2013).

We expect to be able to demonstrate use of the automated sleep assessment system by using the system to assess relevant genetic and biological factors implicated in sleep. We are interested in assessing how neuromodulators affect sleep in young adult *C. elegans*. Neuromodulators allow for an additional neural signaling mechanism separate from neural connections, and is a slower mechanism of action (Bentley et al., 2016). This will include studying the mammalian sleep implicated hormone melatonin, and mutants shown previously by others to have altered arousal due to neuropeptide abnormalities. Candidate mutants showing abnormalities in adult sleep were further studied by attempting to rescue genetic abnormalities under endogenous promoters, with the expectation that if the genetic effects caused sleep abnormalities, rescuing them endogenously will return sleep to wildtype levels.

Results

3.1: What factors influence adult *C. elegans* sleep?

3.1.1: Blue light disturbs adult C. elegans sleep

We measured the impact of light stimuli on sleep by assessing how a blue light illumination source, used for fluorescent imaging in imaging neural activity, affected sleep compared to a green light with brightfield illumination (**Fig. 10a**). As strong blue light can cause arousal by itself (Edwards et al., 2008), we hypothesized that assessment of neural activity in sleep would have to use a system with minimal blue light exposure. When using just blue light for illumination, animals exhibited a significantly lower sleep fraction (55% in green light vs. 25% in blue light, $**p < 0.001$, **Fig. 10b**). The higher sleep fraction was observed for the duration of the experiment after hour 1 (**Fig. 10c**).

3.1.2: Presence of multiple animals, increased flow velocity, and increased arena size do not disturb C. elegans sleep

In order to scale up sleep assessment to larger microfluidic devices, we had to ensure that interaction with other animals and the larger environment of a Population behavior microfluidic device would not impact the frequency or style of sleep we observed. Additionally, due to differing geometries, the two devices have very different velocity flow rates, with the smaller Neural imaging device (**Fig. 11a**) operating around ~15 mm/s flow which is thirty times faster than the ~0.5 mm/s flow seen in Population behavior devices (**Fig. 11b**). The two devices also have very different arena sizes (**Fig. 11c**) with a single arena in the Population behavior device occupying 16 mm x 15 mm as opposed to the 3

mm x 3 mm arena of the Neural imaging device. Despite this, the two arenas share micropost spacing, so the immediate PDMS environment for the animals will be very similar.

To track sleep behavior in the Population behavior devices frame subtraction methods detailed in **Chapter 2** cannot be used. Instead, the base behavioral profiles of each animal in the device were calculated using Arena Worm Tracker software (Albrecht and Bargmann, 2011) which uses centroid tracking and body morphology assessment to determine speed and behavioral type frame by frame. Behaviors are classified by Forward motion, Short Reversals, Pauses, and Omega turns. For the purpose of sleep tracking, pauses become the relevant behavior to track, as by nature they are defined by a subthreshold centroid movement. Similar to sleep assessment detailed in **Chapter 2**, true sleep has a temporal factor as well to distinguish short pauses from longer behavioral quiescent bouts that are characteristic of sleep. Because of this, we developed a post-processing sleep assessment algorithm to determine sleep patterns. Individuals are tracked separately (**Fig. 11d**), allowing us to determine variability between individuals, find outliers, and determine if there are any abnormal sleep profiles. We found that individuals in Neural imaging devices show very similar sleep profiles on average to those in Population behavior devices (**Fig. 11e**), making the two methods cohesive towards understanding the behavioral and neural information underlying sleep and sleep disorder. These factors are discussed in more detail on this method will be discussed in depth in **Chapter 4**.

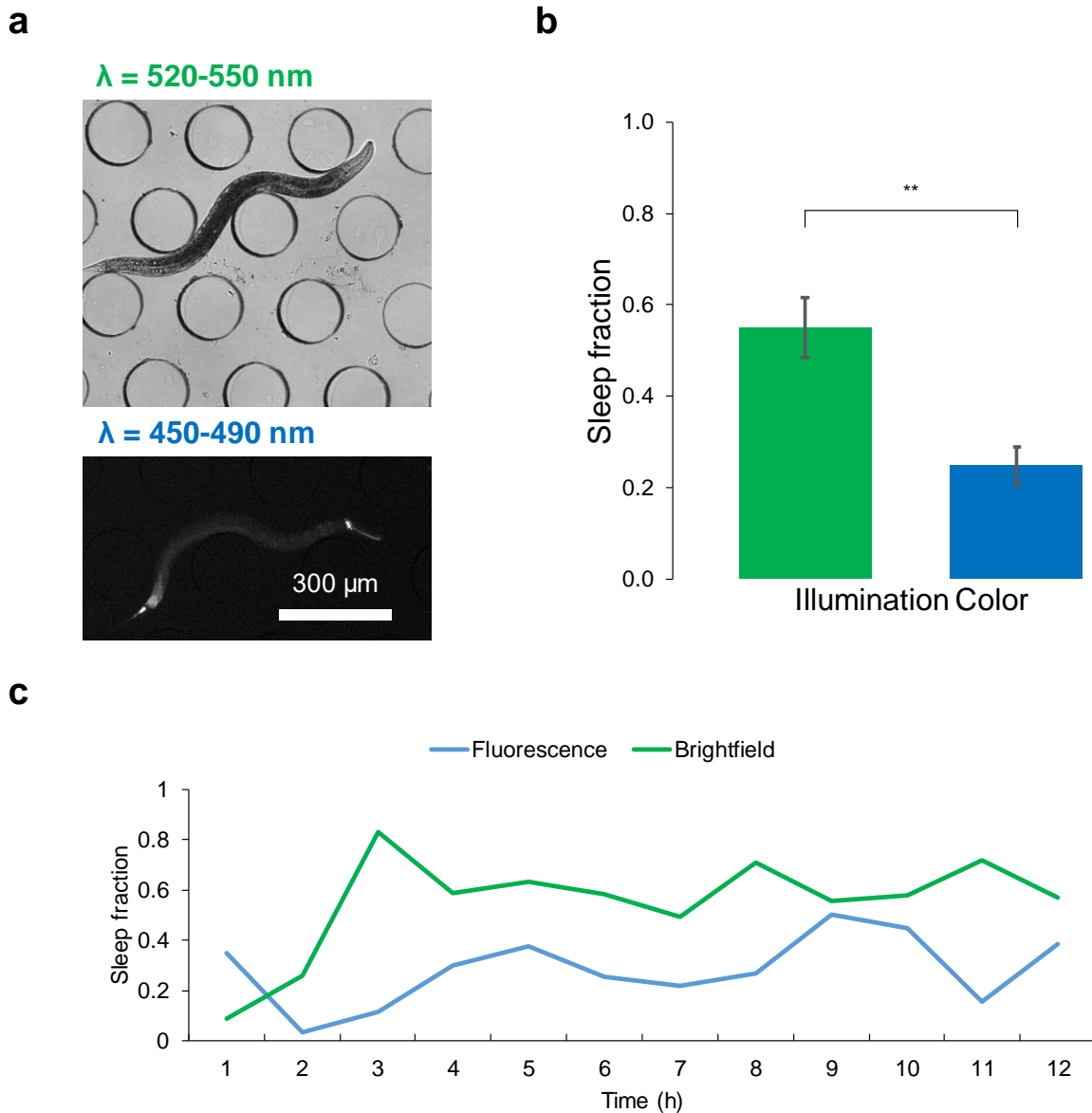


Figure 10. Illumination style impacts sleep behavior

(a) Image of *C. elegans* using brightfield illumination (top) and fluorescent illumination (bottom) in the microfluidic arena. (b) Sleep fraction over 12 h plotted by illumination color (green brightfield, blue fluorescent) ($n=2$ (green), $n=3$ (blue)). (c) Hourly sleep fraction of data from b. Statistics for b performed using an unpaired two-tailed t-test. $**p<0.001$. Error bars signify s.d.

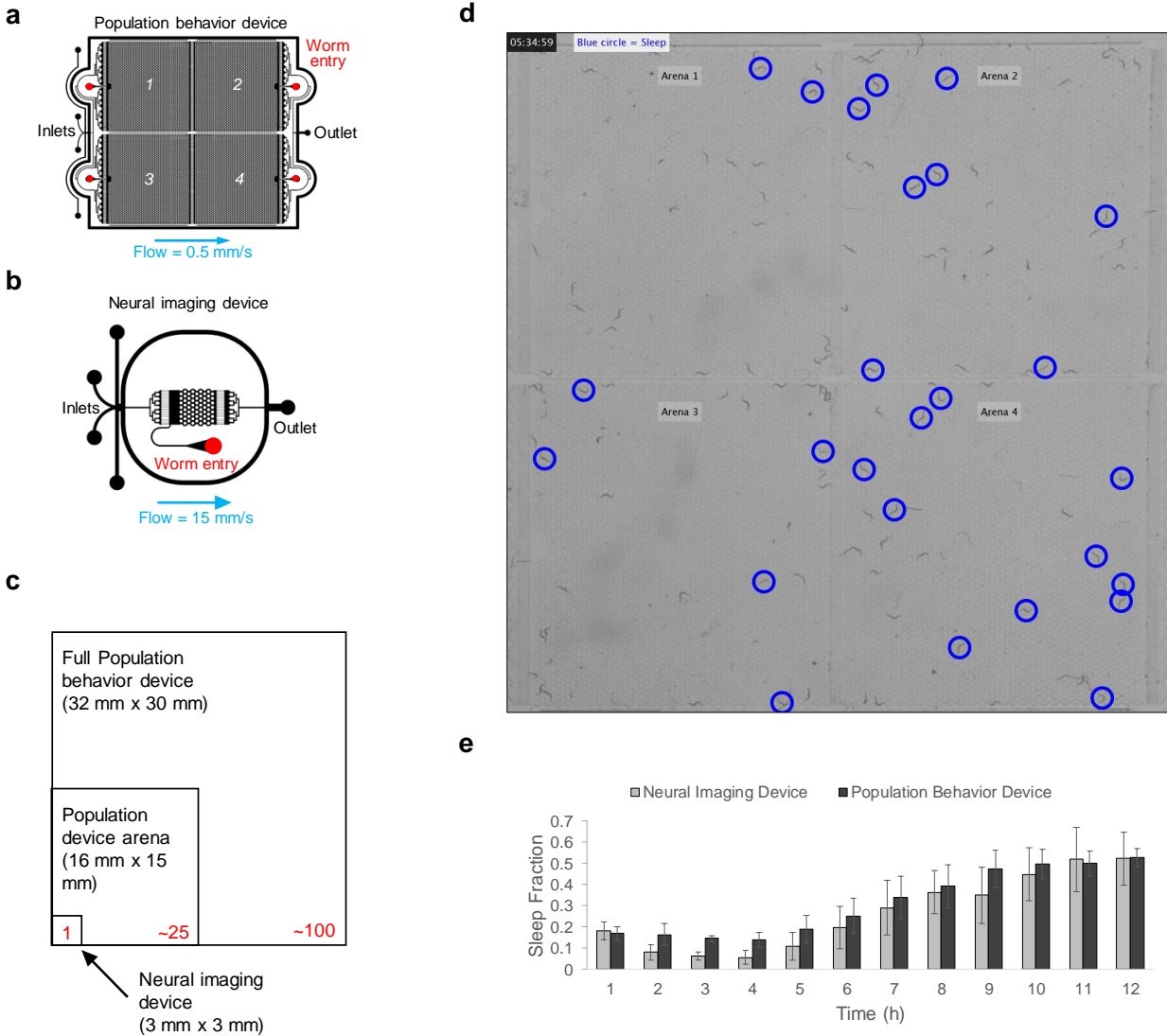


Figure 11. Adult *C. elegans* exhibit similar sleep patterns when isolated or in large microfluidic devices in the presence of other animals

(a) Device design of Population behavior devices. (b) Device design of Neural imaging device. (c) Size comparison between full Population behavior device, single arena of Population behavior device, and Neural imaging device. Ratio of x and y dimensions are accurate between device styles. (d) Snapshot of multi-worm sleep tracking script identifying sleep bouts in Population behavior device. Animals currently in a sleep bout circled in blue. (e) Sleep fraction by hour in Population behavior device vs. Neural imaging device (n = ~100 animals in population behavior device, 7 animals in Neural imaging device). Error bars represent s.e.m.

3.1.3: Exogenous melatonin does not increase sleep behavior in adult *C. elegans*

Next, we looked at how neuromodulators can affect sleep in adult *C. elegans*. The first of which is the neurohormone melatonin. Melatonin is a neural hormone which has been shown to regulate circadian rhythms in mammals (Ganguly et al., 2014). Melatonin is released during darkness, usually at night, which aids animals in assessing day from night during changing seasons. The function of melatonin depends on species, and its role in sleep in *C. elegans* has yet to be determined. Exogenous melatonin however has been demonstrated to cause locomotory slowing in *C. elegans* (Tanaka et al., 2007). We observed the same trend in our microfluidic format during a 15 minute exposure assay (**Fig. 12a**). We tested animals' speed with either 1 μ M Melatonin or a 0.001% ethanol solvent control. Overall average speeds over the 15 minute assay were not significantly different ($p > 0.05$), however speeds in melatonin trended towards being slower than in ethanol control. We also assessed how melatonin exposure would affect later sleep behavior. We found that animals exposed to 1 μ M melatonin for 30 minutes (**Fig. 12c**) showed significantly ($*p < 0.05$) lower sleep fraction over the following 12 hours ($10.9\% \pm 0.7\%$ S.E.M.) than animals exposed to a control solution of 0.001% ethanol ($14.1\% \pm 0.8\%$ S.E.M.) used to dissolve the melatonin (**Fig. 12b**).

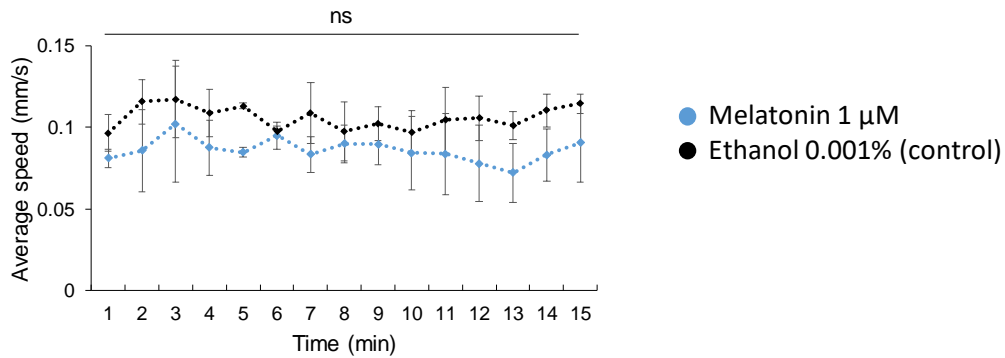
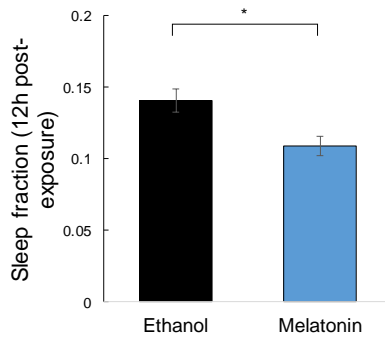
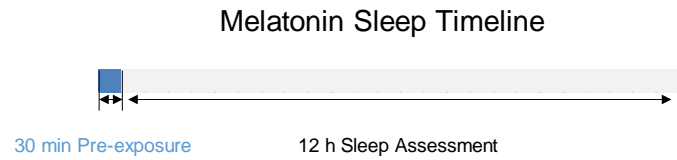
a**b****c**

Figure 12. Melatonin does not increase sleep behavior in adult *C. elegans*

(a) Average speed (mm/s) per minute in 15 minute assay with 1 μ M Melatonin vs. a 0.001% control solution of ethanol. (n = ~100 animals per condition). Statistically insignificant over 15 minute assay. (b) Average 12 h sleep fraction post-exposure for 1 μ M Melatonin vs. a 0.001% control solution of ethanol. (n = 46 animals per condition). (c) Timeline of Melatonin sleep assay. Statistics for a and b performed using an unpaired two-way t-test.; *P<0.05, ns = not significant. Error bars in s.e.m.

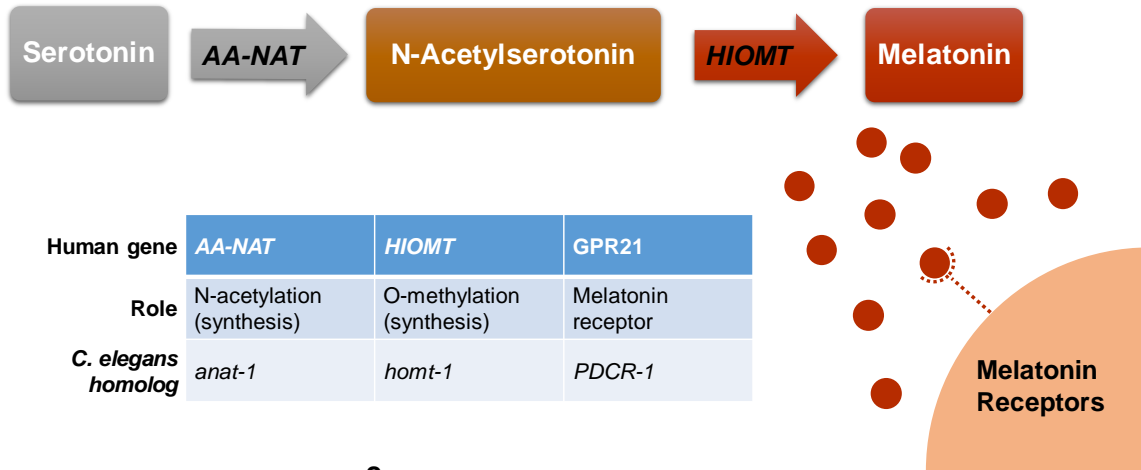
3.2: Genetic effects on adult *C. elegans* sleep

3.2.1: Investigation of melatonin synthesis and receptor mutations on sleep

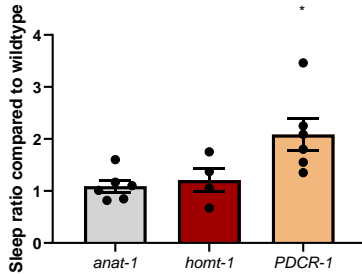
Melatonin synthesis from serotonin in mammals is a two-step process. First by N-acetylation by AA-NAT and then by O-methylation by HIOMT (Tanaka et al., 2007) (**Fig. 13a**). *C. elegans* have homologs to AA-NAT (*anat-1*) and HIOMT (*homt-1*) which show similarity to their mammalian homologs, therefore, to assess melatonin's potential involvement in sleep in adult *C. elegans*, we will assess *homt-1* and *anat-1* mutants for their behavior during adult sleep. Additionally, *PDCR-1* (previously *f59d12.1*) encodes an ortholog of a human G-protein-coupled receptor GPR21 and in *C. elegans* is involved in locomotion and efficient pathogen clearance (Anderson et al., 2019). Phylogenetic analysis predicts *PDCR-1* to encode a receptor for melatonin (Fox et al., 2005), and RNAi knockdown animals appeared slow and paralyzed (Keating et al., 2003). Studying these three mutants will give a sense of melatonin's role in sleep in *C. elegans* by looking both at putative melatonin synthesis mutants, and putative melatonin receptor mutants.

We found that neither *anat-1* (sleep ratio of 1.09 ± 0.11 s.e.m.) nor *homt-1* (1.21 ± 0.23) mutants showed sleep abnormalities compared to wildtype animals (**Fig. 13b**), however *PDCR-1* showed significantly increased sleep fraction (2.08 ± 0.31 , * $p < 0.05$). We developed a rescue line for *pdcr-1* by re-expression under the endogenous promoter (*Pgene::gDNA::SL2::mKate*). When compared in a paired assay (**Fig. 13c**), the rescue line (0.30 ± 0.05 s.e.m.) returned sleep fraction to similar levels to wildtype animals (0.28 ± 0.04), while *pdcr-1* mutants remained with significantly higher sleep fraction (0.48 ± 0.04 , * $p < 0.05$).

a



b



c

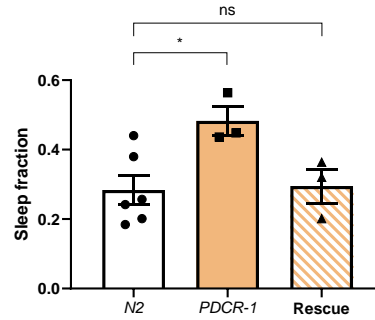


Figure 13. Putative melatonin receptor mutant shows increased sleep fraction

(a) Schematic of the melatonin system from synthesis from Serotonin to receptors. Relevant human genes, their roles in the melatonin system, and *C. elegans* homologs shown in chart. (b) Ratio of sleep fraction over 12 h experiments compared to wildtype animals in the same experiment for *anat-1*, *homt-1*, and *pdcr-1* mutants. Data points represent arenas of ~25 animals with their sleep fraction averaged across all animals in their respective arenas. ($n = 6$ arenas - *anat-1*, 4 arenas - *homt-1*, 6 arenas - *pdcr-1*). (c) Sleep fraction of paired assays with wildtype (N2) animals with *pdcr-1* mutants and a rescue line for *pdcr-1* re-expressing the *pdcr-1* gene in an endogenous promoter. Data from 3 assays each with 1 arena with ~25 *pdcr-1* animals, 1 arena with ~25 rescue line animals, and 2 arenas of ~25 wildtype animals each. Statistics for **b** performed using an unpaired two-way t-test. Statistics for **c** performed using a one-way ANOVA with Bonferroni's correction for multiple comparisons; * $P < 0.05$, ns = not significant. Error bars in s.e.m.

3.2.2: Arousal deficient mutants show reduced sleep

We also studied the effect of neuropeptides in adult sleep. Neuropeptides are short amino acid sequences that act as signaling molecules and may act as neurotransmitters in *C. elegans* (Li, 2008). The two main types of neuropeptides in *C. elegans* are insulin-like peptides and FMRFamide (Phe-Met-Arg-Phe-NH₂)-related peptides (FaRPs) which are called FLPs in *C. elegans*. There are additional neuropeptide-like proteins referred to as NLPs. Most neuropeptides are processed starting from a larger inactive peptide chain (referred to as a pro-peptide or pro-protein) which gets broken down in a series of steps of translation before resulting in individual active neuropeptides. *FLP-20* neuropeptides are necessary for locomotor and sensory arousal (Chew et al., 2018) during wakefulness. Due to the potential links between sleep and arousal, *flp-20* mutants unable to produce *flp-20* neuropeptides were studied to understand if there are any potential sleep effects to animals' sensory arousal. *Flp-20* neuropeptides bind with high affinity to *frpr-3* receptors, which also mediate arousal (Chew et al., 2018). *Frpr-3*, a G-protein-coupled receptor, has been shown to be implicated in SIS as receptor deletion mutants showed decreased quiescence (Turek et al., 2016). Both locomotor arousal and cross-modal sensitization are dependent on *flp-20* and *frpr-3*.

We found that both *frpr-3* (sleep ratio of 0.45 ± 0.03 s.e.m., ** $p < 0.01$) and *flp-20* (0.57 ± 0.09 , ** $p < 0.01$) showed significantly less sleep compared to wildtype animals (**Fig. 14a**). We developed multiple rescue lines for *frpr-3* and *flp-20* by re-expression under their endogenous promoter (*Pgene::gDNA::SL2::mKate*). We found that all 4 rescue lines (AQ4019 – 0.35; AQ4104 – 0.30; AQ4035 – 0.22 ± 0.02 ; AQ4037 – 0.28 ± 0.06 s.e.m.)

showed increased sleep relative to wildtype (0.32 ± 0.03) compared to their mutant counterparts (*frpr-3* – 0.15 ± 0.02 ; *flp-20* – 0.18 ± 0.04) (**Fig. 14b,c**).

The arousal deficiency in *flp-20* and *frpr-3* knockout mutants was seen in awake animals in response to a combination of first mechanical then aversive chemical stimulation. This arousal deficiency is independent of arousal threshold changes that is seen in wildtype animals between sleep and wake states. To assess how this arousal effect translates to sleep abnormalities we assessed the sleep entry (**Fig. 14d**) and sleep exit (**Fig. 14e**) rates for *flp-20* and *frpr-3* mutants compared to wildtype. We found that the increased sleep fraction seen in wildtype animals was primarily through an increased sleep entry rate, exhibiting a higher “sleep pressure” than the arousal deficient mutants. The arousal deficient mutants also showed slightly higher rates of sleep exit, signifying a lower “sleepiness” level during sleep bouts. Because of this, the arousal deficient mutants exhibit less frequent sleep bouts and shorter sleep bouts when they are asleep.

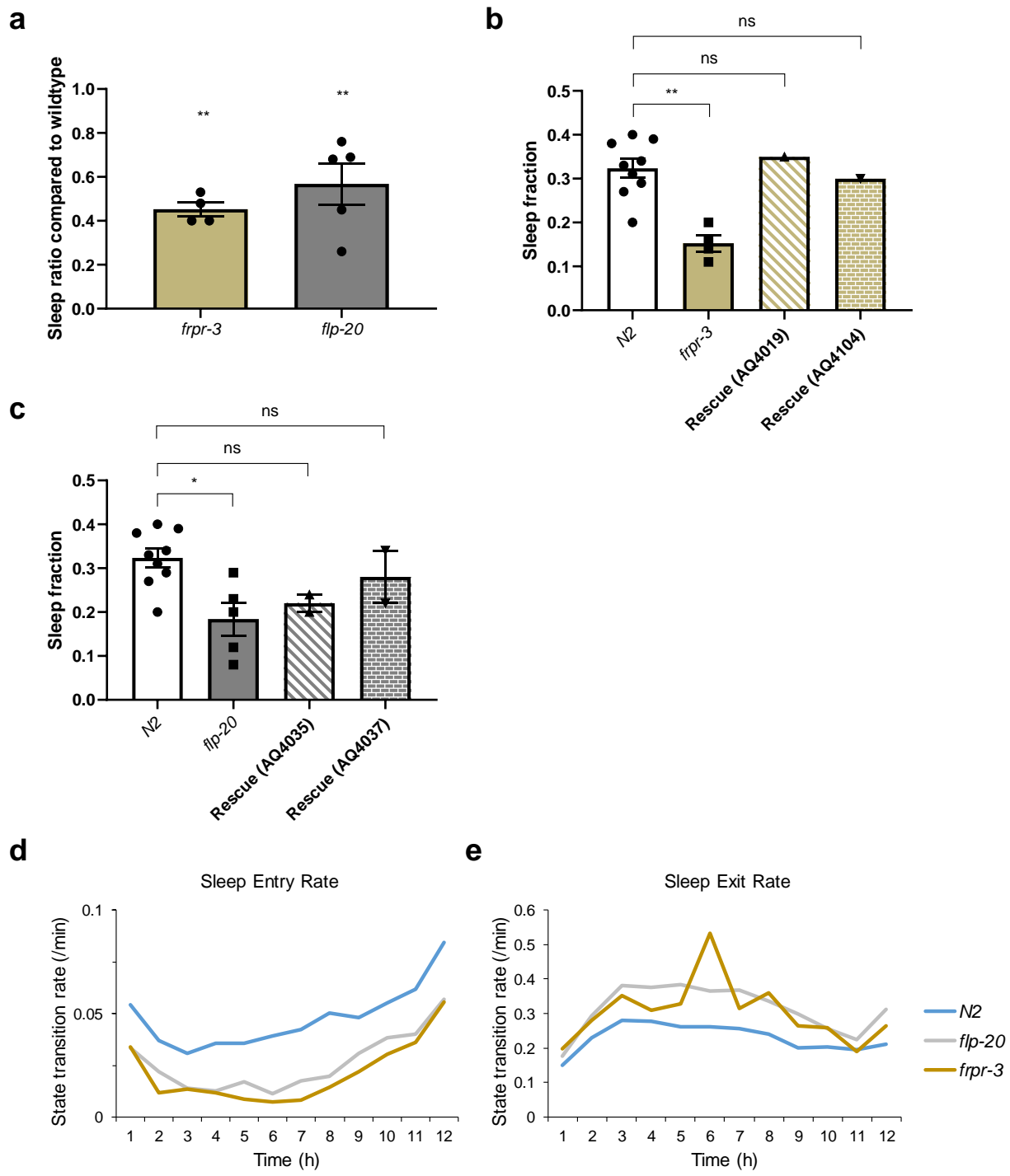


Figure 14. Mutants with decreased locomotor and sensory arousal show reduced sleep

(a) Ratio of sleep fraction over 12 h experiments compared to wildtype animals in the same experiment for *frpr-3*, *flp-20* mutants. Data points represent arenas of ~25 animals with their sleep fraction averaged across all animals in their respective arenas. (n = 4 arenas – *frpr-3*, 5 arenas - *flp-20*). (b) Sleep fraction of unpaired assays with wildtype (N2) animals, *frpr-3* mutants, and rescue lines for *frpr-3* which re-expressed the *frpr-3* gene in endogenous promoters. (n = 9 arenas N2, 4 arenas *frpr-3*, 1 arena rescue (AQ4019), 1 arena rescue (AQ4104)). Arenas of ~25 animals each. (c) Sleep fraction of unpaired assays with wildtype (N2) animals, *flp-20* mutants, and rescue lines for *flp-20* which re-expressed the *flp-20* gene in endogenous promoters. (n = 9 arenas N2, 5 arenas *flp-20*, 1 arena rescue (AQ4035), 1 arena rescue (AQ4037)). Arenas of ~25 animals each. (d) Sleep entry rate for N2, *flp-20*, and *frpr-3* mutants plotted over 12 hour time course. Rates plotted in transitions per minute. (e) Sleep exit rate for N2, *flp-20*, and *frpr-3* mutants plotted over 12 hour time course. Rates plotted in transitions per minute. Statistics for a performed using an unpaired two-way t-test. Statistics for b and c performed using a one-way ANOVA with Bonferroni's correction for multiple comparisons; **P<0.01, *P<0.05, ns = not significant. Error bars in s.e.m.

3.2.3: Sensory processing mutants and their sleep implications

Finally, to understand why sensory processing leads to abnormal arousal behavior, we assessed a group of sensory processing mutants (**Fig. 15a**) each with unique deficiencies later to be related to exposure effects in **Chapter 4**. Sleep fraction was assessed in 12 h experiments where at least one arena contained wildtype animals, and other separated arenas contained mutant strains listed below. Sleep fraction was normalized to the wildtype strain in shared experiments, and it was found that all sensory mutants showed increased sleep over 12 h compared to wildtype animals (**Fig. 15b**). *Daf-2* (an ortholog of human insulin like growth factor 1 receptor and the insulin receptor INSR (Gami and Wolkow, 2006)) animals showed the most elevated sleep behavior ($+0.62 \pm 0.05$ s.e.m.) compared to wildtype animals.

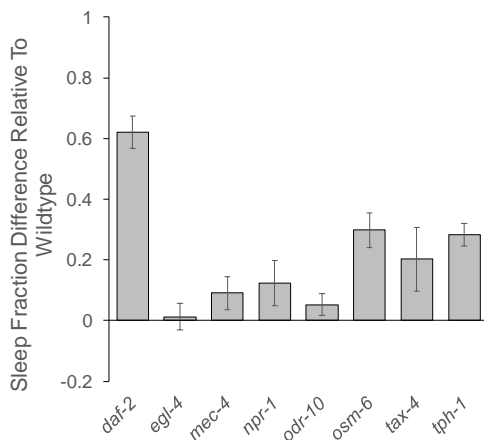
We next selected a group of mutant animals to test our sleep assessment system's ability to assess genetic perturbations through stimulus effects on sleep (**Fig. 15c**). We chose to stimulate with a mild 1 mM concentration of the bitter odorant Quinine which generates a negative chemotaxis in wildtype animals (Tajima et al., 2001). To assess how Quinine affects *C. elegans* sleep, we chose to use *egl-4* mutants who have a hypersensitivity to Quinine (Krzyzanowski et al., 2013), *osm-6* mutants who have limited sensory function to a number of odorants including Quinine (Hilliard et al., 2004), and *mec-4* mutants, who are gentle touch deficient (Driscoll and Chalfie, 1991), but have no related sensory deficiency impacting their Quinine sensation. *Egl-4* mutants showed the most sensitive reaction to Quinine (-0.06 sleep fraction relative to wildtype) with an extremely low sleep fraction of 0.06 over the 12 h assay. *Mec-4* also had sleep reduction from Quinine

stimulation (-0.05 sleep fraction relative to wildtype) as expected as they detect the bitter odorant fully. However, *osm-6* mutants showed far more sleep than wildtype animals (0.40 12 h sleep fraction) which was higher than their 12 h sleep fraction in S. Basal buffer (0.36), confirming that *osm-6* mutants were unaffected by the Quinine stimulus.

a

Gene	Reason for Study	Expectations
<i>egl-4(ad450)</i>	Mutants exhibit abnormal feeding behavior	Lower sleep due to increases in developmental sleep amount because of feeding issues
<i>tax-4(ks28)</i>	Gene involved in proper chemosensation	Lower sleep due to lack of sensory awareness in microfluidic environment
<i>mec-4(e1611)</i>	Mechanosensory deficient control	Lower sleep due to lack of mechanical feedback in microfluidics
<i>npr-1(ky13)</i>	Mutants show aggregation behavior which promotes sleep	Higher sleep due to past results in development and in adults
<i>tph-1(mg280)</i>	Gene required for serotonin biosynthesis	Higher sleep because serotonin promotes wakefulness
<i>osm-6(p811)</i>	Gene required for normal sensory neuron function	Lower sleep due to lack of sensory awareness in microfluidic environment
<i>odr-10(ky32)</i>	Gene required for AWA attractive response to diacetyl	Lower sleep due to lack of sensory awareness in microfluidic environment
<i>daf-2(e1370)</i>	Mutants are hypoxia resistant	Higher baseline sleep due to impaired insulin signaling, but unaffected by oxygen depletion

b



c

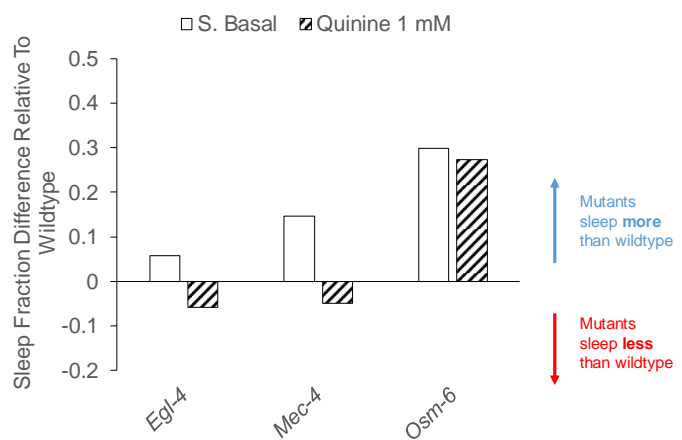


Figure 15. Sensory processing mutants show increased sleep compared to wildtype

(a) Table of genes used to study sensory processing deficiencies and their reason for study along with expected results. (b) Sleep fraction for mutant strains from a compared to wildtype animals in the same experiment (n = 2 arenas for *daf-2*, *egl-4*, *mec-4*, *odr-10*, *tax-4*, *tph-1*; n = 3 arenas for *npr-1* and *osm-6*. Each arena contained ~25 animals and sleep fraction calculated as average for each arena; Error bars represent s.e.m.). (c) Comparison of sleep fraction (difference relative to wildtype) in S. Basal buffer compared to 1 mM Quinine for *egl-4*, *mec-4*, and *osm-6* mutants.

$$\begin{aligned}
 & \text{"Sleep Fraction Difference Relative To Wildtype"} \\
 & = \text{Sleep Fraction}_{\text{Mutant}} - \text{Sleep Fraction}_{\text{Wildtype}}
 \end{aligned}$$

3.3: Investigating the effects of sleep on stimulus-evoked response in sensory neurons

3.3.1: ASH sensory neurons respond reliably despite delayed arousal

One of the behavioral characteristics that is used to define behavioral quiescence as sleep is an increased arousal threshold. Researchers have demonstrated that *C. elegans* also have an increased arousal threshold (Cho and Sternberg, 2014; Raizen et al., 2008a) during periods of lethargus during develop, helping coin the state “developmentally timed sleep.” As we are studying sleep phenomenon in a novel presentation with adults in a microfluidic environment, we too wanted to determine if these sleep states showed an increased arousal threshold.

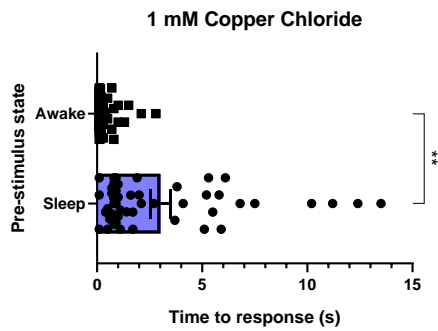
We subjected animals to a 10s pulse of odor, 5 seconds into measurement of neural activity and tracked neuron position over time. In tracking the time to response after stimulus was delivered, we found that 1 mM Copper Chloride (**Fig. 16a**) showed significantly delayed arousal response when stimulated in a sleep state compared to that of an awake state.

It also been suggested that this arousal delay is coupled with a dampening of neural activity across the entire nervous system (Nichols et al., 2017) forming a global brain state that supports sleep behavior as well as reduced sensory response (Cho and Sternberg, 2014). We sought to find out if adult *C. elegans* also display a reduced sensory response by testing the sensory neurons AWA and ASH. Using a 10s odor pulse stimulus paradigm we found that 1 mM Copper Chloride, pH 3.5 HCl, pH 4.1 HCl, 10 mM Quinine, and 1.1

μM Diacetyl all showed reliable peak sensory response regardless of strength of stimulus or behavioral state pre-stimulation (**Fig. 16b-f**).

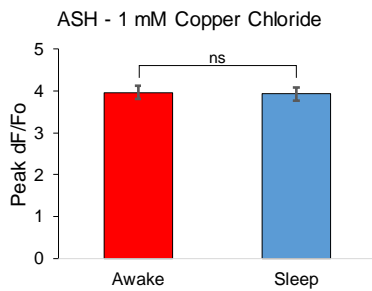
Increased arousal threshold during sleep

a

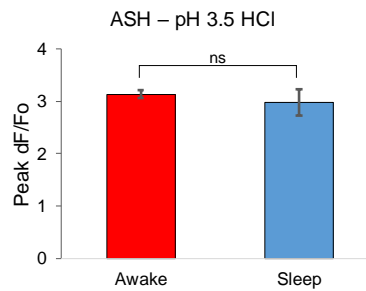


Consistent peak sensory response sleep vs. awake

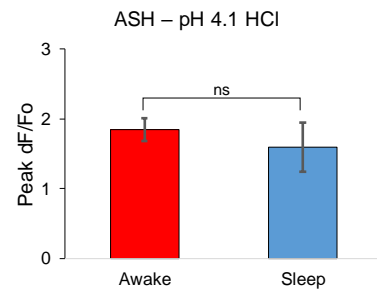
b



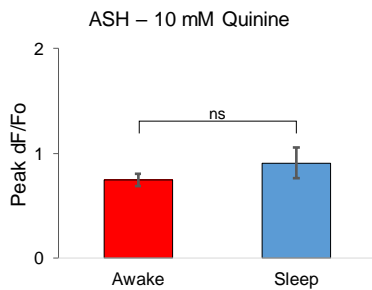
c



d



e



f

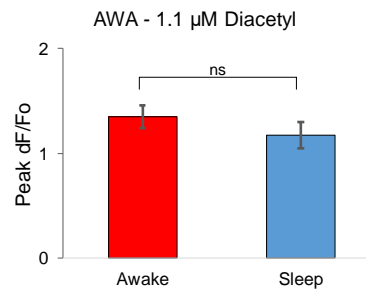


Figure 16. Adult *C. elegans* show increased arousal threshold during sleep but varied sensory response

(a) Average time to a behavioral response in sleeping and awake animals when stimulated with 1 mM Copper Chloride ($n = 48$ sleep, 49 awake). (b) Peak $\Delta F/F_0$ in ASH neuron in response to 1 mM Copper Chloride during sleep and awake states ($n = 18$ sleep, 19 awake). (c) Peak $\Delta F/F_0$ in ASH neuron in response to pH 3.5 HCl during sleep and awake states ($n = 3$ sleep, 3 awake). (d) Peak $\Delta F/F_0$ in ASH neuron in response to pH 4.1 HCl during sleep and awake states ($n = 3$ sleep, 7 awake). (e) Peak $\Delta F/F_0$ in ASH neuron in response to 10 mM Quinine during sleep and awake states ($n = 4$ sleep, 10 awake). (f) Peak $\Delta F/F_0$ in AWA neuron in response to 1.1 μ M Diacetyl during sleep and awake states ($n = 7$ sleep, 10 awake). Statistics for a-f performed using an unpaired two-tailed t-test; ** $P < 0.001$; * $P < 0.05$, ns = not significant $P > 0.05$. Error bars in s.e.m.

3.3.2: AWA sensory neuron shows modulated response during sleep state

Sleep-dependent modulation of neural activity may present as an altered baseline activity, changed strength of response, modular response timing or a combination of these factors. Using identical stimulation parameters to copper chloride measurements, we assessed the response in the appetitive sensory neuron AWA to 1.1 μM diacetyl. Unlike aversive stimulation with copper chloride which provokes reversal behavior, appetitive stimulation promotes continuation of behavior (often forward locomotion). Additionally, sleeping animals most often respond with only head movement, not engaging in any locomotion post-stimulation. When behavioral response was measured to 1 mM copper chloride (**Fig. 16a**), tracking of the neuron followed both head movement and body movement in both sleep and wake cases. We tracked movement in the AWA neuron in sleep and awake cases, capturing both the head movement during sleep trials and overall movement during awake trials (**Fig. 17a**), while simultaneously measuring neuronal activity (**Fig. 17b**).

As with copper chloride, animals who were sleeping prior to stimulation showed a significantly delayed first movement (3.25 ± 0.15 s after stimulation onset, $**P < 0.001$) compared to the rise in AWA activity (1.21 ± 0.05 s) (**Fig. 17c**). First movement in awake animals cannot be properly compared to establish an arousal threshold increase as animals' first response to appetitive stimuli is often to continue behaving how they were previously behaving, providing no instantaneous behavioral change to quantify. The pattern of response in AWA showed differences between sleep and awake states. Over the course of the 30 s stimulation paradigm, animals while awake would exhibit a peak

and fall in AWA activity during the 10 s stimulus exposure, and return roughly to baseline 15 s later at the end of the 30 s trial (**Fig. 17d**). Contrarily, sleeping animals showed a continuous rise during the 10 s stimulus exposure and maintained higher neural activity post-exposure, not returning to baseline. On average (**Fig. 17e**) sleeping animals showed significantly ($0.54 \pm 0.04 \Delta F/F_0$, $**P < 0.001$) higher average fluorescence post-stimulation (15- 30 s) compared to awake animals ($0.19 \pm 0.05 \Delta F/F_0$). However, peak neural response in AWA to 1.1 μM diacetyl was not significantly (ns $P > 0.05$) different between sleep and awake cases, as was seen with ASH in response to 1 mM copper chloride (**Fig. 17f**).

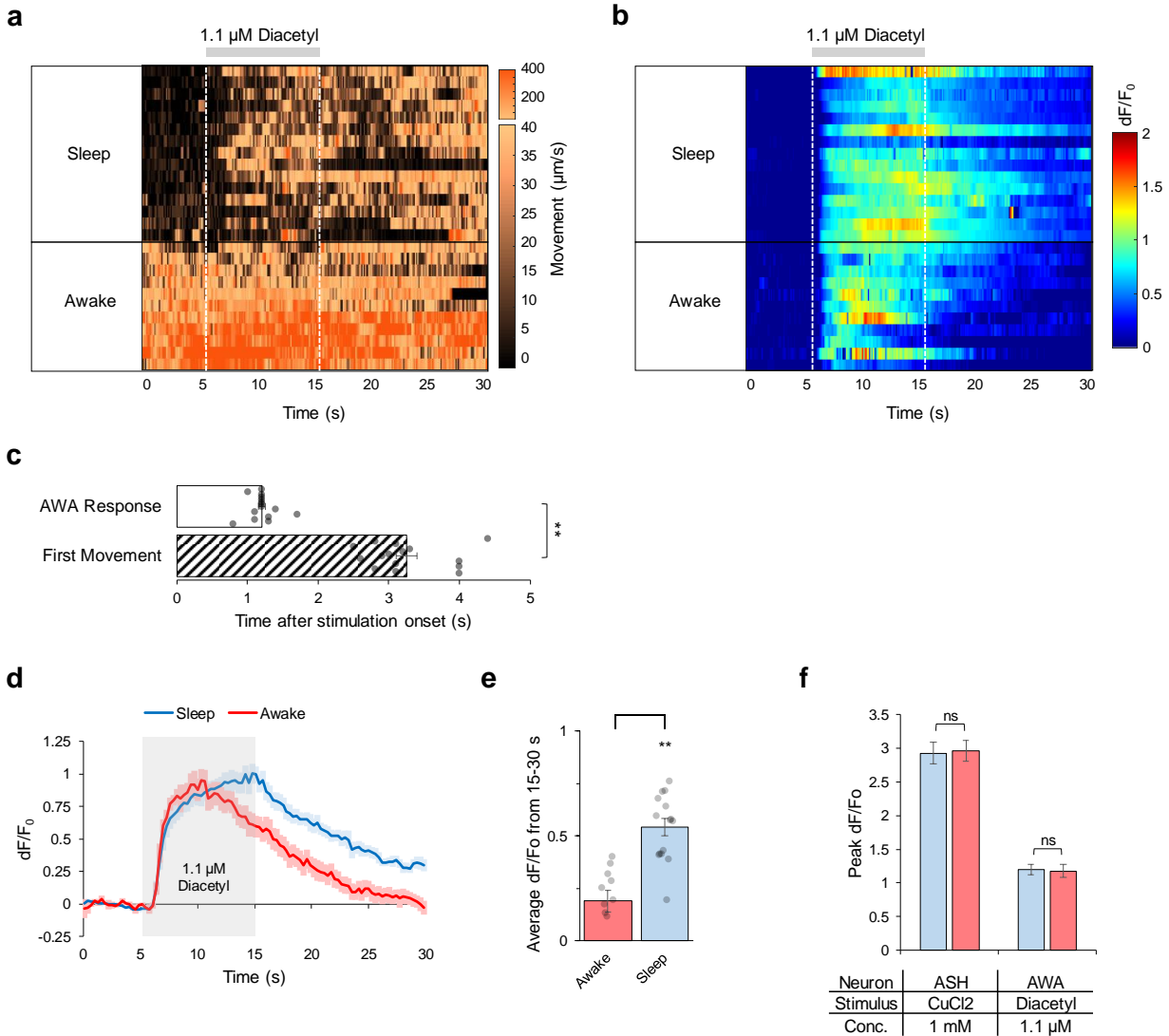


Figure 17: Appetitive sensory neuron shows elongated neural response during sleep state.

(a) Heatmap showing movement of AWA neuron per frame (0.1 s) across 26 pulsed stimulation trials (rows). Stimulus of 1.1 μM diacetyl applied between 5–15 s during each 30 s trial. Data sorted by average movement 5 s prior to stimulus, indicating the sleep/awake state for each recording. (b) Heatmap of individual $\Delta F/F_0$ AWA responses from a. (c) First movement in sleeping animals quantified by time of head movement after stimulus onset, compared to time of rise in AWA neural activity ($n = 15$ trials). (d) Average $\Delta F/F_0$ AWA neural responses in Sleep/Awake states to 10 s diacetyl pulses ($n = 15$ Sleep, 11 Awake). (e) Average $\Delta F/F_0$ post-stimulation in sleep ($n = 15$ trials) and awake ($n = 11$ trials) animals. (f) Peak $\Delta F/F_0$ in AWA and ASH neurons in response to stimuli during sleep and awake states ($n = 26$ -35 trials per condition). Statistics for c, e and f performed using an unpaired two-tailed t-test; ** $P < 0.001$; ns $P > 0.05$. Error bars represent s.e.m.

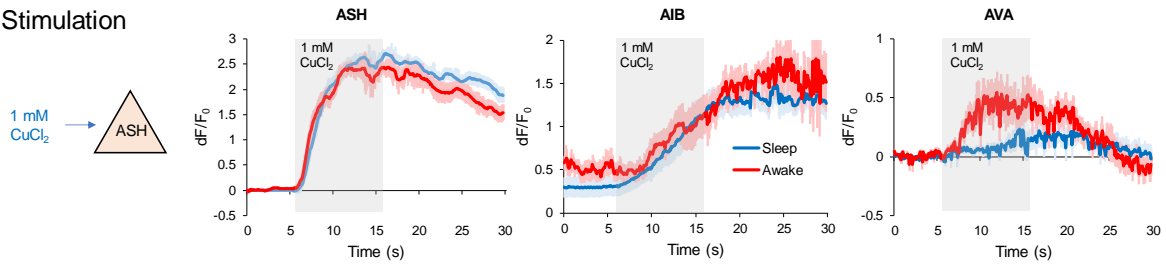
3.3.3: Sensory processing differences arise between aversive and appetitive stimulation

C. elegans must detect and respond to a plethora of sensory information in their environment. Changes in stimulus strength, presentation, and type all influence responsiveness to the environment. As sleep is associated with an increased arousal threshold (Raizen et al., 2008b), and some sensory systems have been shown to have diminished response in sleep states in *C. elegans* (Cho and Sternberg, 2014) it was commonly thought that decreased arousal thresholds arise due to dampening of global neural systems (Kato et al., 2015; Nichols et al., 2017; Skora et al., 2018). Based on information gathered here in **Chapter 3** and information to be discussed in detail in **Chapter 4** it is clear that not all types of sleep or all types of sensory information will modulate neural activity in the same way.

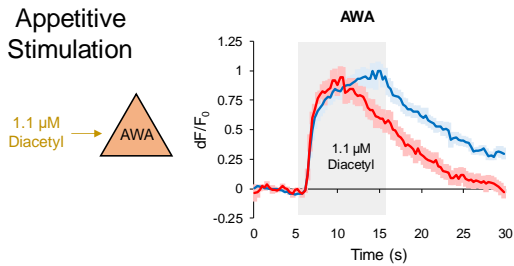
In **Chapter 4** the aversive sensorimotor subcircuit of ASH-AIB-AVA is probed in more depth, but briefly it was discovered that in adults sleep does not alter the stimulus-evoked sensory response in ASH, or response in the first-layer interneuron AIB, but strength and timing of response in AVA was altered between sleep and wake states in response to copper chloride (**Fig. 18**). This diminished and delayed behavior in the premotor interneuron AVA resulted in a delayed response in sleeping animals, compared to a nearly instantaneous reversal responses in awake animals. AVA responds reliably with reversal behavior in freely moving awake animals, so it is not surprising that sleeping animals do not show AVA depolarization until coordinated movement occurs.

It was anticipated that a similar comparison could be made with other sensory modalities, however the differences seen in appetitive stimulation highlight the complexity in sleep-dependent neural modulation. We saw that AWA neurons showed similar peak response to stimulation with diacetyl, however sleeping animals exhibited a prolonged response during and after stimulation. Assessing arousal threshold with appetitive stimulation is also difficult, as sleeping and awake animals do not exhibit similar reactionary behavior. Awake animals typically respond to appetitive stimulation by continuing behavior, not allowing for a timepoint to assess sudden response. Sleeping animals often showed no coordinated locomotion after stimulation, only responding by head movement. The differences in this behavior are highlighted in **(Fig. 18)**. It is evident that sleep-dependent modulation occurs with specificity across different neural subcircuit and different sleep states (DTS vs. SIS).

Aversive Stimulation



Appetitive Stimulation



Behavior

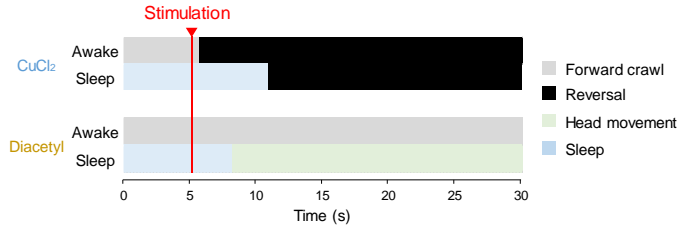


Figure 18: Schematic of neural responses and behavior in aversive and appetitive stimulation

Schematic shows summary of average neural responses and behavior shifts in appetitive and aversive stimulation cases. Data taken from **Fig. 16**, **Fig. 17**, **Fig. 24**, and **Fig. 26**.

Discussion

The field of sleep research in *C. elegans* has seen exponential growth in recent years. From (Raizen et al., 2008a) first making the argument that periods of quiescence observed during lethargus represent a sleep-like state, to calls for the field to simply refer to these states as sleep by (Trojanowski and Raizen, 2015) just 4 years ago, establishment of sleep measurement systems and sleep phenomena in *C. elegans* have risen dramatically. Sleep is a challenging behavior to be confident in studying because its behavioral characteristics are dynamic, unable to be sorted away from animals being dead, pausing, resting, etc. Sleep as we think of it in humans is a restoration period. In our culture, getting a “good night’s rest” is not necessarily correlated with inactivity, but rather with a change in consciousness (Brown et al., 2010). But still, loss of consciousness can be a result of anesthesia or severe brain injury, so researchers developed measurements of brain waves using EEG as the gold standard to define sleep. This presents a challenge in establishing organisms like *C. elegans* as animals that sleep, but the field has demonstrated through thorough investigation of behavioral patterns with sleep that periods of behavioral quiescence observed during DTS (Raizen et al., 2008a) and SIS (Hill et al., 2014) are true sleep states. We also studied these criteria in depth for the investigation of spontaneous behavioral quiescence in young adult *C. elegans* in the microfluidic environment, which will be discussed in more detail in **Chapter 4**, as such we sought to assess how chemical and genetic perturbations affect this format of sleep, and establish criteria for understanding the behavioral plasticity associated with sleep.

First, we had to determine the appropriate methods to study sleep behavior. Our first observations detailed in **Chapter 2** were conducted with individual isolated animals, testing their sleep with pulses of blue light to illuminate their entire body due to autofluorescence. As we suspected though, blue light was found to be an aversive stimulus towards sleep in adults (**Fig. 10**) reducing their sleep fraction by more than half. As such, we needed to find formats to observe sleep behavior using less harmful wavelengths of illumination, so we developed systems to use green LEDs to present brightfield illumination. To translate this method to higher throughput assessment of sleep behavior, we saw that when we loaded ~25 animals into a 16 mm x 15 mm arena their overall sleep patterns did not change despite instances of animal-to-animal encounter. This allowed us to assess the chemical and genetic perturbations we sought to with much higher throughput.

Our interest first was in studying how neuromodulators impact sleep, and melatonin was an obvious first choice of a neuromodulator to study. Melatonin has been shown to control circadian rhythms in mammals (Ganguly et al., 2014) however its role in sleep in *C. elegans* had yet to be determined. We found that melatonin synthesis pathways involved in the conversion of serotonin to melatonin likely do not play a role in adult sleep in *C. elegans* as mutants lacking the homologous pathway enzymes did not show differences in sleep from wildtype animals (**Fig. 13b**). On the other hand, a putative melatonin receptor that has been shown to be involved in pathogen clearance, *pdcr-1*, showed significantly increased sleep and animals were slow and sluggish. We were able to rescue this phenotype, returning sleep levels to baseline and eliminating the possibility that this

strain had sleep abnormalities due to off target effects (**Fig. 13c**). Additionally, the return of sleep phenotypes in a rescue line were extremely promising in assessing the systems' capability in elucidating genetic effects on sleep behavior when future studies will involve the assessment of human disease models impacting sleep. It is possible that melatonin does not impact adult *C. elegans* sleep that is driven by the conditions of microfluidic exposure, however the rhythmic nature of DTS provides an alternative sleep presentation that is more likely to be influenced by melatonin exposure.

One of the key behavioral markers of sleep is an increased arousal threshold. It has been shown that animals during lethargus show delayed response to mechanical and chemical stimuli (Raizen et al., 2008a) and neural activity to sensory stimulation is dampened (Cho and Sternberg, 2014), resulting in downstream miscoordination of interneuron circuits thought to contribute to motor circuit state dependent modulation. Using a closed-loop system described in greater detail in **Chapter 4** we assessed a plethora of sensory stimulants in both the AWA and ASH chemosensory neurons (**Fig. 16-17**), seeing that adult *C. elegans* do show an increased arousal threshold in our system (**Fig. 16a**) but unlike during lethargus, peak sensory neuron response is consistent between sleep and awake states (**Fig. 16b-f**) through chemosensory attractants and repellants of various degrees of magnitude. This result challenges the generally thought of idea of how sleep regulates arousal in *C. elegans*, an idea that has been adopted to understand sensory regulation in higher level organisms. It is possible that differences may lie in physiological changes between DTS and adult sleep. Potentially, the presence of an additional cuticle layer during molting could cause physical differences in how molecular interactions occur

with amphid sensory neurons like ASH. Also possible is that sleep states exhibited during DTS have additional important consequences for the growth and health of *C. elegans* commanding differences in how stimulation and neural activity are modulated between sleep and wake states. It has been shown that sleep effects the global brain state (Nichols et al., 2017), leading to reduced baseline activity in neurons across the nervous system, but it is unclear the differences in how this global brain state is regulated during adult sleep, DTS, and SIS. We did however see a difference in the pattern of neural activity following appetitive stimulation (**Fig. 17d,e**), highlighting the potential differences of neural regulation not only across different sleep modalities, but also different sensory responsibilities.

As arousal and sensory processing clearly have implications in sleep in *C. elegans* we also sought to assess genetic perturbations related to these phenomena. We tested an array of sensory processing mutants and found nearly all of them to have increased sleep compared to wildtype (**Fig. 15a**) potentially suggesting that sleep behavior in the microfluidic device could arise due to the sensory deprivation of the microfluidic environment, as these sensory deficient mutants have even greater levels of sensory deprivation than wildtype animals, potentially leading to more prevalent sleep behavior. Many of our expected results were not seen in these mutant screening assays, which leads us to believe that test-to-test variability and the variability of sleep behavior may not have elucidated all of the potential genetic effects seen in adult sleep. Further exploration of these mutants may yield new findings of how sensory processing effects sleep. We also studied mutants implicated in proper arousal from mechano- and chemosensory

stimulation (Chew et al., 2018). We observed that both neuropeptide and receptor mutants exhibited lower levels of sleep compared to wildtype (**Fig. 14a**), again able to be rescued by re-expression under endogenous promoters (**Fig. 14b,c**). The decrease in sleep with mutants with deficient arousal suggests that their diminished capability of arousal may lessen the sleep pressure normally exhibited in the microfluidic device. Arousal deficient mutants exhibited lower sleep entry rates and higher sleep exit rates than wildtype animals (**Fig. 14d,e**). Based on this, we believe that *C. elegans* exhibit a balance between the sleep and arousal systems to regulate their environmental decision making, and that arousal from sleep and arousal during wakefulness are carried out by different processing systems.

Methods and Materials

Strains and *C. elegans* culture

All *C. elegans* strains were maintained under standard conditions on NGM plates and fed OP50 *E. coli* bacteria seeded onto each plate. Wild-type animals were Bristol strain (N2). The following mutant strains were used: **AQ3683**, *anat-1* (lj102); **AQ3652** *homt-1* (lj100); **AQ3585**, *pdcr-1* (gk1122) of which a rescue line was generated for the gene *f59d12.1* (**unnamed**) (*Pf59d12.1::gDNA::SL2::mKate*). **AQ3832**, *frpr-3(ok3302)*; **AQ4000**, *flp-20(ok2964)*; **AQ4019**, *frpr-3(ok3302)*; *ljEx1090[Pfrpr-3::frpr-3 gDNA::SL2-mKate(pYLC149)(25); unc-122::gfp(50)]*; **AQ4037**, *flp-20(ok2964);ljEx1093[Pflp-20(3kb)::flp-20 gDNA + 3' UTR::SL2-mKate2 (pYLC155) (50); unc-122::gfp(50)]*; **AQ4035**, *flp-20(ok2964)*; *ljEx1094 [Pmec-4::flp-20 gDNA + 3' UTR::SL2-mKate2 (pYLC152) (50); unc-122::gfp(50)]*; **AQ4104**, *frpr-3(ok3302)*; *ljEx1135 [Pflp-2::frpr-3::SL2-mKate2 (50)(pYLC196);unc-122::gfp(50)]*. **CB1370**, *daf-2 (e1370)*; **DA521**, *egl-4 (ad450)*; **CB1611**, *mec-4 (e1611)*; **CX32**, *odr-10 (ky32)*; **FK103**, *tax-4 (ks28)*; **GR1321**, *tph-1 (mg280)*; **DA609**, *npr-1 (ad609)*; **PR811**, *osm-6 (p811)*. Neural imaging strains expressing GCaMP in specific neurons were: (ASH (Larsch et al., 2013)) **CX10979**, *kyEx2865 [Psra-6::GCaMP3; Pofm-1p::GFP]*; (AWA (Larsch et al., 2013)) **CX14887**, *kyIs598 [Pgpa-6::GCaMP2.2b 50 ng/μL, unc-122p::dsRed]* expressing GCaMP integrated in AWA neurons. Some strains were provided by the CGC, and others provided by Y.L. Chew of the Schafer Lab. To synchronize for age, we picked L4 larval stage animals one day prior to experimentation such that all animals tested were at the young adult stage.

To prepare for an experiment, animals were isolated by genotype and/or arena placement and then transferred to an unseeded NGM plate immediately prior to experimentation. The plates were then flooded with the control buffer used for their respective experiment: S. Basal buffer (100 mM NaCl, 50 mM KPO₄; pH 6.0) for the majority of experiments, or a saline buffer (80 mM NaCl, 5 mM KCl, 20 mM D-glucose, 10 mM HEPES, 5 mM MgCl₂, 1 mM CaCl₂; pH 7.2) for copper chloride stimulus experiments. Animals were then collected into loading tubing using a 1 mL syringe prior to injection into the microfluidic arena.

Microfluidic device fabrication

“Population behavior” and “Neural imaging” microfluidic devices were fabricated as previously described (Lagoy and Albrecht, 2015). Briefly, transparency photomasks were printed at 25,000 dpi from designs sketched using DraftSight CAD software. SU-8 mold masters were prepared on silicon wafers using standard photolithography techniques, and microfluidic devices were fabricated by pouring degassed PDMS (Sylgard 184, Dow Corning) onto the mold and heat curing. Individual devices were then cut out and punched to provide inlet and outlet flow. A hydrophobic glass substrate was created by vapor deposition of tridecafluoro-1,1,2,2-tetrahydrooctyl trichlorosilane (TFOCS, Gelest) and then sealed reversibly to the microfluidic channels. An upper glass slide, with holes drilled over inlet and outlet ports with a diamond-coated drill bit, was sealed above the device, which was then placed into a metal clamp.

Stimulus preparation

All odor dilutions were freshly prepared on the day of experimentation. Melatonin powder (Sigma) was dissolved in 100% ethanol at 100 mM before being dissolved in S. Basal buffer to a testing solution of 1 μ M with 0.001% ethanol. For neural imaging experiments, 1 mM copper chloride and 10 mM quinine solution were prepared the day of the experiment using copper chloride powder and quinine powder respectively. Diacetyl (1.1 μ M) was prepared from a 10^{-3} dilution (11 mM) stock solution immediately prior to experimentation. Hydrochloric acid solutions were prepared by slowly titrating stock solution into a stirring beaker of S. Basal while a pH meter was submerged in the solution. Samples were removed at the respective 4.1 and 3.5 pH readings.

Microfluidic device setup

Microfluidic devices were cleaned, assembled, and degassed in a vacuum desiccator for 30–60 min prior to experimentation. Degassing devices accelerates the absorption of air bubbles within the device. For behavioral experiments, devices were filled with 5% (w/v) Pluronic F127 through the outlet port to prevent bacterial and molecular absorption by passivation of the microfluidic surfaces and to minimize bubble entrapment via its surfactant properties. Neural imaging devices were filled with control buffer alone. Reservoirs of loading solutions were prepared as previously described (Lagoy and Albrecht, 2015), purging the reservoir system of bubbles and connecting the tubing into the inlets of the device. Once flow was properly established, animals were gently loaded into their respective arenas and allowed to roam for 15–20 min prior to

experimentation. For neural imaging experiments, a control valve is used to switch between stimulus and control buffer conditions within 0.5 s.

Population behavior imaging and identification of sleep events

Videos of sleep behavior were captured using a 6.6 MP Pixellink FireWire Camera at 1 fps for 12 h with an image resolution of ~30 pixels/mm. Videos were processed after experimentation as described in detail in **Chapter 4** using MATLAB to extract behavioral data (Albrecht and Bargmann, 2011), and then further analyzed to identify sleep events. A minimum sleep entry window of 20 s and exit window of 5 s were used to quantify state transitions. All behavior data was collected using “Population behavior” devices with four 16 mm x 15 mm arenas capable of housing ~25 animals per arena for simultaneous study.

Neural calcium imaging, sleep detection and data analysis in closed-loop system

Neural imaging videos and light assessment were acquired at 5x magnification (NA=0.25) with a Hamamatsu Orca-Flash 4.0 sCMOS camera using MicroManager/ImageJ software. The system has a green ($\lambda = 520\text{-}550$ nm) LED mounted overhead to provide pulsed brightfield illumination for tracking animal behavior and a Lumencor SOLA-LE solid-state lamp pulsed to excite GCaMP during fluorescence calcium imaging. Arousal threshold and sensory response data in **Fig. 16** were collected using a closed-loop state detection system described in depth in **Chapter 4**. To achieve autonomous experimentation for a closed-loop system, custom Arduino, MicroManager, and ImageJ scripts work together to control illumination timing, image acquisition, stimulus delivery, and sleep/wake state identification. An Arduino Uno microcontroller was

programmed to control fluidic valves through a ValveLink 8.2 (AutoMate Scientific) controller and to control illumination sources for brightfield and fluorescent imaging. A MicroManager script allows the user to configure all camera and illumination settings prior to experimentation as well as all testing conditions for sleep assessment. Assessment of blue vs. green light was performed using illumination previously described at equal 0.1 fps frame rates. Greater detail about the image capture and sleep identification process is detailed in **Chapter 4**.

Calcium imaging was performed on freely-moving animals as previously described (Larsch et al., 2013) using lines expressing GCaMP in selected neurons. Calcium imaging in ASH and AWA neurons was performed at 10 fps, using closed-loop stimulation to record responses to 10 s chemical stimulation from 5–15 s within a 30 s trial. Videos were analyzed for neural fluorescence and locomotion using NeuroTracker software in ImageJ, which tracks the position of the neuron over time and integrates fluorescent intensity of the soma using a 4 x 4 pixel box. Fluorescence (F) was normalized by dividing by the initial baseline fluorescence in the first 4 s of each trial before stimulation (F_0), and the peak was collected for each stimulation.

Statistical analysis

Statistics were performed using one-way ANOVA with Bonferroni's correction for multiple comparisons or an unpaired two-tailed t-test when specified for 2 sample comparison, using the Statistics and Machine Learning Toolbox in MATLAB. Data represented as mean \pm s.e.m. unless otherwise stated. In behavioral experiments, animals were excluded when valid behavioral tracks comprised <8% of recording time,

indicating an animal not viable or not present during the test. In neural recordings, the top and bottom 1% of instantaneous fluorescent intensity was removed to reduce noise in peak fluorescence calculations.

Chapter 4: Automated analysis of sleep in adult *C. elegans* with closed-loop assessment of state-dependent neural activity

The work presented in this chapter has been submitted for publication, and is posted in preprint form on biorvix (Lawler et al., 2019). Dr. Yee Lian Chew, Dr. Josh Hawk, Dr. Ahmad Aljobeh, Dr. William Schafer, and Dr. Dirk Albrecht are also co-authors on the manuscript. Several undergraduate students, graduate students, and faculty members are acknowledged as supporting the work. This work was supported in part by an NSF IGERT award (DGE 1144804) and by the Burroughs Wellcome Fund Career Award at the Scientific Interface, and the National Science Foundation NSF CBET 1605679 and EF 1724026, NIH R01DC016058.

Abstract

Sleep, a state of quiescence associated with growth and restorative processes, is conserved across species. Invertebrates including the nematode *Caenorhabditis elegans* exhibit sleep-like states during development and periods of satiety and stress. Here we describe two methods to study behavior and associated neural activity during sleep and awake states in adult *C. elegans*. A large microfluidic device facilitates population-wide assessment of long-term sleep behavior over 12 h, including effects of fluid flow, oxygen, feeding, odors, and genetic perturbations. Smaller devices allow simultaneous recording of sleep behavior and neuronal activity, and a closed-loop sleep detection system delivers chemical stimuli to individual animals to assess sleep-dependent changes to neural responses. Sleep increased the arousal threshold to aversive chemical stimulation, yet sensory neuron (ASH) and first-layer interneuron (AIB) responses were unchanged. This localizes adult sleep-dependent neuromodulation within interneurons presynaptic to the AVA premotor interneurons, rather than afferent sensory circuits.

Introduction

Sleep is a physiological state during which voluntary muscle activity ceases, sensory processing is modulated (Velluti, 1997), and anabolic, growth, and restorative processes occur in the brain and other tissues (Adam and Oswald, 1977). Sleep is observed across species, from mammals to invertebrates (Campbell and Tobler, 1984), where it controls energy usage (Schmidt, 2014), metabolism, macromolecular biosynthesis (Mackiewicz et al., 2007), and neural plasticity and memory consolidation (Frank and Benington, 2006). Sleep pathologies include improper duration or control (e.g., insomnia, narcolepsy),

altered sleep behavior (e.g., sleepwalking), and altered sensation (e.g., restless leg syndrome). In humans, these sleep deficiencies are associated with reduced productivity (Rajaratnam et al., 2013) and increased prevalence of cardiovascular disease (Newman et al., 2000), diabetes (Gottlieb et al., 2005), and obesity (Hasler et al., 2004).

The initiation and cessation of sleep is often mediated by circadian rhythms, which are controlled by environmental factors (Reppert and Weaver, 2002) and timing genes that are generally conserved across species (Panda et al., 2002). A number of molecular pathways (Kramer et al., 2001; Saper et al., 2005; Sehgal and Mignot, 2011; Siegel, 2004; Tsunematsu et al., 2011; Weber et al., 2015; Yamuy et al., 1999) are involved in promoting sleep states and inhibiting arousal behavior. However, it is currently unclear how these pathways modulate circuit-level sensory processing during sleep states (Hennevin et al., 2007), and how misregulation of neural activity may contribute to sleep disorders.

The nematode *C. elegans* provides distinct advantages for direct observation of neurological function in freely-behaving animals. They are small (<1 mm), exhibit short generational times, and have a compact and fully mapped connectome of 302 neurons in hermaphrodites and 387 in males (Molina-García et al., 2019). Noninvasive optical measurements of neural activity can be made in living, behaving animals via genetically-encoded fluorescent calcium indicators such as GCaMP (Tian et al., 2009), and genetic tools are available for rapid generation of mutants and transgenic strains for mechanistic

studies (Antoshechkin and Sternberg, 2007; Boulin and Hobert, 2012; Friedland et al., 2013).

C. elegans demonstrate states of quiescence during lethargus between larval stages (Raizen et al., 2008a) (developmental sleep) and during periods of stress (Hill et al., 2014), satiety (Gallagher and You, 2014; You et al., 2008), starvation (McCloskey et al., 2017; Skora et al., 2018), and hypoxia (Nichols et al., 2017). Additionally, adult *C. elegans* undergo quiescent periods after 1–2 h of swimming in liquid (Ghosh and Emmons, 2008) and in microfluidic chambers with open and constrictive geometries (Gonzales et al., 2019). These quiescent states share fundamental characteristics with sleep in other species (Singh et al., 2013), including putative human sleep functions such as processing of synaptic plasticity (Dabbish and Raizen, 2011) and metabolic control (Driver et al., 2013), and typical behavioral characteristics such as increased arousal threshold (Cho and Sternberg, 2014; Raizen et al., 2008a), stereotypical posture (Iwanir et al., 2013; Schwarz et al., 2012; Tramm et al., 2014), homeostatic response to sleep deprivation (Driver et al., 2013; Nagy et al., 2014a; Raizen et al., 2008a), and rapid reversibility (Raizen et al., 2008a; Trojanowski et al., 2015). Together, these connections make a strong case that these quiescent bouts represent sleep in *C. elegans* (Trojanowski and Raizen, 2015), enabling its use as a model organism to study the molecular basis of sleep.

C. elegans sleep has been observed on a variety of experimental platforms, including agar (Raizen et al., 2008a) or agarose pads (Churgin et al., 2017; Turek et al., 2015) and microfluidic chambers that house individual animals (Gonzales et al., 2019; Huang et al.,

2017; Nagy et al., 2014b; Singh et al., 2011) throughout multiple development stages. Agar pads are useful for studying developmentally-timed sleep, by permitting feeding and growth across multiple larval stages, but they are difficult to use for assessing neural responses to sensory stimulation. Neural activity measurements typically require immobilization by agarose pads (Spies and Bringmann, 2018) or microfluidic traps (Cho and Sternberg, 2014), which prevent locomotory behavior and limit their use to developmentally-timed sleep in which sleep state is inferred by timing rather than by behavior. Alternatively, whole brain imaging in immobilized adult animals (Nichols et al., 2017; Skora et al., 2018) showed cessation of spontaneous neural activity during presumed sleep states induced by hypoxia. However, spontaneous sleep events in adult animals are best assessed by analysis of locomotion and quiescent behaviors. Therefore, new methods are needed for monitoring sleep state and stimulated neural responses in freely-moving animals, in order to assess the functional circuit changes that occur during adult sleep.

Here we demonstrate two systems to quantify the behavioral and neural characteristics of sleep in young adult *C. elegans*, using microfluidic devices that allow a natural sinusoidal crawling motion in a well-controlled liquid environment enabling rapid chemical stimulation (Albrecht and Bargmann, 2011). A larger device is used for population-wide assessment of over 100 animals and up to 4 conditions at once, and a smaller device allows simultaneous behavioral and neural recording in individual animals (Larsch et al., 2013). We show that sleeping behavior exhibited by young adult *C. elegans* follows characteristic dynamics over 12 h in microfluidic devices and is impacted by fluid flow,

oxygen, bacterial food, food signals, and genetic perturbations affecting sensory input. In this platform, the onset of adult sleep correlates with increased activity of the RIS interneuron (Steuer Costa et al., 2019; Turek et al., 2013). Using a closed-loop chemical stimulation system, we observed an increased arousal threshold during adult sleep states as before (Raizen et al., 2008a) and also monitored simultaneous neural activity. A sleep-dependent delay in response to aversive copper chloride corresponded to diminished and delayed responses in AVA command interneurons. Responses in the ASH sensory neurons and AIB interneurons were not modulated by sleep in young adult animals, localizing sleep-state neural circuit modulation within interneurons of the aversive sensorimotor subcircuit. These results suggest that sleep specifically alters the linkage between sensory stimuli and command neurons without changing processing within high-level interneurons, and provide an experimental system to dissect the molecular processes that produce this specificity.

Results

High-throughput analysis of adult sleep

Sleep behavior, defined by periods of behavioral quiescence, was observed in young adult *C. elegans* over 12 hours in microfluidic behavior arenas (Albrecht and Bargmann, 2011). A hexagonal array of 70 μm tall microposts enables free sinusoidal crawling behavior in a dynamic, switchable liquid environment with continuous flow (**Fig. 19a,b**). Each device contained four 16 mm x 15 mm arenas housing four independent populations of ~25 freely crawling animals that share the same fluidic environment. Wild-type animals roam around microfluidic arenas with predominantly forward locomotion, separated by momentary pauses, spontaneous short reversals (<1 s), and long reversals coupled with reorienting “omega” turns (Albrecht and Bargmann, 2011; Gray et al., 2005). Awake animals may pause briefly to feed if bacterial food is present (Flavell et al., 2013), to probe the physical barriers of arenas, or when encountering other animals. Other times, animals enter a prolonged quiescence state that lasts for ~20 s to several minutes. These bouts begin with animals gradually slowing their mean forward locomotion speed over 10–20 s (**Fig. 20a**), often pausing briefly a few times (**Fig. 20b**) during slow, creeping motion. Animals then gradually adopt a relaxed body posture (Schwarz et al., 2012) over about one minute (**Fig. 20c,d**) and cease further movement. Sleeping animals are apparent visually in microfluidic arenas by their straight head and contact with only one micropost (**Fig. 20d**), whereas awake animals actively wrap around several posts (e.g., **Fig. 19b**). After typically one or more minutes, animals quickly wake and resume forward (or occasionally reverse) locomotion, accelerating to a typical 0.15 mm/s forward velocity within 5 s.

Since pauses reflect both the extended quiescent states of sleep bouts and the momentary pauses of awake animals, true sleep states were automatically identified by centroid tracking filtered by the characteristic duration, history, and body shape of sleep. Using temporal parameters based on sleep entry and exit dynamics (onset after 20 s continuous pausing and ending at 5 s non-pausing), automatic classification of sleep bouts showed 95.2% agreement with human observation, with slight underestimation of sleep states (1.9% false discovery rate; 7.9% false omission rate; $n = 500$ randomly selected bouts; **Fig. 20e**). These detected sleep bouts exclude the brief pauses that precede a sleep bout, and include momentary “twitch” movements during sleep which can be caused by contact from other animals, flow disturbance, or presumed involuntary movements, and do not signal exit of a sleep state.

We analyzed 535 wild-type (N2) animals for 12 h in continuous 0.5 mm/s flow of S. Basal buffer (**Fig. 19c**). Hourly sleep fraction, defined by the fraction of time the animal spends in a sleep state during each hour, decreased on average across the population from 22% \pm 0.8% s.e.m. in the first hour to 8% \pm 0.5% in hour 3, then increased steadily to 38% \pm 1% in hour 12 (**Fig. 19d**). A wide range of sleep behavior was observed among individual wild-type animals, with 95% exhibiting a 12 h total sleep fraction ranging from 4% to 43%. To assess variability in sleep dynamics, we divided animals into quartiles by total sleep fraction. Sleep dynamics were similar in all quartiles, with sleep fraction increasing over time after 3 h (**Fig. 19d**), but median sleep fraction over 12 h varied greatly across quartiles from 3% to 24%. Median sleep duration remained between 1.3–1.9 min for each

quartile (**Fig. 19e**), whereas median awake duration varied more greatly, with the top quartile of sleeping animals remaining awake for a median of 7 min, about one-quarter of the most active animals (27 min). The increase in sleep fraction over time from hours 3–12 was associated with both an increased rate of sleep entry (more sleep pressure) and a decreased rate of sleep exit (more sleepiness) (**Fig. 19f**), resulting in more frequent and longer sleep bouts and shorter awake periods over time (**Fig. 21a**). The rate of sleep exit remained consistent across total sleep quartiles (**Fig. 21b**), while the rate of sleep entry varied greatly (**Fig. 21c**). Together, these results indicate that sleep bouts were similar across wild-type animals, while individual variability in sleep fraction among wildtype animals predominantly arose due to variation in the rate of sleep entry, or equivalently, the duration of awake bouts, and in the frequency of sleep bouts.

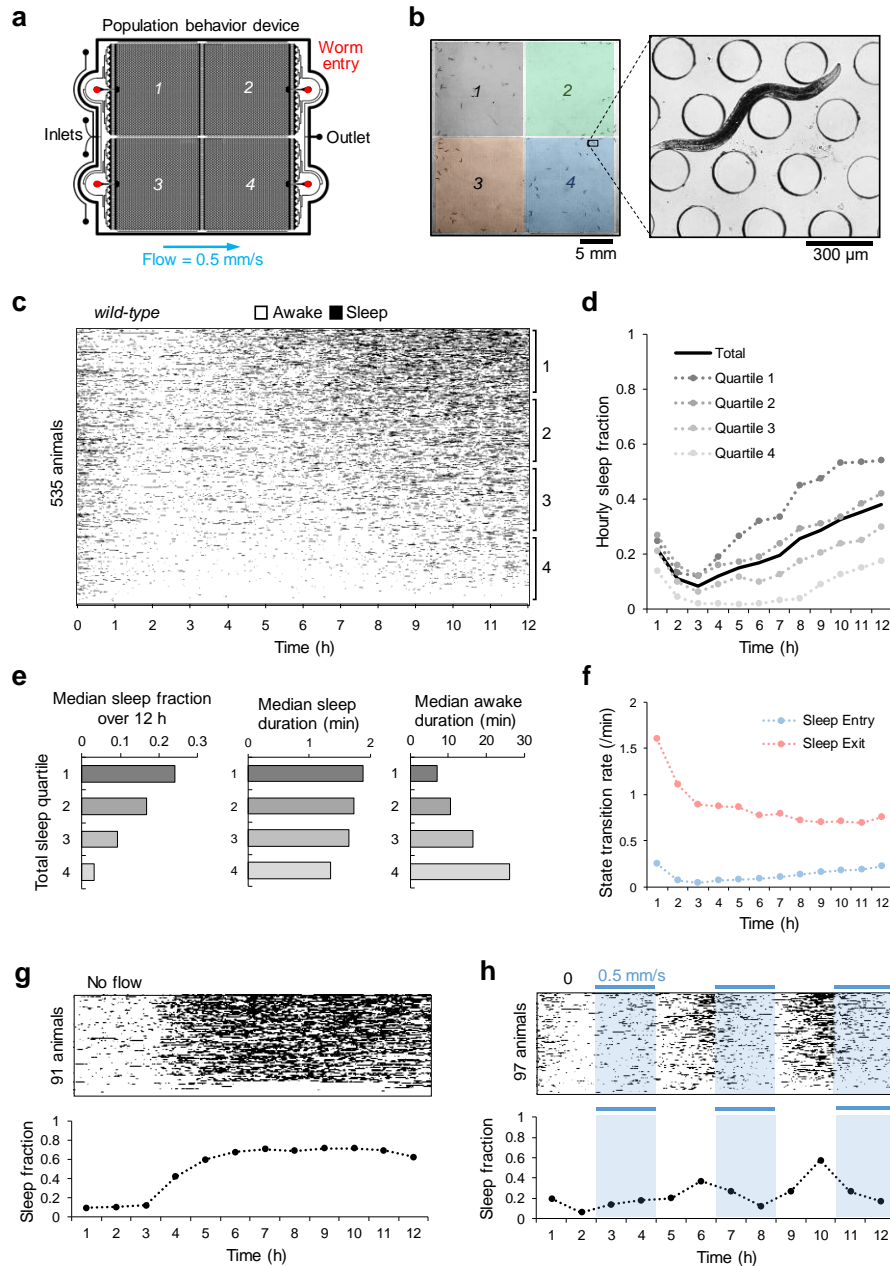


Figure 19. Young adult sleep in wild-type *C. elegans* in “Population behavior” microfluidic devices

(a) Schematic of the “Population behavior” microfluidic device, including multiple inlets to switch fluids, four worm entry ports to introduce separate worm populations, and a flow outlet. (b) Image frame of a device containing about 100 animals, 25 in each of four separated 16 mm x 15 mm arenas. Awake animals roam freely between 200 μm diameter microposts (inset). (c) Heatmap of sleep events (black) over 12 h, sorted by total sleep fraction ($n = 535$ animals). (d) Hourly sleep fraction for all animals from c and grouped into four quartiles by their total 12 h sleep fraction as in c (quartile 1 = most sleep). (e) Median sleep fraction, sleep bout duration, and awake bout duration from data in c, separated by total sleep quartiles as in c. (f) Sleep entry/exit transition rate plotted during each hour of experimentation from data in c. (g) Effect of stationary fluid on sleep behavior over 12 h ($n = 91$ animals). Heatmap of sleep events shown above, and mean hourly sleep fraction below. (h) Effect of pulsed buffer flow on sleep behavior over 12 h ($n = 97$ animals). Fluid flow alternated between moderate flow (0.5 mm/s) or no flow every 2 h. Heatmap of sleep events shown above, and mean hourly sleep fraction below.

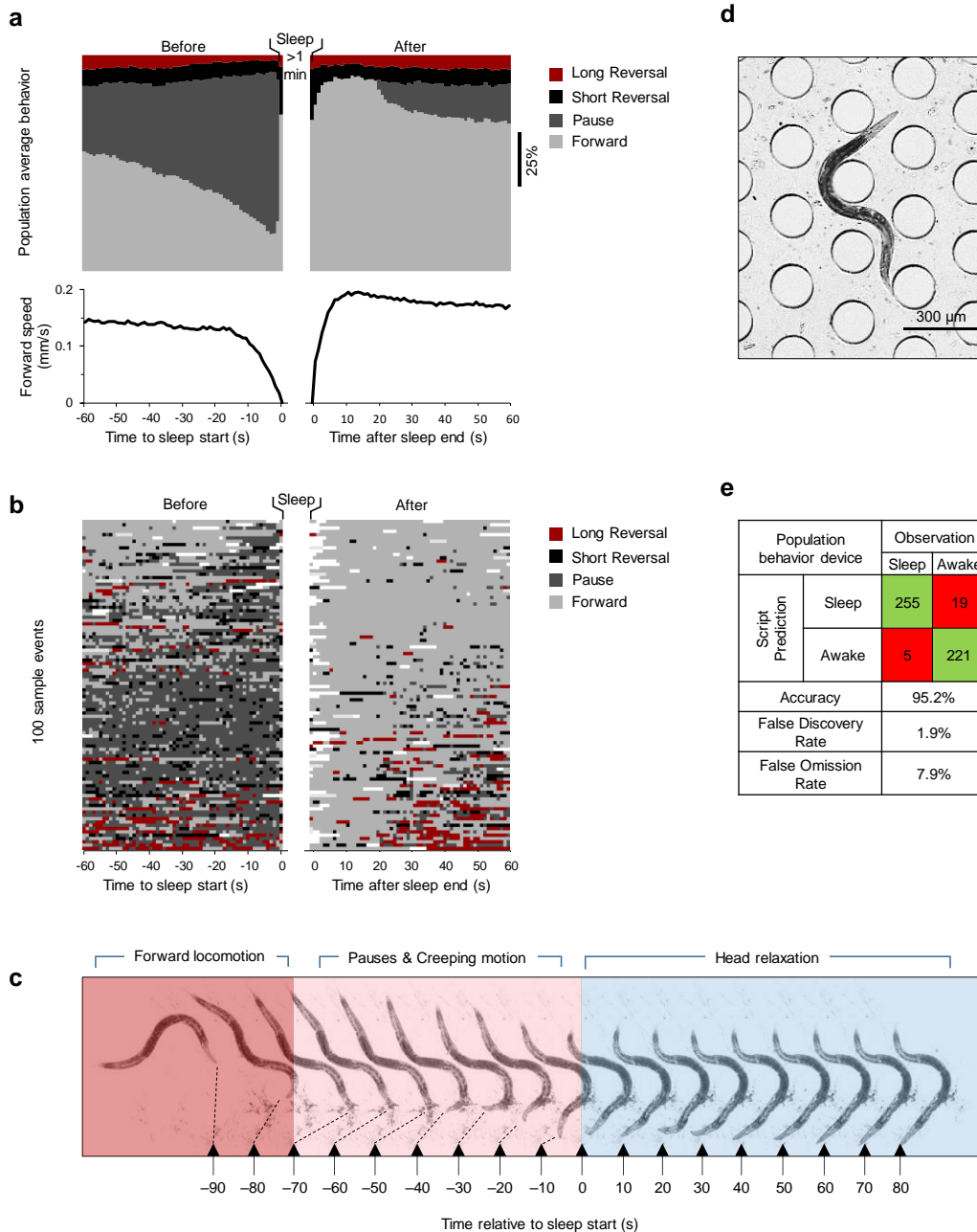


Figure 20. Spontaneous adult sleep transitions in microfluidic devices

(a) Distribution of behavior probability and average speed in the 60 s before and after a sleep bout of at least 1 minute. Data are from 697 wild-type (N2) animals observed for 12 h (4359 qualified bouts, 32% of all sleep bouts >60 s). Examples exclude sleep bouts that preceded or followed another sleep bout within 60 s. (b) Ethogram of behavior state of 100 randomly selected animals in the 60 s before and after a sleep bout, sorted such that animals with more frequent forward behavior pre-sleep are at the top, and with more prevalent turning behavior at the bottom. White coloring denotes unknown behavior. (c) Montage of an animal transitioning between awake forward motion (red), pausing/creeping motion (pink) and sleep with characteristic head relaxation (blue). (d) Image of a sleeping animal in the microfluidic device. Head exhibits straight posture, as opposed to curling around posts as seen in awake animals. (e) Table of accuracy verification for automatic sleep tracking in the "Population behavior device".

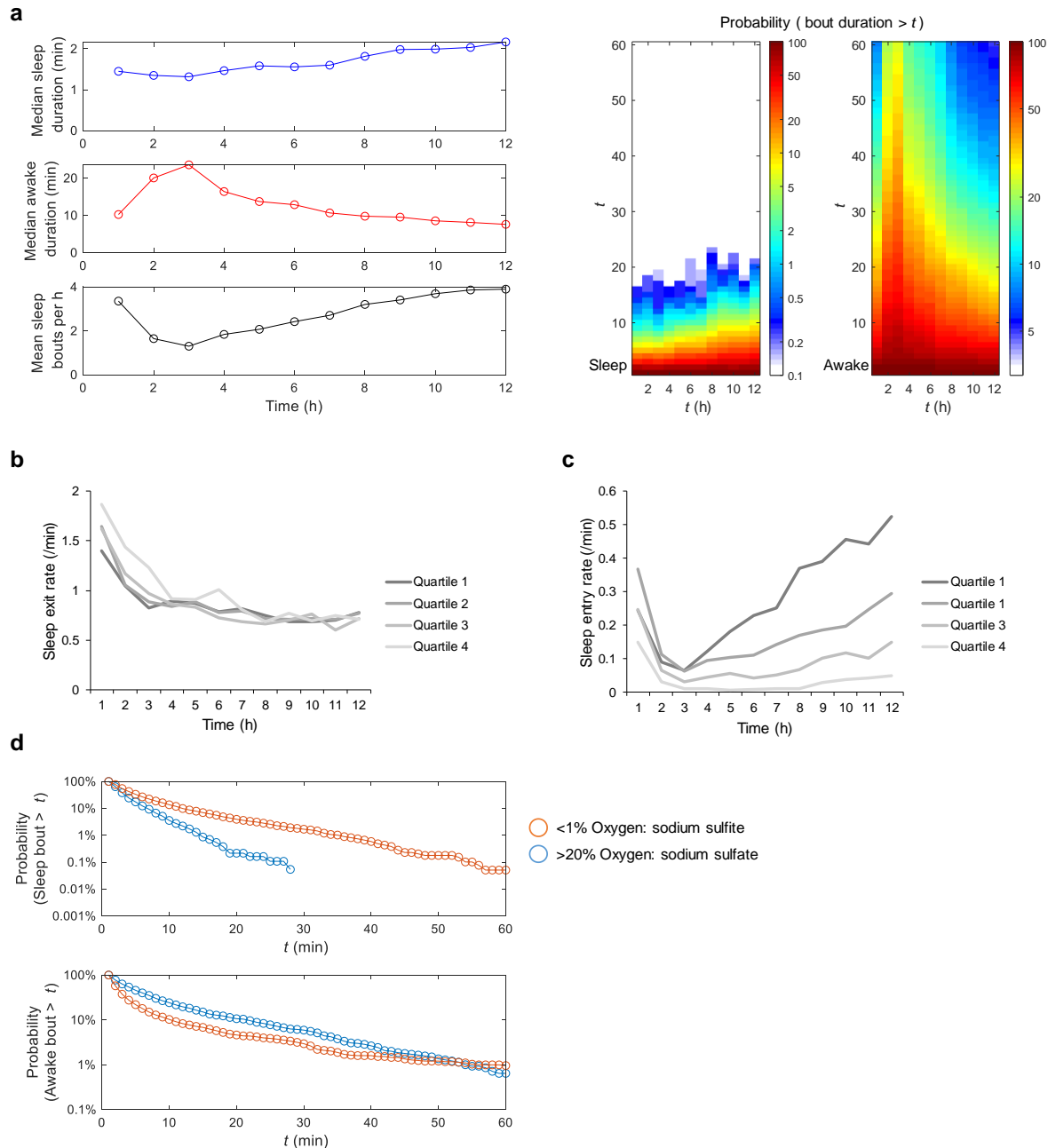


Figure 21. Characteristics of spontaneous wild-type adult sleep and wake periods

(a) Dynamics of sleep behavior over 12 h from Fig. 19c. Median sleep bout duration, median awake bout duration, and average number of sleep bouts plotted per hour. Heatmap shows probability (%) of sleep and awake bout durations greater than the specified times. (b) Sleep exit rate (average transitions per minute) as in Fig. 19f for each total sleep quartile in Fig. 19d,e, showing little inter-quartile variation from most sleep (quartile 1) to least sleep (quartile 4). (c) Sleep entry rate for each total sleep quartile in Fig. 19d,e, showing large inter-quartile variation across wild-type animals. (d) Sleep and awake bout duration distributions for high and low oxygen from data in Fig. 19a, plotted as probability of durations larger than the specified times. Low oxygen increases sleep duration and frequency, and shortens awake periods.

Environmental and sensory effects on sleep dynamics

Sleep entry and exit are sensitive to environmental conditions and sensory input. To test the role of sensory input on sleep, we first assessed the effect of flow in the microfluidic environment, comparing sleep amounts with a moderate flow rate (0.5 mm/s), no flow, and periodic pulsing of flow conditions (**Fig. 19g,h**). Without flow, sleep fraction was similar to moderate flow conditions for the first 3 h, but rose dramatically from 12% to 42% around 3 h and remained high for the duration of the 12 h experiment (**Fig. 19g**). To test whether resumption of flow would return sleep fraction to baseline rates, we pulsed flow every 2 h, alternating between 0.5 mm/s flow or no flow. Again, sleep fraction remained low for the first 3 h regardless of flow condition, then sleep fraction became flow-dependent, increasing after about 30 mins without flow and decreasing sharply when flow was resumed (**Fig. 19h**). Under static conditions, animals can deplete the microfluidic environment of oxygen (Huang and Lin, 2018; Suda et al., 2005), and hypoxia has been shown to induce sleep behavior (Kim and Jin, 2015) especially in starved animals (Skora et al., 2018).

We therefore assessed the role of oxygen in adult sleep in microfluidic devices. With continuous flow of 0.5 mm/s, a hypoxic buffer (<1% O₂, 30 mM sodium sulfite (Jiang et al., 2011)) significantly increased total sleep fraction (48% ± 1.1%, P<0.0001) compared to the same solution reoxygenated to >20% O₂ (16% ± 1.3%) (**Fig. 22a-c**). During hypoxia, 13% of sleep bouts were >10 min long, including some bouts lasting hours, compared to only 3.5% in the reoxygenated buffer (**Fig. 21d**). Notably, hypoxia increased sleep fraction only after 4 h in the device (P<0.0001, **Fig. 22c**), in line with past results

suggesting that starvation and hypoxia work together to promote sleep behavior (Skora et al., 2018). The rapid rise in sleep behavior after 4 h mimicked a similar rise in static no-flow conditions (**Fig. 19g**), suggesting that gentle flow replenishes oxygen to suppress sleep behavior.

Because feeding state impacts arousal (Chao et al., 2004; Ezcurra et al., 2016) and starvation may regulate the impact of hypoxia on sleep (Skora et al., 2018), we next assessed the role of feeding and satiety on adult sleep dynamics within our microfluidic chamber (**Fig. 22d-f**). The presence of bacterial food (NA22 *E. coli*) suppressed total 12 h average sleep fraction ($3.8\% \pm 0.6\%$, $P < 0.0001$) compared to S. Basal control ($33\% \pm 0.5\%$) (**Fig. 22e**). Serotonin, which mimics the feeding response (Horvitz et al., 1982), presented at a moderate concentration of $10 \mu\text{M}$ similarly reduced total sleep fraction ($8\% \pm 1.1\%$, $P < 0.0001$) compared to control buffer conditions. Whereas bacterial food suppressed sleep continuously for 12 h, serotonin suppressed sleep for ~ 9 h. Similarly, a moderate behaviorally attractive food odor (Chuang and Collins, 1968) ($1.1 \mu\text{M}$ diacetyl) suppressed total sleep fraction compared to control buffer ($28\% \pm 0.9\%$, $P < 0.0001$), although to a lesser extent than food or serotonin. Diacetyl suppressed sleep fraction up to hour 9 ($P < 0.0001$), consistent with adaptation to the odor over hours (Larsch et al., 2015; Matsuura et al., 2009) (**Fig. 22f**). Animals also showed increased hourly sleep fraction when starved on a plate without food prior to entry to the microfluidic environment (**Fig. 23a**). These results suggest that adult sleep behavior in microfluidic devices is driven in part by feeding state and perception of hunger.

To observe how sensory information influences sleep, we tested wild-type animals and three sensory mutants (**Fig. 22g-i**) loaded into separate arenas of each “Population behavior” device (**Fig. 19a**). Since the odorant diacetyl reduced sleep (**Fig. 22f**), we tested *odr-10* mutants, which lack the diacetyl receptor normally present in the AWA sensory neurons and should not perceive this odor. In the presence of 1.1 μM diacetyl, *odr-10* mutants exhibited a higher total sleep fraction ($40\% \pm 1.0\%$, $P < 0.0001$) compared to wild-type ($28\% \pm 1.2\%$) (**Fig. 22h**), and similar to wild-type animals in control conditions (**Fig. 23b**). In diacetyl, *odr-10* mutants showed a significant increase in hourly sleep fraction compared to wild-type only up to 6 h (**Fig. 23c**), after which habituation to the odor may reduce its influence. Sensory deficient *tax-4* mutants lack a cyclic GMP-gated ion channel necessary for signal transduction in many sensory neurons (Komatsu et al., 1996) and are defective in multiple sensory behaviors, failing to respond to temperature or to water-soluble or volatile chemical cues. However, *tax-4* is not present in AWA neurons; hence, diacetyl-mediated sleep suppression should be preserved in this mutant. Indeed, while *tax-4* showed a moderate decrease in total sleep fraction ($20.7\% \pm 1.0\%$, $P < 0.0001$) compared to wild-type over 12 h in 1.1 μM diacetyl, no significant differences in hourly sleep fraction were observed except during the first hour (**Fig. 22i**). Strong suppression of early quiescence bouts in hour 1 in *tax-4* animals (4% vs. 21%, **Fig. 23d**) suggests that sensory information other than from AWA neurons contributes to elevated quiescence in the first hour. Animals transferred into microfluidic devices experience a novel mechanical environment, including gentle touch of the microposts and continuous fluid flow. While gentle touch deficient *mec-4* mutants showed a slightly lower total sleep fraction than wild-type ($24\% \pm 1.0\%$ vs. $28\% \pm 1.2\%$, $P < 0.05$), *mec-4* mutants had no

significant difference in first hour sleep fraction compared with wild-type (18% vs. 21%, **Fig. 23d**), suggesting that any sensory information leading to elevated initial quiescence did not come from the *mec-4*-expressing touch receptor neurons ALM, AVM, or PLM. Together, these data demonstrate the role of sensory information in sleep regulation, and the testing of multiple mutants at once in multi-arena microfluidic devices to investigate regulators of sleep dynamics.

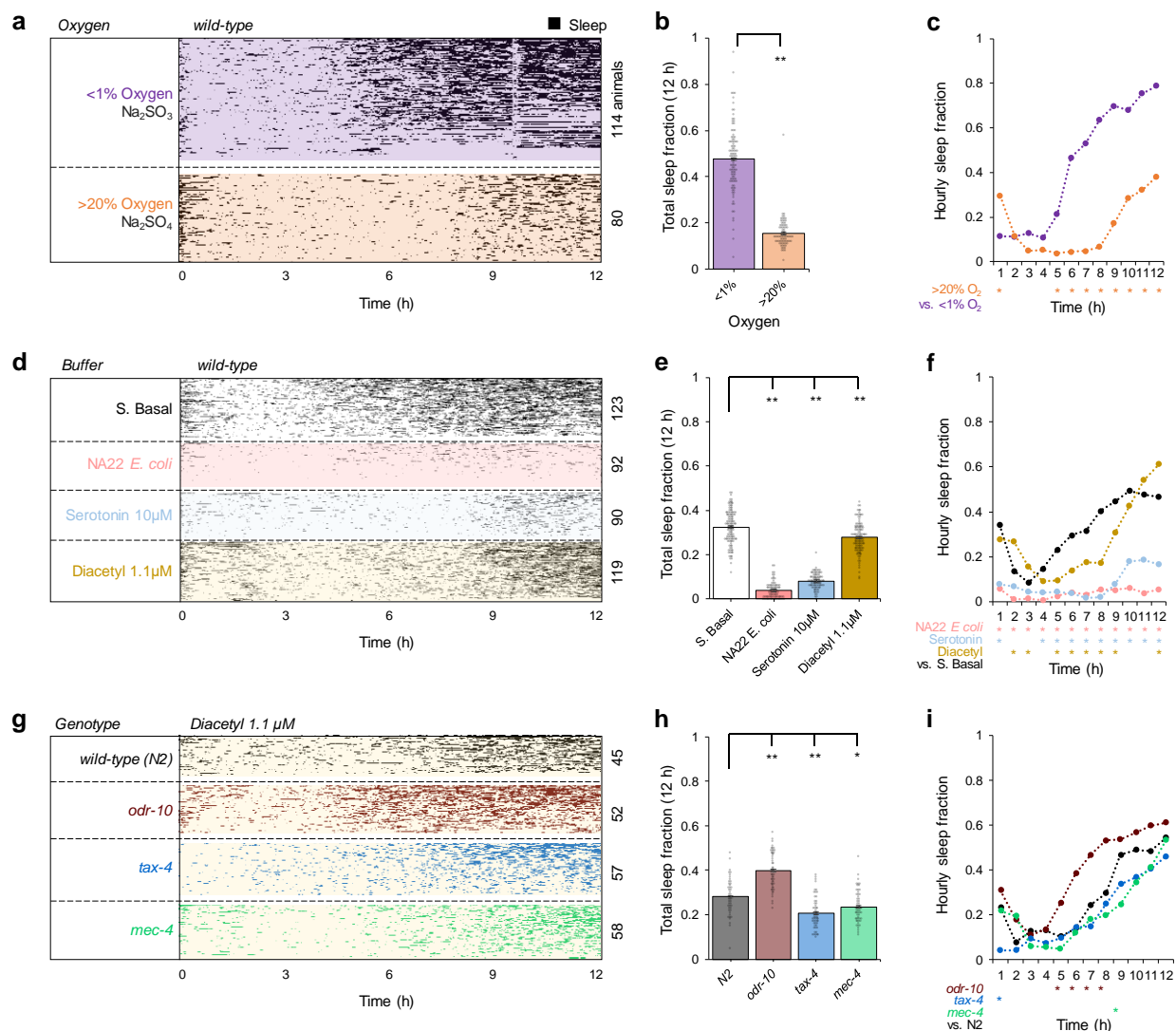


Figure 22. Effects of oxygen, feeding, food signals, and sensory input on young adult sleep dynamics

(a) Effect of hypoxia on sleep dynamics ($n = 80$ – 114 animals). Within each group, animals (heatmap rows) are sorted by total sleep fraction. (b) 12 h total sleep fraction assessing effect of hypoxia on sleep behavior from a with bars representing population mean \pm s.e.m. and points indicating individual animals. (c) Hourly sleep fraction from data in a. (d) Effect of feeding and food signals comparing sleep behavior in S. Basal buffer vs. bacterial food (NA22 *E. coli*, OD600 = 0.35), serotonin 10 μ M to mimic feeding response, and a food odor diacetyl 1.1 μ M ($n = 90$ – 123 animals). (e) 12 h total sleep fraction assessing feeding effect on sleep behavior, as in panel b. (f) Hourly sleep fraction from data in d. (g) Sensory mutant sleep behavior assessed in diacetyl 1.1 μ M ($n = 45$ – 58 animals). (h) 12 h total sleep fraction assessing effect of sensory mutations on sleep behavior, as in panel b. (i) Hourly sleep fraction from data in g. Statistics for all plots were performed using one-way ANOVA with Bonferroni's correction for multiple comparisons. For 12 h total sleep fraction plots (b, e, h): ** $P < 0.0001$; * $P < 0.05$. For hourly sleep fraction (c, f, i), significance is noted for * $P < 0.0001$ as indicated within data of that hour.

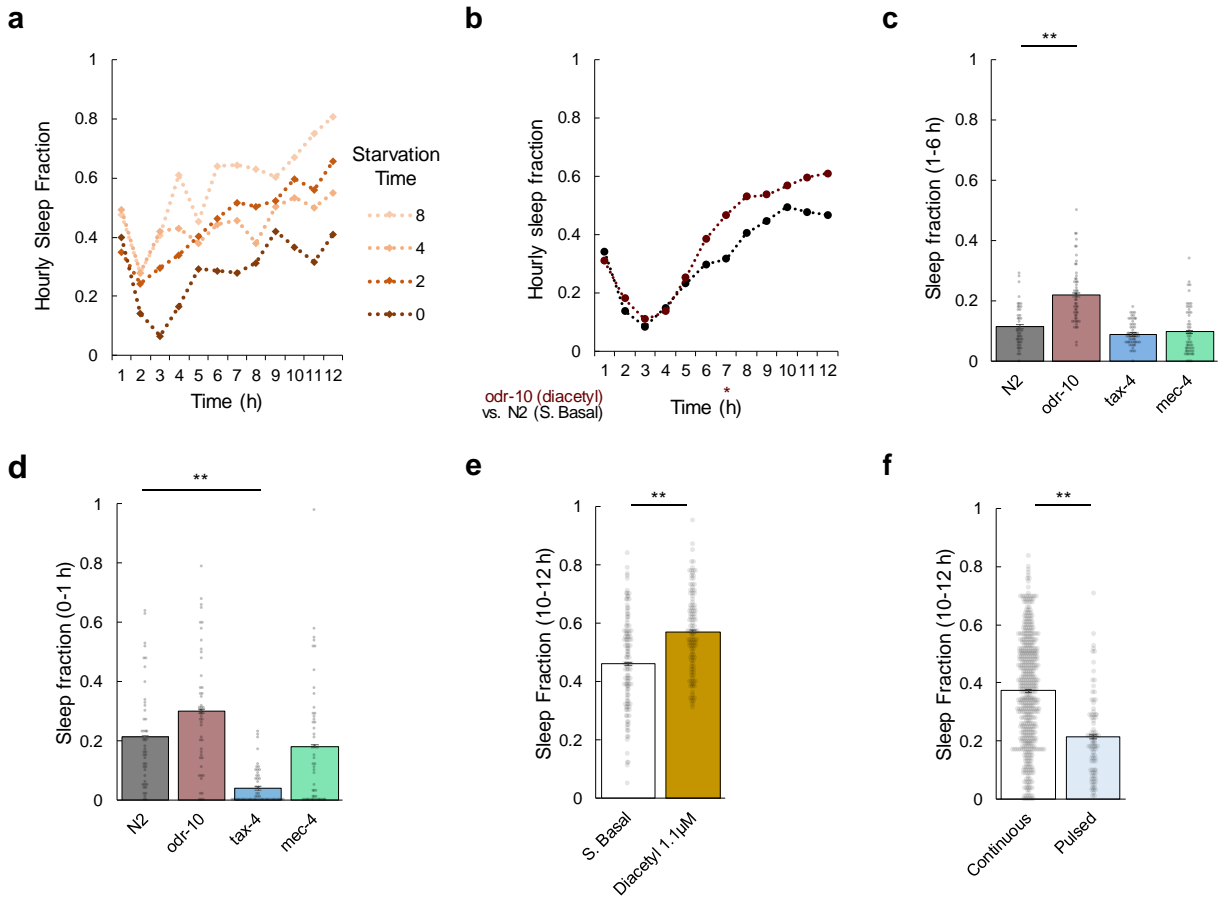


Figure 23. Comparisons of sleep fraction among specific groups and time ranges

(a) Hourly sleep fraction comparison following wild-type starvation times from 0–8 h on agar dishes prior to loading in the microfluidic device. (b) Hourly sleep fraction comparison between *odr-10* mutants under constant exposure to 1.1 μ M diacetyl from Fig. 22g to N2 animals in S. Basal from Fig. 22d. (c) Total sleep fraction from hour 1 to hour 6 from data in Fig. 22g. (d) Total sleep fraction during the first hour of experiment from data in Fig. 22g. (e) Total sleep fraction during hours 10–12 comparing S. Basal and diacetyl conditions from data in Fig. 22d. (f) Total sleep fraction during hours 10–12 comparing continuous flow of S. Basal (Fig. 19c) vs. pulsed flow while flow is on (Fig. 19h). Statistics for b were performed using one-way ANOVA with Bonferroni's correction for multiple comparisons. For hourly sleep fraction, significance is noted for * $P < 0.0001$ as indicated within data of that hour. Statistics for plots c and d were performed using one-way ANOVA with Bonferroni's correction for multiple comparisons; ** $P < 0.001$. Statistics for plots e and f were performed using an unpaired two tailed t-test; ** $P < 0.001$.

Automatic sleep tracking, chemical stimulation, and neural imaging

To understand how neural activity changes during sleep cycles, we designed smaller “Neural imaging” microfluidic devices, containing a single 3 mm x 3 mm arena with the same micropost array as the “Population behavior” device (**Fig. 24a**) but sized to fit the entire field of view at 5x magnification on an epifluorescence microscope (**Fig. 24b**). Sleep behavior of animals was tracked using brightfield illumination every 10 s, using frame subtraction similar to previous methods (Nagy et al., 2014b) (**Fig. 25a,b**), and correctly identified sleep bouts with 93.4% agreement with human observers (**Fig. 25c**). Wild-type *C. elegans* sleep dynamics in the small “Neural imaging” device were equivalent to the larger “Population behavior” devices, dropping from 18% to 6% over the first 3 h, then steadily rising to 50% by 12 h, despite a faster flow velocity in the neural imaging microfluidic device (15 mm/s vs. 0.5 mm/s) (**Fig. 24c**).

The “Neural imaging” device provides fast temporal control of chemical stimuli, capable of reproducible fluid switching in <0.5 s (**Fig. 25d**) without disturbing natural behaviors. We assessed arousal from sleep by testing sensory responsiveness of sleeping and awake wild-type animals to aversive 10-s pulses of 1 mM copper chloride solution. Sleep or wake states were determined by average pixel movement 5 s prior to stimulation (**Fig. 24d**), which was significantly higher in awake vs. sleeping states ($5.8 \pm 1.5 \mu\text{m}/\text{frame}$ vs. $0.32 \pm 0.07 \mu\text{m}/\text{frame}$, $P < 0.05$) (**Fig. 24e**). We recorded the time elapsed between chemical onset and the first reversal movement. Responses in a sleep state were about eight times slower ($6.0 \text{ s} \pm 1.2 \text{ s}$, $P < 0.001$) than in an awake state ($0.76 \text{ s} \pm 0.14 \text{ s}$), consistent with an increased threshold for sensory responsiveness in sleeping young

adult animals (**Fig. 24f**) as has been shown during lethargus to mechanical and chemical stimuli (Raizen et al., 2008a).

RIS interneuron activity correlates with the onset of developmentally-timed sleep (Turek et al., 2013) and quiescent behavior in adults (Steuer Costa et al., 2019). To demonstrate neural imaging during spontaneous sleep-wake cycles in the microfluidic device, we recorded activity in the RIS interneuron expressing GCaMP3 (**Fig. 24g**) in freely moving animals while simultaneously assessing movement behavior. As expected, RIS activity increased at the onset of adult sleep (**Fig. 24h**).

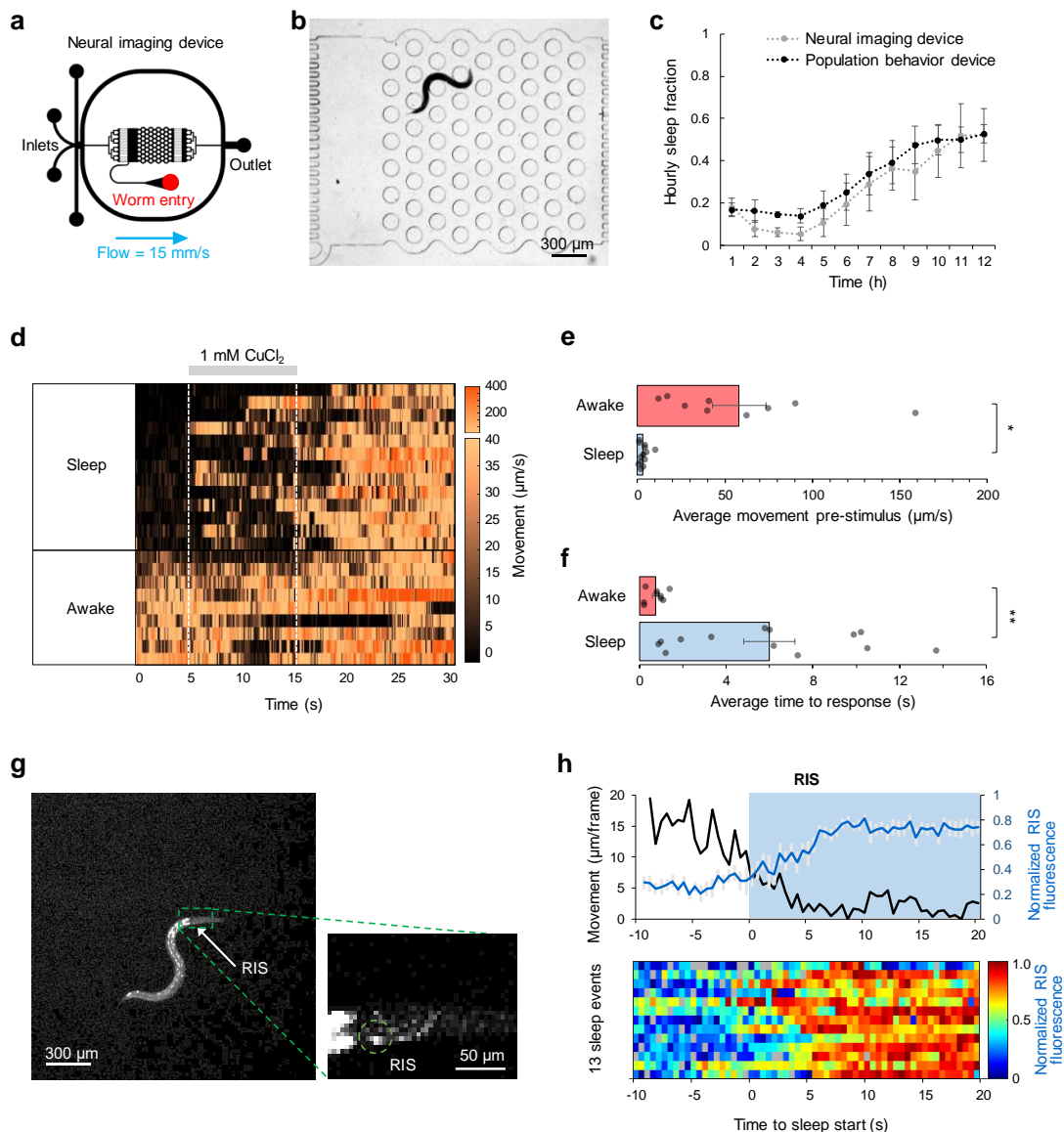


Figure 24. Neural activity during sleep and awake states in “Neural imaging” microfluidic devices

(a) Design of microfluidic device for closed-loop sleep assessment, chemical stimulation, and neural imaging. Device contains a single 3 mm x 3 mm arena. (b) Individual animals tracked using pulsed brightfield illumination ($\lambda = 520\text{--}550\text{ nm}$). An awake animal is shown. (c) Comparison of sleep fraction in “Neural imaging” ($n = 7$ animals) vs. “Population behavior” ($n = \sim 100$ animals) devices. (d) Heatmap showing movement of AIB neuron per frame (0.1 s) across 22 pulsed stimulation trials (rows). Stimulus of 1 mM CuCl_2 applied between 5–15 s during each 30 s trial. Data sorted by average movement 5 s prior to stimulus, indicating the sleep/awake state for each recording. (e) Average movement pre-stimulus (0–5 s) in d grouped by sleep or awake state ($n = 13$ Sleep, $n = 9$ Awake). (f) Average time to a reversal or avoidance behavior response in d for sleeping and awake animals. Statistics for e and f performed using an unpaired two-tailed t-test; ** $P < 0.001$; * $P < 0.05$. (g) Image of an animal expressing GCaMP in the RIS neuron during sleep onset. (h) Average RIS neuron fluorescence ($n = 13$ traces) and average neuron centroid movement per frame (2 fps). Neural activity normalized to minimum and maximum intensity of each RIS neuron trace during the 30 s before and after the awake to sleep transition at time = 0 s. Heatmap of all neural recordings shown below.

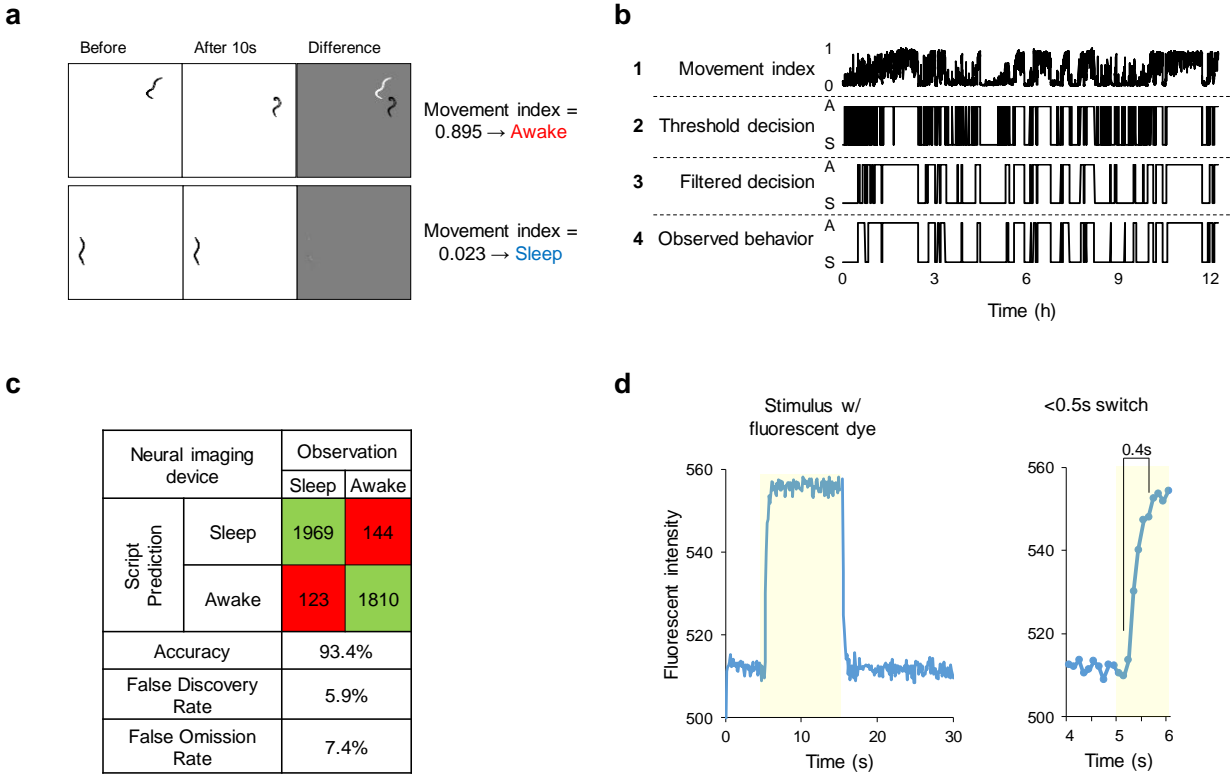


Figure 25. Sleep detection in “Neural imaging” microfluidic devices

(a) Examples of the frame subtraction method for sleep detection showing awake and sleep cases. Movement Index represents fraction of body pixels moved between 10 s frames. (b) Schematic of sleep decision processing in a single wild-type animal over 12 h in S. Basal, top-to-bottom: 1. Movement Index (MI); 2. Result of threshold $MI < 0.125$; 3. Temporal-filtering for 5 consistent state frames (40 s); 4. Human observation. (c) Table of accuracy verification for automatic sleep tracking in the “Neural imaging” device. (d) Raw fluorescent pixel intensity measurement over time from a 5–15 s pulse of fluorescent dye, switching within 0.4 s (right).

Closed-loop stimulation and neural imaging of a reversal circuit

An increased threshold for sensory responsiveness during sleep suggests sleep-dependent modulation to neural activity in *C. elegans*, either in sensory responses to stimulation, or in downstream interneurons or motor neurons. For example, diminished ASH sensory neuron activity to aversive chemical pulses (1 mM copper chloride) was reported during lethargus states in developmentally-timed sleep (Cho and Sternberg, 2014). However, it is unclear whether sensory-level modulation occurs during adult sleep as well. Since adult sleep is not synchronized across animals, or within an individual, we developed a closed-loop system that monitors sleep state every 10 s and triggers a stimulation and neural recording when user-programmable conditions are met (**Fig. 26a**). Here, we chose to stimulate one minute after a sleep state transition, allowing a 15-minute recovery period between stimulation trials (**Fig. 26b**). Brief pulses of blue light excitation were used for fluorescent imaging to measure calcium activity during each 30-s trial (**Fig. 26c**), as strong blue light can cause arousal by itself (Edwards et al., 2008), and sleep state was monitored by behaviorally-neutral green light.

We measured neural responses to 10-s pulses of 1 mM copper chloride in the ASH sensory neurons over 12 h in individual animals. A typical closed-loop experiment with 15-minute recovery per stimulation showed no significant adaptation (**Fig. 27a**) and recorded about one sleep and one awake response per hour over >10 hours (**Fig. 26d**, **Fig. 27b**). ASH neurons responded strongly and consistently to each copper chloride pulse, regardless of sleep or awake state during stimulation (**Fig. 26e,f**).

Since ASH chemosensory responses were equivalent in sleep and awake states, the elevated arousal threshold in sleep could result from diminished activity in interneurons, motor neurons, or in the muscles themselves. ASH is directly presynaptic to AVA, but also has secondary connections through AIB, AVD, and RIC interneurons (**Fig. 27c**). As AIB shares a gap junction with the sleep-inducing neuron RIS, and ablation of AIB reduces long reversals (Gray et al., 2005), we recorded AIB and AVA neural activity in sleep and awake states in response to 1 mM copper chloride. Neural responses in AIB were not significantly different between awake and sleep states (**Fig. 26g,h**). In contrast, animals in sleep states had diminished AVA responses, increasing average relative GCaMP fluorescence 55% when awake and 23% when asleep ($P < 0.05$). AVA neural responses were also delayed relative to the copper pulse (**Fig. 26i,j**), consistent with delayed and shortened reversal behaviors (**Fig. 24f**). AIB activity often increased before reversal behavior in sleeping animals but coincided with reversal responses in awake animals (**Fig. 27d**), suggesting a sleep-dependent behavioral delay downstream of (or bypassing) AIB and presynaptic to AVA, that contributes to the apparent arousal threshold increase in sleeping animals.

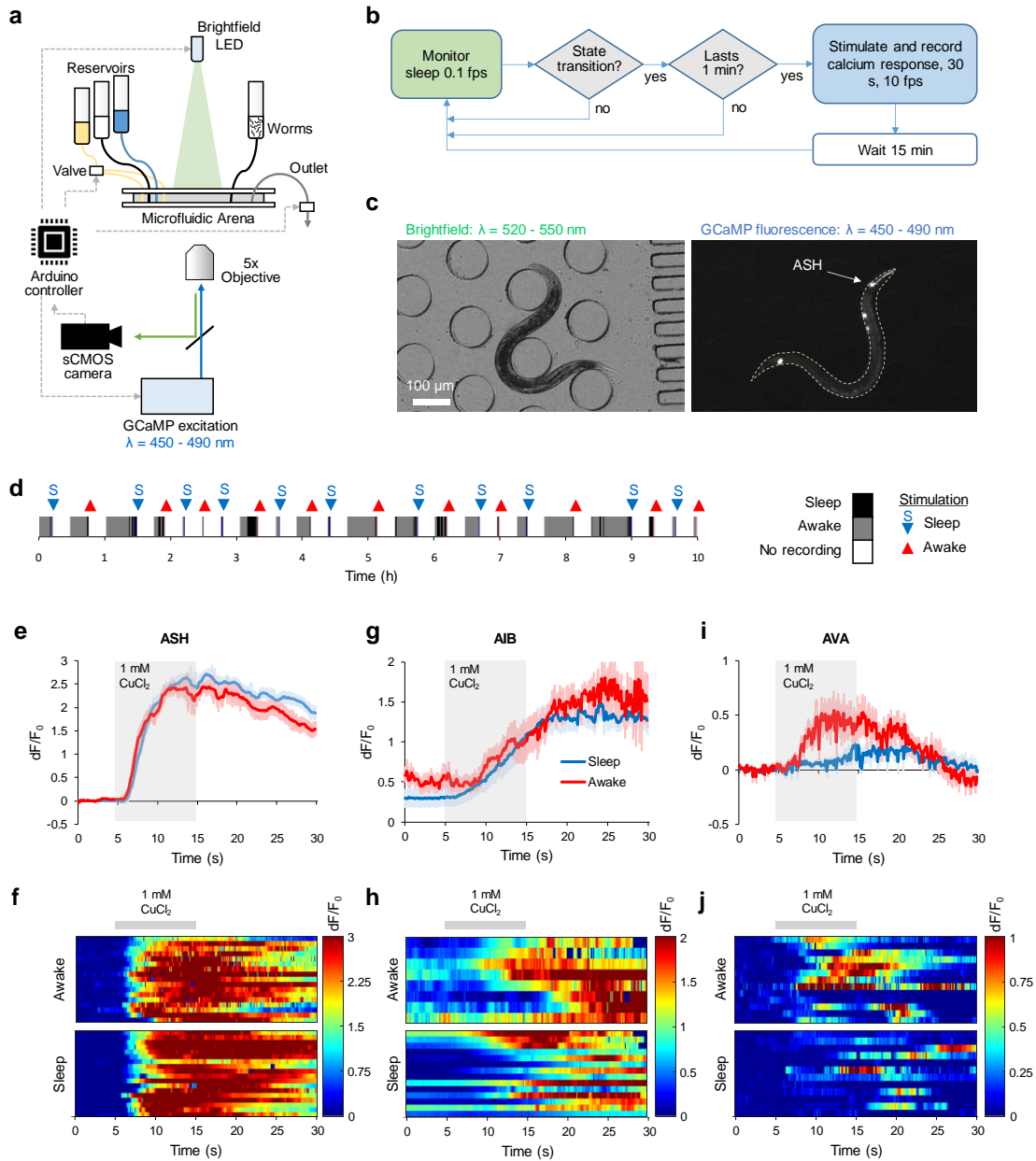


Figure 26. Closed-loop stimulation and neural recording in individual free-behaving animals

(a) Schematic of closed-loop neural recording set-up for sleep/awake response tracking. Video recording, valve control, and LED triggering are controlled through an Arduino microcontroller. Brightfield images are used for tracking sleep behavior and fluorescent images are used for measuring calcium transients. Image capture, sleep/awake determination, and chemical stimulation are controlled by computer in a closed-loop without user intervention. (b) Decision process schematic of closed-loop experiment. Green (brightfield) and blue (fluorescent) shading of decision nodes indicate corresponding illumination source during frame capture. (c) Brightfield ($\lambda = 520\text{--}550\text{ nm}$) and fluorescent ($\lambda = 450\text{--}490\text{ nm}$) images of a freely-moving animal expressing GCaMP in ASH neurons. (d) Example showing behavior and neural recording trials in a typical 10 h closed-loop experiment. (e) Average ASH neural responses in Sleep and Awake states to 10 s CuCl_2 pulses ($n = 18$ Sleep, 17 Awake). (f) Heatmap of individual ASH responses from e. (g) Average AIB neural responses in Sleep/Awake states to 10 s CuCl_2 pulses ($n = 13$ Sleep, 8 Awake). (h) Heatmap of individual AIB responses from g. (i) Average AVA neural responses in Sleep/Awake states to 10 s CuCl_2 pulses ($n = 13$ Sleep, 12 Awake). (j) Heatmap of individual AVA responses from i.

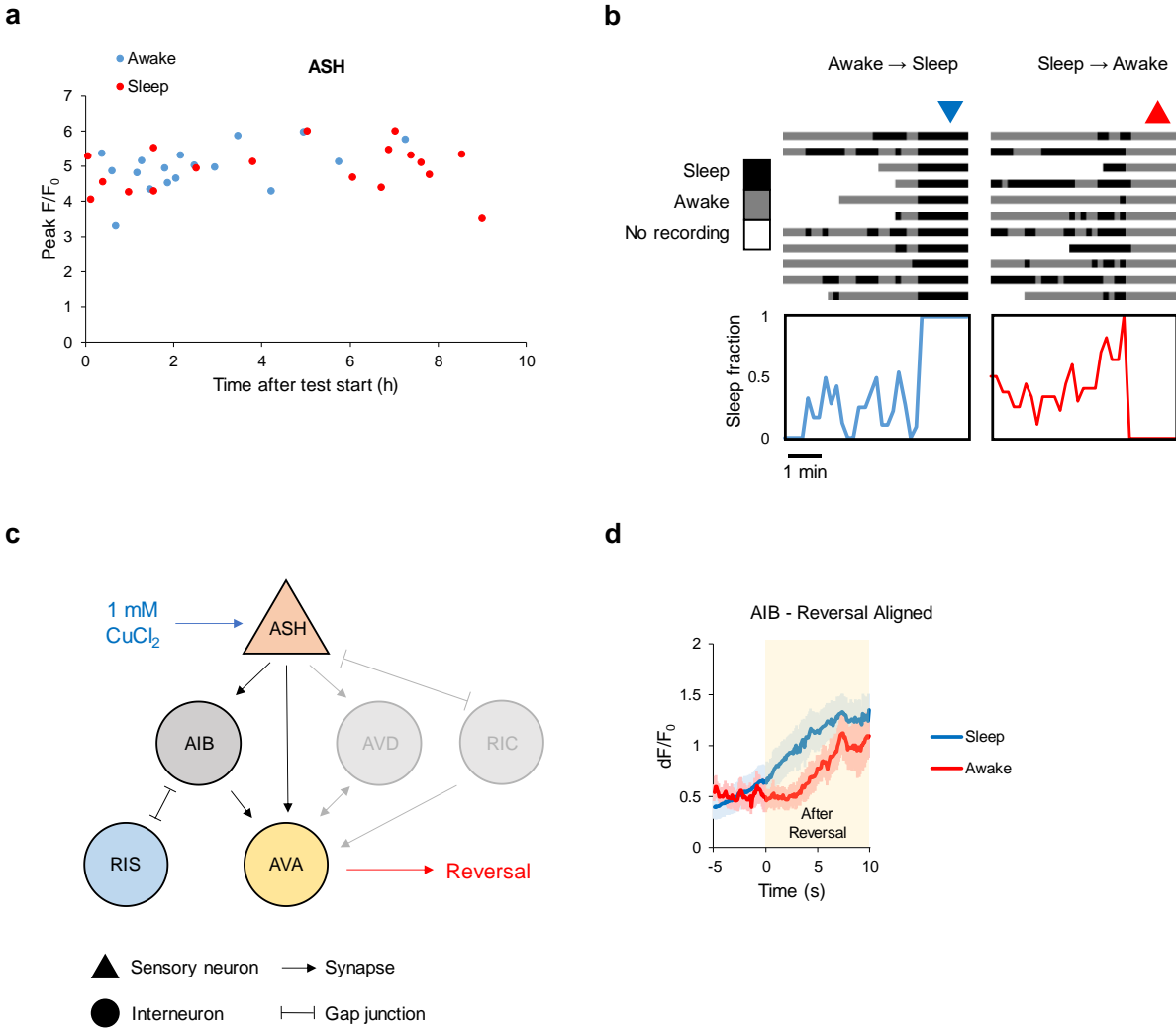


Figure 27. Neural imaging during closed-loop experiments

(a) Peak F/F_0 response in ASH to 1 mM $CuCl_2$ plotted by time after animal started closed loop experiment. Data from **Fig. 26e,f**. (b) Pre-stimulus behavior up to 5 min before 22 stimulation trials during an example closed-loop experiment from **Fig. 26d**. Average sleep fraction is plotted below. (c) Neural connections linking copper chloride sensation for reversal behavior upon arousal by stimulus in sleep and wake states in **Fig. 26e-j**. (d) Neural activity from AIB aligned to point of first reversal response. Data from **Fig. 26g,h**. Lines indicate mean response; shading s.e.m.

Discussion

C. elegans sleep has been studied previously during developmentally-timed transitions (lethargus) and after induction by satiety or various stresses. Spontaneous adult sleep has been technically more difficult to assess. Here we present two microfluidic tools to study spontaneous or induced sleep in young adult *C. elegans*, complimentary to related methods for use in larval stages. Both devices share the same microfluidic arena geometry and elicit the same sleep dynamics over 12 h. The larger “Population behavior” device quantifies sleep dynamics to compare up to four different environmental conditions or genetic perturbations at once. The smaller “Neural imaging” device identifies sleep state-dependent neural circuit modulation, by correlating simultaneous recordings of sleep behavior and stimulated neural responses in individual animals. Unlike previous microfluidic methods, these designs used microposts structured for natural crawling behavior without mechanical constriction. Some features of spontaneous adult sleep in this environment differ from previous studies, such as the role of oxygen and flow, and it remains to be seen whether this mode of sleep behavior is unique to stress-induced sleep states previously observed.

Adult quiescence behavior in these devices displays several common behavioral characteristics of sleep. For example, quiescent adults exhibit: (1) an increase in arousal threshold to an aversive chemical stimulus by a delay in behavioral response (**Fig. 24f**), (2) rapid sleep reversibility upon changes in fluid flow (**Fig. 19h**), and (3) a characteristic relaxed posture (**Fig. 20c,d**). Additionally, our results are consistent with (4) a

homeostatic sleep response, in which periods of elevated sleep are followed by reduced sleep, and vice versa. For example, sleep suppression by diacetyl odor elicited a higher fraction of rebound sleep at later times ($46\% \pm 1.4\%$ for control buffer alone vs. $57\% \pm 1.4\%$ for diacetyl in hours 10-12, $P < 0.0001$, **Fig. 22f, 22e**). Conversely, elevated sleep during static fluid conditions later suppressed sleep after flow was resumed ($21\% \pm 1.9\%$ for pulsed flow vs. $37\% \pm 0.8\%$ for continuous flow in hours 10-12, $P < 0.0001$, **Fig. 19h, S3f**).

Sleep behavior is sensitive to environmental conditions presented in microfluidic devices. For example, fluid flow in the microfluidic environment is important for maintaining a fresh and constant environment, and cessation of flow increased sleep behavior dramatically. Static fluid conditions may decrease mechanical stimulation, deplete nutrients and oxygen, and increase concentrations of byproducts and CO_2 . As sleep behavior increased dramatically in a hypoxic buffer, oxygen depletion by animals may be a primary factor driving elevated sleep in static microfluidic conditions. While hypoxia increased sleep behavior only after 4 h in freely-behaving animals, sudden hypoxia was shown to suppress most spontaneous neural activity across the whole brain of trapped *C. elegans* in 16 h starved animals (Skora et al., 2018). In mammals, intermittent hypoxia may cause excessive sleepiness (Sanfilippo-Cohn et al., 2006), but also cause disturbed and superficial sleep with frequent waking via chemoreceptor reflex pathways (Laszy and Sarkadi, 1990). Thus, there is an interplay between arousing and somnolent environmental cues. Further studies in *C. elegans* may be useful to distinguish between

these contrasting hypoxic effects and to understand the role of sleep in regulating metabolic and energetic systems.

Sleep behavior is also dependent on the availability of food. Wild-type animals in buffer without a food source increased their sleep fraction over time away from food, due to both increased “sleepiness” extending sleep bouts and increased “sleep pressure” shortening awake bouts. Feeding bacteria in the device suppressed sleep bouts for at least 12 h, whereas presenting exogenous serotonin to mimic feeding response or a food odor suppressed sleep for 9 h, consistent with adaptation to these food signals.

Sensory neural activity also modulates sleep. For example, sleep suppression by diacetyl was absent in *odr-10* mutants that lack only the diacetyl odor receptor and are unable to detect this odor. Sensory information also contributes to the initial elevated sleep behavior seen in the first hour of testing as animals acclimate to the microfluidic environment. The general sensory mutant *tax-4* suppressed first-hour sleep whereas mechanosensory-deficient *mec-4* animals did not, suggesting that sensation of flow or gentle touch of microfluidic structures do not contribute to early sleep behavior. Instead, other *tax-4* dependent sensation, such as from various thermo- and chemosensory neurons (Komatsu et al., 1996), may be involved in detecting the novel microfluidic environment.

We observed freely-moving behavior and simultaneous activity of several neurons during sleep and awake states. We verified the RIS interneuron is active at the onset of spontaneous adult sleep, as has been shown during developmentally-timed lethargus

sleep (Turek et al., 2013). The automated closed-loop stimulation system operates without user intervention, resulting in unbiased measurements of neural responses during alternating sleep and awake bouts within the same animal. The ability to record response differences in individuals over time is particularly important given the wide variation in sleep dynamics observed across individual animals. Isogenetic animals, even when raised on the same plate from the same parental animal, exhibited total sleep fractions varying from zero to nearly one half over 12 h. Given the sensitivity of adult sleep to oxygen, feeding state, chemicals, and likely other sensory stimuli, it is possible that even animals cultured identically experience slight variations in their sensitivity to these parameters to induce differences in their sleep dynamics. The ability to automatically monitor individual animals allows for longitudinal studies capturing dozens of events per animal to identify intra-animal differences in sensory processing irrespective of population-wide variation in sleep patterns.

An increased arousal threshold in sleeping animals suggests modulation to sensorimotor neural circuit activity in *C. elegans* during sleep. Responses of the AVA command interneurons, which are required for backward locomotion (Gray et al., 2005; Piggott et al., 2011; Zheng et al., 1999) were indeed diminished and delayed during adult sleep, coinciding with delayed behavioral responses. Similarly, diminished AVA activity was previously observed during lethargus (Cho and Sternberg, 2014). However, sensory responses in ASH neurons were not modulated by sleep state in adults, in contrast to the lower ASH responses observed in larval stages during developmentally-timed sleep (Cho and Sternberg, 2014), suggesting that spontaneous adult sleep is a distinct phenomenon.

The first layer interneuron AIB, which shares synaptic connection with ASH and the command interneuron AVA, and also with sleep-induction neuron RIS, also showed no sleep-dependent difference in response. Together, these results suggest that modulation in sensory processing that leads to reduced arousal response in sleep occurs presynaptic to AVA, either from ASH, AIB, or another interneuron (**Fig. 27c**), or perhaps via neuropeptides from other sources. One possibility is that sleep increases arousal threshold predominately by diminishing the efficacy of monosynaptic shortcuts to the command interneurons (here, ASH to AVA), whereas sensory information is preserved to first layer interneurons (such as AIB) to allow for rapid arousal from more salient polymodal stimuli from multiple sensory neurons. However, animal survival should benefit from maintaining rapid arousal to potentially harmful stimuli, yet for aversive ASH sensory neurons, this does not appear true. Alternatively, the dampened brain state apparent in sleep⁷⁴ may broadly suppress activity in premotor interneurons like AVA, increasing arousal thresholds equally to all types of sensory input. These data highlight the hierarchy of altered sensorimotor processing, and further study of response modulation to additional sensory stimuli should provide insight into the architecture and mechanisms of sleep-dependent modulation of arousal.

These flexible microfluidic systems for studying adult sleep in *C. elegans* are applicable to any neuron, stimulus, environment, and genetic perturbation for thorough assessment of sleep behavior and underlying neural responses. For example, it will be informative to compare neural responses in various sleep modes, including hypoxia and starvation-induced sleep as shown here, as well as heat shock and satiety-related sleep. Microfluidic

devices are easily customized to different animal sizes by adjusting arena post geometry, for example, to observe L4 animals in lethargus transition stages in developmentally-timed sleep. Other types of oxidative or metabolic stress (such as by chemical oxidants or varying food quality), or sleep disruption via mechanical stimulation or light, can be applied using the same microfluidic devices and tracking methods. Overall, this platform can be used to uncover molecular and neural circuit pathways underlying altered sensation during sleep, toward establishing connections between nematode sleep and associated regulatory mechanisms and human sleep disorders.

Methods and Materials

Strains and *C. elegans* culture

All *C. elegans* strains were maintained under standard conditions on NGM plates and fed OP50 *E. coli* bacteria seeded onto each plate. Wild-type animals were Bristol strain (N2). The following mutant strains were used: CB1611, *mec-4* (*e1611*); FK103, *tax-4* (*ks28*); CX32, *odr-10* (*ky32*). Neural imaging strains expressing GCaMP in specific neurons were: (ASH (Larsch et al., 2013)) CX10979, *kyEx2865* [*Psra-6::GCaMP3*; *Pofm-1p::GFP*]; (AIB) DCR6035, *olals94* [*Pinx-1::GCaMP6f*; *Punc-122::GFP*]; (AVA) QW607, *zfls42* [*Prig-3::GCaMP3::SL2::mCherry*] gifted by the Alkema lab; (RIS) AQ4064, *ljEx1119* [*Pflp-11::GCaMP3::SL2-tagRFP*; *unc-122::rfp*]. To make the RIS imaging line, a 2643 bp region immediately upstream of the ATG of the *flp-11* gene was amplified, similar to previously reported methods (Turek et al., 2016). This promoter was shown to express consistently in RIS and occasionally in other neurons (Turek et al., 2016). To synchronize for age, we picked L4 larval stage animals one day prior to experimentation such that all animals tested were at the young adult stage.

To prepare for an experiment, animals were isolated by genotype and/or arena placement and then transferred to an unseeded NGM plate immediately prior to experimentation. The plates were then flooded with the control buffer used for their respective experiment: S. Basal buffer (100 mM NaCl, 50 mM KPO₄; pH 6.0) for unfed behavioral experiments, S. Medium buffer (1 L S. Basal, 10 mL 1 M potassium citrate pH 6.0, 10 ml trace metals solution, 3 ml 1 M CaCl₂, 3 ml 1 M MgSO₄) for feeding experiments, or a saline buffer (80 mM NaCl, 5 mM KCl, 20 mM D-glucose, 10 mM HEPES, 5 mM MgCl₂, 1 mM CaCl₂; pH 7.2) for copper chloride stimulus experiments.

Animals were then collected into loading tubing using a 1 mL syringe prior to injection into the microfluidic arena.

Microfluidic device fabrication

“Population behavior” and “Neural imaging” microfluidic devices were fabricated as previously described (Lagoy and Albrecht, 2015). Briefly, transparency photomasks were printed at 25,000 dpi from designs sketched using DraftSight CAD software. SU-8 mold masters were prepared on silicon wafers using standard photolithography techniques, and microfluidic devices were fabricated by pouring degassed PDMS (Sylgard 184, Dow Corning) onto the mold and heat curing. Individual devices were then cut out and punched to provide inlet and outlet flow. A hydrophobic glass substrate was created by vapor deposition of tridecafluoro-1,1,2,2-tetrahydrooctyl trichlorosilane (TFOCS, Gelest) and then sealed reversibly to the microfluidic channels. An upper glass slide, with holes drilled over inlet and outlet ports with a diamond-coated drill bit, was sealed above the device, which was then placed into a metal clamp.

Stimulus preparation

All odor dilutions were freshly prepared on the day of experimentation. NA22 *E. coli* stock solutions were prepared using previously described methods (Keil et al., 2017). Briefly, NA22 *E. coli* was cultured, concentrated into pellet form, and suspended in S. medium buffer. A stock solution was diluted to an OD600 of 7.0, and 50 µg/ml of kanamycin was added to prevent bacteria from growing. Chemical solutions were prepared at a 1:20 dilution of stock solution and filtered through a 5 µm filter. Diacetyl (1.1

μM) was prepared from a 10^{-3} dilution (11 mM) stock solution immediately prior to experimentation. Serotonin was prepared by dissolving serotonin creatine sulfate monohydrate powder (Sigma). Sodium sulfite (Sigma) solution was prepared moments before experimentation at 30 mM. We found that a 30 mM sodium sulfite solution would remain at nearly 0% oxygen with stirring for 12 h and without stirring for 5 days (Ocean Optics Neofox O₂ probe kit), so the testing solution would be devoid of oxygen for entire 12 h testing period. The control solution of sodium sulfate was created by allowing for reoxygenation of the sodium sulfite solution for greater than 5 days. For neural imaging experiments, 1 mM copper chloride solution was prepared the day of the experiment using copper chloride powder.

Microfluidic device setup

Microfluidic devices were cleaned, assembled, and degassed in a vacuum desiccator for 30–60 min prior to experimentation. Degassing devices accelerates the absorption of air bubbles within the device. For behavioral experiments, devices were filled with 5% (w/v) Pluronic F127 through the outlet port to prevent bacterial and molecular absorption by passivation of the microfluidic surfaces and to minimize bubble entrapment via its surfactant properties. Neural imaging devices were filled with control buffer alone. Reservoirs of loading solutions were prepared as previously described (Lagoy and Albrecht, 2015), purging the reservoir system of bubbles and connecting the tubing into the inlets of the device. Once flow was properly established, animals were gently loaded into their respective arenas and allowed to roam for 15–20 min prior to

experimentation. For neural imaging experiments, a control valve is used to switch between stimulus and control buffer conditions within 0.5 s (**Fig. 25d**).

Population behavior imaging and identification of sleep events

Videos of population behavior were captured using a 6.6 MP PixelLink FireWire Camera at 1 fps for 12 h with an image resolution of ~30 pixels/mm. Videos were processed after experimentation as previously described using MATLAB to extract behavioral data (Albrecht and Bargmann, 2011), and then further analyzed to identify sleep events. A minimum sleep entry window of 20 s and exit window of 5 s were used to quantify state transitions. To verify accuracy in parameters for sleep detection, user observed behavioral state was compared to script calculated state on randomly chosen 60 second traces of an individual animals (**Fig. 20e**). All behavior data was collected using “Population behavior” devices with four 16 mm x 15 mm arenas capable of housing ~25 animals per arena for simultaneous study.

Neural calcium imaging, sleep detection and data analysis in closed-loop system

Closed-loop neural imaging videos were acquired at 5x magnification (NA=0.25) with a Hamamatsu Orca-Flash 4.0 sCMOS camera using MicroManager/ImageJ software. The system has a green ($\lambda = 520\text{-}550$ nm) LED mounted overhead to provide pulsed brightfield illumination for tracking animal behavior and a Lumencor SOLA-LE solid-state lamp pulsed to excite GCaMP during fluorescence calcium imaging. To achieve autonomous experimentation for a closed-loop system, custom Arduino, MicroManager, and ImageJ scripts work together to control illumination timing, image

acquisition, stimulus delivery, and sleep/wake state identification. An Arduino Uno microcontroller was programmed to control fluidic valves through a ValveLink 8.2 (AutoMate Scientific) controller and to control illumination sources for brightfield and fluorescent imaging. A MicroManager script allows the user to configure all camera and illumination settings prior to experimentation as well as all testing conditions for sleep assessment. Once the experiment is underway, the script initiates brightfield image capture at the desired framerate, and analyzes movement compared with the prior image in real time to determine the animal's behavioral state. If the current state and timing match the desired and preprogrammed conditions for neural imaging, the script initiates a fluorescence image stack recording and communicates with the Arduino via serial commands to control epifluorescence illumination and chemical stimulation with the desired timing.

Tracking of behavior of a single animal in the closed-loop neural imaging system was done using brightfield illumination with images captured at 0.1 fps. The current sleep/awake state of the animal was determined by an ImageJ script which calculates a movement index for each frame, represented as the fraction of body pixels moved since the previous frame, ranging from 0 – 1 (**Fig. 25a**). A sleep state was defined as movement below the empirically-optimized threshold (0.125) for 3 consecutive frames (i.e., for 20–30 s). Optimization of detection parameters was done by maximizing accuracy from user observed behavioral states to script calculated states (**Fig. 20e**). One minute of consistent sleep or wake state frames were used to increase confidence in the animals' current state before neural imaging.

Calcium imaging was performed on freely-moving animals as previously described

(Larsch et al., 2013) using lines expressing GCaMP in selected neurons. Neural activity was recorded in RIS neurons at 2 fps with no stimulation from the closed-loop system, however motion was detected post-processing to identify sleep bouts. Calcium imaging in ASH, AIB, and AVA neurons was performed at 10 fps, using closed-loop stimulation to record responses to 10 s chemical stimulation from 5–15 s within a 30 s trial. Videos were analyzed for neural fluorescence and locomotion using NeuroTracker software in ImageJ, which tracks the position of the neuron over time and integrates fluorescent intensity of the soma using a 4 x 4 pixel box. Fluorescence (F) was normalized by dividing by the initial baseline fluorescence in the first 4 s of each trial before stimulation (F_0). As AIB fluorescence may not be at baseline at the beginning of each trial, baseline AIB intensity was determined for each animal across all trials, and individual AIB traces were excluded when animals engaged in reversal behavior immediately prior to stimulation.

Statistical analysis

Statistics were performed using one-way ANOVA with Bonferroni's correction for multiple comparisons or an unpaired two-tailed t-test when specified for 2 sample comparison, using the Statistics and Machine Learning Toolbox in MATLAB. Data represented as mean \pm s.e.m. unless otherwise stated. In behavioral experiments, animals were excluded when valid behavioral tracks comprised <8% of recording time, indicating an animal not viable or not present during the test. In neural recordings, the top and bottom 1% of instantaneous fluorescent intensity was removed to reduce noise in peak fluorescence calculations.

Chapter 5: Associative learning in a microfluidic format in *C. elegans*

The beginning stages of this project were developed with the help of an undergraduate student Dina Abedi who worked in the Albrecht lab during the summer of 2017 in the Research Experience for Undergraduates (REU) program at WPI. She assisted with experimental preparation on many of the assays assessing associative learning. Additionally, the associative learning project in the Albrecht lab was begun by a former masters student Karen Tran, who first translated the butanone enhancement assay partially in gradient microfluidic devices (Karen Tran, 2015). This work was supported in part by an NSF IGERT award (DGE 1144804) and by the Burroughs Wellcome Fund Career Award at the Scientific Interface, and the National Science Foundation NSF CBET 1605679 and EF 1724026, NIH R01DC016058.

Abstract

Our capacity to learn changes over time, during development and aging, and in specific neurological diseases. Studying the genetic and neuronal factors that affect memory capacity can potentially help devise memory preservation strategies. However, learning assays in mammals or larger invertebrates can be laborious, low-throughput, and difficult to achieve reliable results. The quick life cycle and large brood size of *C. elegans* allow for rapid assessment of learning capabilities in many animals. Researchers have utilized *C. elegans*' natural inclination to taxis to attractive odors or away from aversive odors to determine behavioral preferences, setting a baseline for naïve behavior, and have used these preference measurements to observe instances of learned behavior. However, the majority of these assays are developed on agar dishes. The open environment of the agar dish and variable diffusion effects of odorants in the agar limit experimental robustness. To address these limitations, we have developed a series of robust associative learning assays in the model organism *C. elegans* contained entirely in the microfluidic environment based on their behavioral responses to chemical cues in microfluidic devices. Microfluidics allow us to maintain precise stimulus control to pre-program odorant exposure to test behavioral preference, and institute a stable environment for reliable measurement. We have found that in young adult *C. elegans*, combining a neutral chemical (the conditioned stimulus, CS) with bacterial food (an attractive unconditioned stimulus, US) causes animals to become strongly attracted to the formerly neutral CS, demonstrating associative learning.

Introduction

Despite their simple nervous system, *C. elegans* are able to navigate towards desirable locations based on environmental cues such as water soluble attractants/repellents, temperature, pH, and oxygen levels (Bono and Maricq, 2005; Troemel, 1999). Learning and memory have been behaviorally demonstrated in *C. elegans*. Rankin et al. (Rankin et al., 1990) were the first to demonstrate non-associative learning and memory in *C. elegans*. They showed that *C. elegans* was capable of learning in response to a mechanical stimulus. They demonstrated this habituation style learning was both short-term and long-term lasting over 24 hours. The first study demonstrating learned behavior in *C. elegans* came from (Hedgecock and Russell, 1975) who demonstrated that *C. elegans* had associative learning based on thermotaxis to temperatures they were grown at. Since these first studies, a number of associative learning paradigms have been tested including pairing 1-propanol with HCl in an aversive olfactory learning experiment (Amano and Maruyama, 2011) as well as pairing butanone with food in a positive learning assay (Torayama et al., 2007). Additionally, the effects of associative learning on a neural level have been studied by (Stetak et al., 2009) demonstrating that changes on the interneuron level were necessary for memory consolidation however not on the sensory neuron level.

Many methods have been developed to assess learning in *C. elegans* making use of the organism's capability for various forms of taxis. When studying chemotaxis, commonly, these assays calculate a chemotaxis index by tracking behavioral preference to dissolved odorants on an agar dish, however these assays can be inexact due to variable environmental conditions in an open environment and variable concentrations of

dissolved odorants in the agar. To combat these issues, we translated the butanone enhancement assay into a controlled microfluidic environment to present odorants in a consistent fashion and assess behavior. We formed an attraction index based on behavior profiles upon exposure to the paired stimulus. Additionally, our method allows us to do all training and testing in the microfluidic environment, including application of food, to avoid potential damage or variability due to transfer of animals. The microfluidic assay also lends itself to an easy transition for studying neural activity, allowing for functional measurements of changes to a neural circuit upon a learning paradigm.

Results

5.1: Development of new associative learning assay

5.1.1: Translation of the butanone enhancement assay into an all-microfluidic platform

The butanone enhancement assay was first demonstrated by (Torayama et al., 2007), where animals who were pre-exposed to butanone on their feeding plates later showed elevated attraction to butanone compared to animals who had not been exposed to the pairing of butanone and food (**Fig. 28a**). This paradigm of learning is commonly referred to as “associative learning.” While successful, there were a number of potential issues with this assay to be addressed, as well as some positive qualities that should be mimicked in assay developments (**Table 4**). First, naïve response to butanone is slightly attractive, so in the Torayama assay the chemotaxis index for naïve animals who were not trained showed a high baseline, making the learned behavior less convincing and more susceptible to test-to-test variability. Second, their scoring method involved paralyzing animals once they reach an odorant choice, relying on discovery of an odorant as the assessment metric rather than a more robust behavioral phenotype that can be further probed for insight on the learning mechanism. Third, as mentioned previously, plate-based assays lead to variable exposure conditions, again making the experiment susceptible to variability.

In turn, Karen Tran (a former MS student) developed a butanone enhancement assay where testing occurred in a microfluidic gradient device (Karen Tran, 2015) to improve reliability of associative learning assessment. In her assay, animals were selected from plates, placed in micro-centrifuge tubes with the given training condition for one hour,

then loaded to their testing microfluidic device for a 15-20 minute acclimation period prior to testing (**Fig. 28b**). The associative pairing in this assay involved the conditioned stimulus of 1.1 mM butanone paired with an unconditioned stimulus of OP50 *E. coli* (food). The assay also trains animals using 3 other control groups to compare response: “Naïve”, “Food Only”, “Butanone Only” all of whom represent cases without associative pairing. Chemotaxis index is scored based on standards discussed for gradient based assays (**Fig. 2**) in response to a gradient of with the maximum concentration of 11 μ M butanone. Briefly, chemotaxis index is calculated as the difference in animals in the middle 50% of the arena to animals in the outer 25% regions of the arena divided by the total number of animals in the area. In an ideal scenario, pure attraction would result in all animals in the center 50% therefore chemotaxis index would be +1.0. Conversely, pure aversion would result in a chemotaxis index of -1.0. Karen showed that young adult *C. elegans* demonstrate associative learning of butanone to OP50 *E. coli* when pre-trained with the pairing of Butanone and Food (0.54 CI \pm 0.17 s.d., n = 8), showing significantly (*p<0.05) higher chemotaxis than Naïve (0.10 \pm 0.09, n=7), Food only (0.24 \pm 0.14, n=6), and Butanone only (0.02 \pm 0.12, n = 6) groups, recapitulating the Torayama assay (**Fig. 28c**).

Karen’s assay did not come without limitations though. First, the process of training animals had to occur outside of the microfluidic device, as OP50 *E. coli* has a tendency to sediment and clump within the small channels of the device. Despite efforts to keep mixtures well mixed, OP50 proved too difficult to use as a stimulant within microfluidic devices, necessitating their application outside of the device in micro-centrifuge tubes. Loading *C. elegans* into micro-centrifuge tubes can be agitating for animals, potentially

affecting their motility necessary in chemotaxis assessment. Second, because animals take time to acclimate to the microfluidic environment, a 15-20 minute acclimation period had to be installed in between training and testing. This additional time loses potentially valuable insight on potentially the strongest preference demonstrations post-learning, and adds experimental time. Third, the gradient assessment format while applicable to studying chemotaxis, leads to challenging translation of the assay for finding associated neural activity in learning, limiting the assay's potential long-term benefits.

Thus, we developed a pulse-based associative learning assay contained entirely in the microfluidic environment making use of the less clumpy bacterial food source of NA22 *E. coli* (Keil et al., 2017). Wildtype animals showed strong and persistent attraction to a stripe of flowing NA22 *E. coli* bacteria (**Fig. 2d**), indicating its suitability as an unconditioned attractive stimulus. Our method operates similarly to past butanone enhancement assays, presenting animals with an hour of pre-stimulus training solution followed by a brief testing period where the attraction to butanone is assessed in response to 10 μ M pulses of the odorant (**Fig. 28d**). Pulses were applied 30s every 5 min, and were counterbalanced with a light stimulus of 10 nM Diacetyl to neutralize their behavior in native conditions. Animals are loaded in the assay with all necessary solutions situated in their respective channels (**Fig. 28e**), so the acclimation period can occur as animals are being trained with exposure conditions. Using 4-arena microfluidic devices that house ~25 animals per 16 mm x 15 mm arena, we present 2 training solutions per experiment, separating animals and solutions at a central border (**Fig. 28f**). Testing occurs immediately after a 1 h training period, and control of fluidic valves to generate all training and testing stimulation

paradigms are pre-programmed by the user. This allows us to capture data on many animals in a rapid fashion, but also test isogenetic animals from the same generational and culture groups to the training pair and a control training together, identifying any outlier cases. The method also eliminates potential handling issues with animals, as animals are allowed plenty of time to acclimate to the microfluidic environment prior to testing. Lastly, as assessment of attraction in this assay utilizes pulse-assay microfluidics, the assay is more readily translatable to neural imaging assessment.

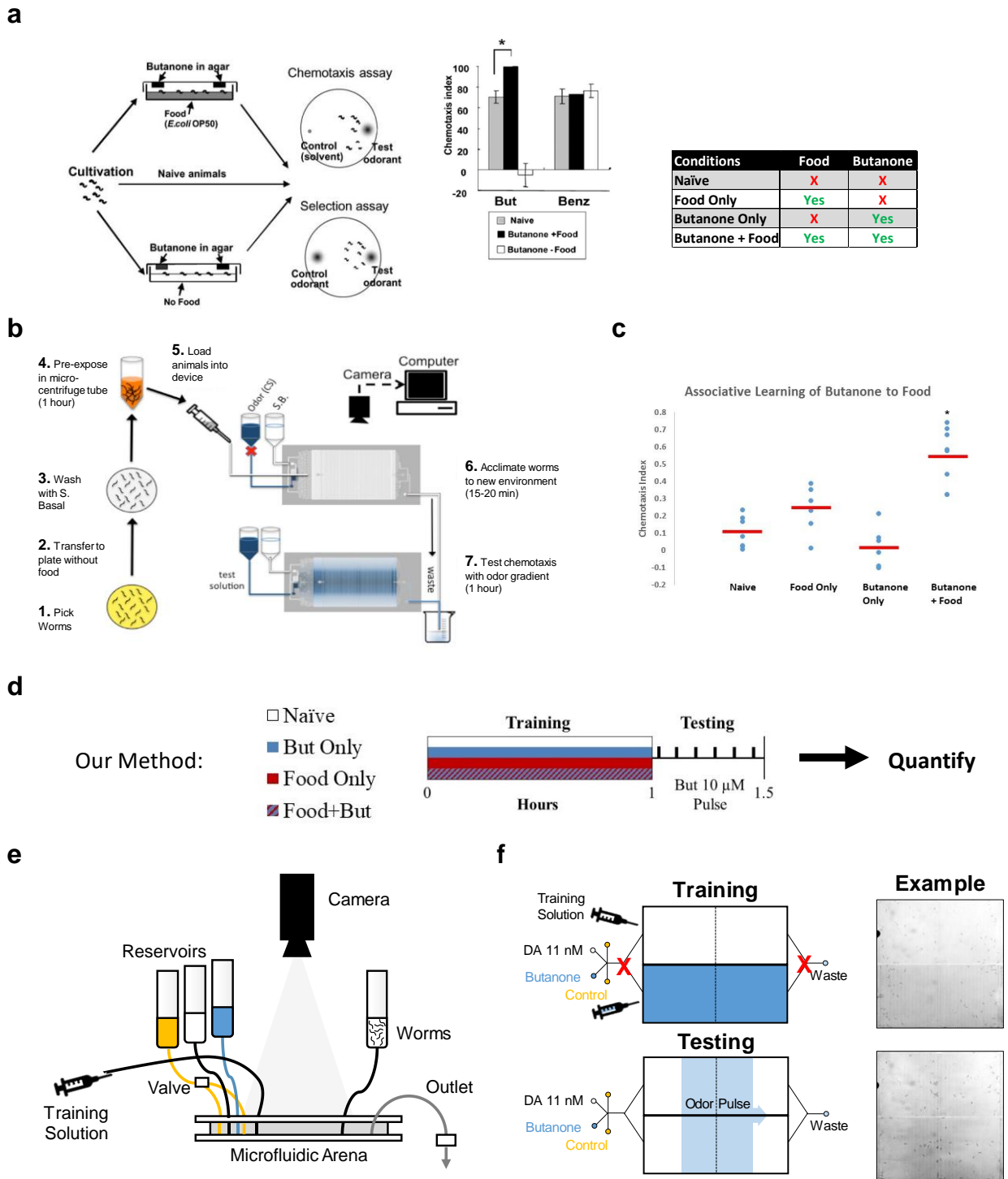


Figure 28. Development of the microfluidic butanone enhancement assay

(a) Schematic and results of the butanone enhancement assay in a plate-based format by (Torayama et al., 2007). Copyright 2007 Society of Neuroscience. (b) Step by step protocol for microfluidic adaption of the butanone enhancement assay by (Karen Tran, 2015). Method involves pre-training in micro-centrifuge tubes followed by animal transfer into a microfluidic device, and testing chemotaxis to a gradient of odor. (c) Results of an associative learning assay of butanone to food by (Karen Tran, 2015). Data points represent per-arena chemotaxis index showing enhanced attraction when animals are trained with butanone + food (n = 6-8 arenas of ~25 animals each condition). (d) Proposed all-in-one microfluidic assay where animals are trained and tested in a butanone enhancement assay without any user intervention or acclimation time. (e) Schematic side-view of the microfluidic system on top with three reservoir inlets (one for S. Medium buffer, one for odorant, and one for control fluid with a 3-way valve to split flow depending on valve actuation. (f) Bird's eye view schematic of the training and testing phases for d with example images. Statistics for c performed using a one-way ANOVA with Bonferroni's correction for multiple comparisons; *P<0.05.

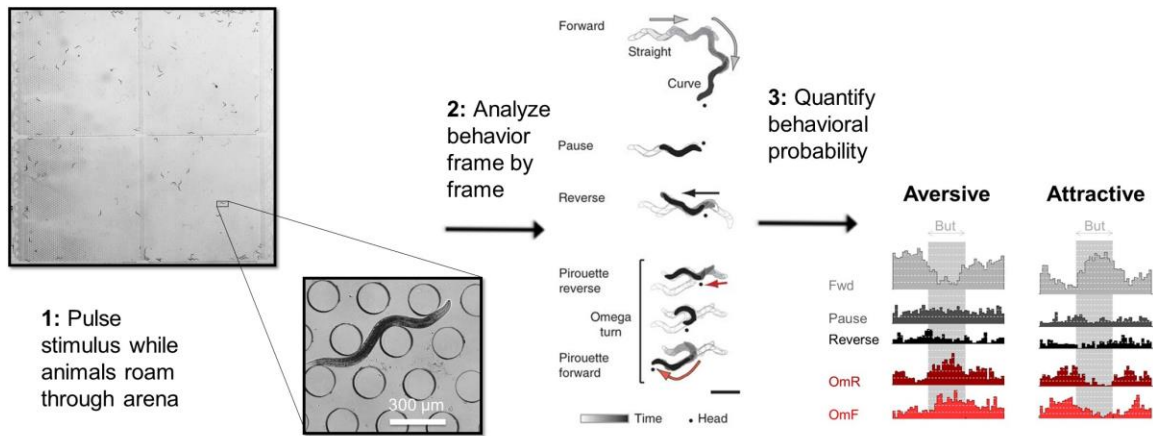
Table 4: Comparison of butanone enhancement assay formats

Format	Pros	Cons
<p>Plate based (Torayama et al., 2007)</p>	<ul style="list-style-type: none"> -Easy assay set up -Location based quantification is simple and clear for odor preferences 	<ul style="list-style-type: none"> -Difficult translation of assay to neural activity measurements -Lacked food alone assessment vs. no food -Baseline attraction is high, less increase in “learned” condition
<p>Microfluidic – Gradient (Karen Tran, 2015)</p>	<ul style="list-style-type: none"> -Mimics commonly used plate-based chemotaxis assay format in controlled environment -Additional study of food only and naïve conditions -Can assess strength of attraction through positional information 	<ul style="list-style-type: none"> -2-part assay requires more animal handling, more room for variability of experience -Gradient assay makes neural activity measurements difficult -Cannot study older animals due to movement deficiencies
<p>Microfluidic – Pulse</p>	<ul style="list-style-type: none"> -Uses controlled environment of microfluidics -Pulse assay formation allows all animals to encounter the stimulus regardless of position -Devices can accommodate testing across ages -Assay format works well for neural imaging assessment -Animals are handled only once, reducing handling concerns 	<ul style="list-style-type: none"> -Use of counterbalancing diacetyl alters control results, changing assay conditions -Instantaneous behavior is more difficult to assess and quantification requires interpretation: less straightforward

5.2: Learning assessment in pulse-based microfluidic butanone enhancement assay

5.2.1: *Quantifying attraction in an automated all-microfluidic pulse-based butanone enhancement assay*

To improve the ability for this assay to be converted into a neural activity assessment, we sought to convert the style of behavior assessment from chemotaxis in a stripe or gradient assay to utilizing a pulse format with behavior assessment. To do so, association to typical “attraction” and “aversion” behaviors were used. The process of analysis is shown in (**Fig. 29**), including an example of behavioral probabilities of an adverse and attracted group to their stimulus odor. An increase in forward motion and decrease in omega turns is seen in attractive behavior, and the opposite is seen in aversive behavior. Behavior was monitored using Arena Worm Tracker software in MATLAB (Albrecht and Bargmann, 2011). An Attraction Index was calculated from population-average forward motion (indicative of attraction) prior to stimulation, during stimulation and after stimulation of the butanone pulse. To balance the index to match the easy to understand scoring of a chemotaxis index (negative = aversive, 0 = neutral, positive = attractive) we also subtract 1 from the index.



$$\text{Attraction Index} = \frac{2 * \text{Fraction of forward motion during middle 10s of stimulus}}{\text{Fraction of forward motion in 10s pre- and post-stimulus}} - 1$$

Figure 29. Analysis schematic of the automated pulse-based butanone enhancement assay

Step-by-step process of analyzing butanone enhancement. After training period, animals are exposed to pulses of butanone in the testing period and roam in the microfluidic environment. Their behavior is classified frame-by-frame using previously described methods (Albrecht and Bargmann, 2011). Probability of behavior is calculated as an average of recorded behaviors during the pulse time. Pulses in the assay last 30s, and the middle 10s of pulse exposure gives a view of how attracted to the present stimulus of butanone animals are. Attraction index is calculated by taking the ratio of forward motion during the middle 10s of stimulus over forward motion pre- and post- stimulus and subtracting 1 to normalize to a more similar scale of the standard chemotaxis index scoring. Horizontal white dashed lines represent 10% probability.

Behavioral schematic in the middle adapted by permission from Springer Nature Customer Service Centre GmbH: Albrecht DR and Bargmann CI. High-content behavioral analysis of *Caenorhabditis elegans* in precise spatiotemporal chemical environments. *Nature Methods* 8(7):599-605 (2011). License Number 4725421152425

5.2.2: Young adults show association of the neutral butanone to food

Wild-type animals were trained by exposure to 1 mM butanone paired with NA22 *E. coli* (bacterial food) for 1-hour in a 4 arena (16 mm x 15 mm each) PDMS microfluidic device, then tested for butanone attraction in the same device by applying six pulses of 10 μ M butanone. Pulses were applied for 30 s once every 5 minutes, and a counter stimulus of 10 nM Diacetyl balanced the naïve response to butanone. Control conditions included mock training with buffer, food alone, and butanone alone at the paired concentrations. The bacteria did not clump or clog the device over 1-hour of flow in a microfluidic device, unlike the conventional OP50 strain, swiftly flowing out of the device leaving no food on posts or in channels after removal. Animals trained with bacterial food + butanone for 1-hour showed a significant (* $p < 0.05$) increase in attraction ($0.25 \text{ AI} \pm 0.06 \text{ s.e.m.}$) over the next 30 min, compared with food alone (-0.34 ± 0.04), butanone alone (0.00 ± 0.08), and buffer (naïve) control (-0.04 ± 0.11) training groups (**Fig. 30a**). Thus, pairing 1 mM butanone with food strongly enhanced the animals' response to butanone odor, indicating a conditioned response.

It was also observed (**Fig. 30b**) that when animals were trained in the presence of food (whether it was food alone or food and butanone), their forward motion probability with just the counterbalance buffer containing 10 nM Diacetyl was lower (0.32 Food Only, 0.33 Food + Butanone) than without food (0.43 Butanone only, 0.48 Naïve). The paired training group showed higher forward motion probability when butanone was pulsed during the testing phase (0.42) than the food alone group (0.22) leading to a higher attraction index in the paired group. Both the butanone only and naïve case had similar probabilities of

forward motion during butanone exposure to the counterbalanced buffer control, resulting in neutral attraction indices.

We have preliminary data which suggests that there may be some modulation on the sensory level in response to the butanone enhancement associative learning pairing (**Fig. 30c**), however more investigation is required. After removal of butanone (**Fig. 30d**), post-trained animals (0.63 ± 0.03 F/F₀ s.e.m.) show significantly (*p<0.05) higher neural activity than they do pre-training (0.51 ± 0.05 F/F₀ s.e.m.), suggesting they show stronger response to the removal of butanone.

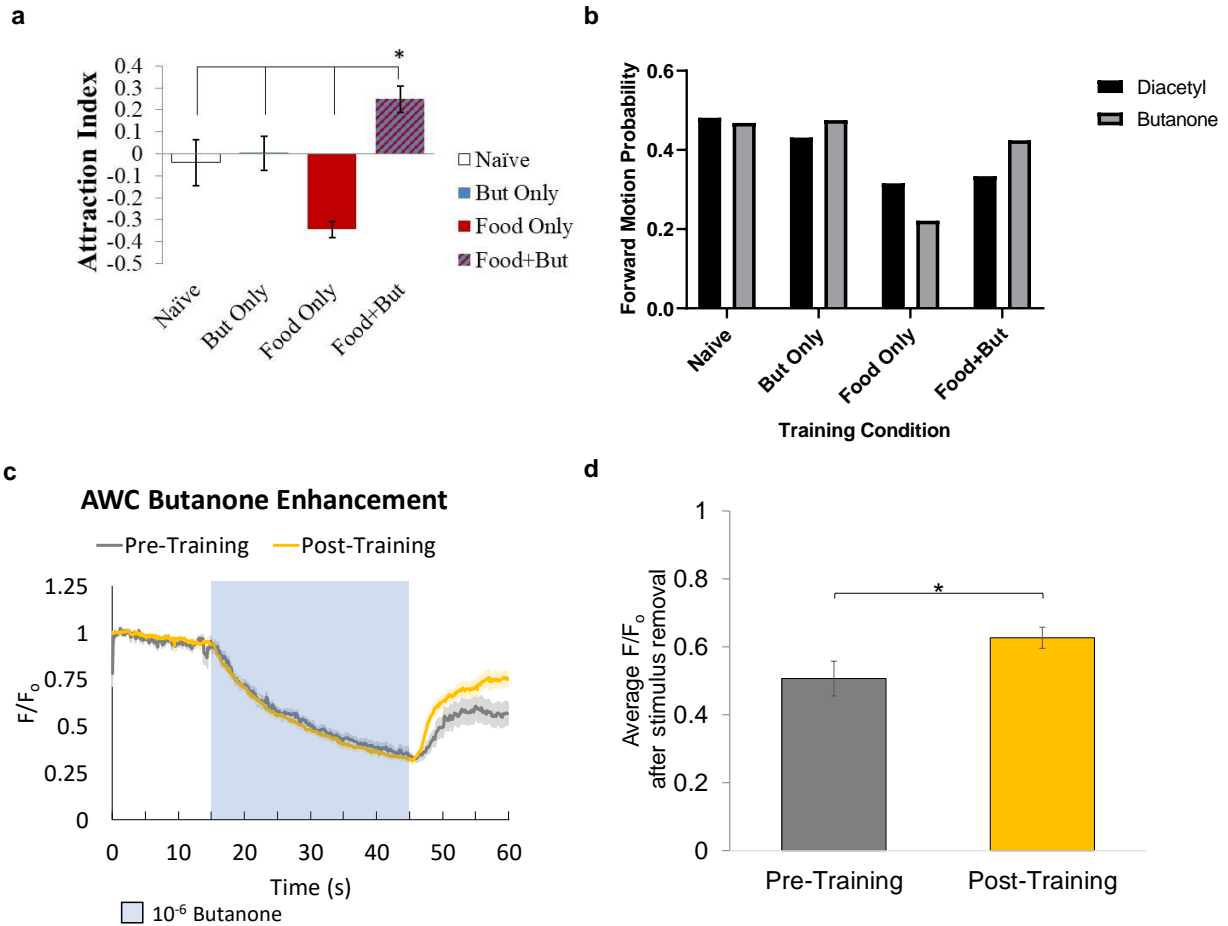


Figure 30. Butanone enhancement assay results in pulse-assay format

(a) Attraction index plotted for all 4 training groups: Naïve ($n = 3$), Butanone only ($n = 8$), Food only ($n = 4$), and Food + Butanone ($n = 8$). (b) Cumulative probability of forward motion for each training group with Butanone (during pulse) or Diacetyl (outside of pulse) in stimulus. (c) Preliminary neural imaging data shows potential strength of AWC response after removal of butanone following training through associate learning paradigm ($n = 17$ animals). Shading represents s.e.m. (d) Average F/F_0 after stimulus removal (45-60s) from data in c ($n=17$ animals). Statistics for a performed using a one-way ANOVA with Bonferroni's correction for multiple comparisons; $*P < 0.05$. N's represent an arena of ~ 25 animals with average probability of behavior. Statistics for d performed using a paired two-tailed t-test. $*P < 0.05$. Error bars represent s.e.m.

Discussion

In this chapter we established a new assay for associative learning through butanone enhancement contained entirely with a microfluidic device. The method represents a substantial improvement over original methods (Torayama et al., 2007) and previous microfluidic adaptations (Karen Tran, 2015) used to characterize associative learning in *C. elegans*. We addressed issues associated with plate-based chemotaxis assays by presenting controlled stimulus delivery in the closed environment of a microfluidic device. To reduce handling issues, we were able to train and test young adult *C. elegans* giving plenty of time for animals to acclimate to the testing environment after handling and assessing many animals in high throughput pulse-based attraction assays. These changes highlight a number of pros and cons that each of the butanone enhancement assay types mentioned possess (**Table 4**).

Using this system, we replicated past results indicating young adult *C. elegans* are able to associate a CS of neutral butanone to the US of food, in this assay NA22 *E. coli*. NA22 *E. coli* allowed us to flow and stimulate animals in the microfluidic device, allowing them to feed but also for the bacteria to be completely cleared when flushed out, leaving no residue on micro-posts and channels. Control results were slightly different though, with the food only exposure group showing the strongest aversion to butanone rather than the adapted butanone only group as expected (**Fig. 30**). It is likely that this difference in control preference is related to the addition of a counterbalancing stimulus of weak diacetyl. The goal of adding diacetyl as a counterbalancing stimulus was to reach an even attraction in naïve animals between butanone and the buffer, helping to demonstrate the

attraction shift in trained animals. It is possible that animals who are well fed have shifted preference against weak diacetyl compared to the tested butanone concentration. Additionally, it has recently been shown that diacetyl inhibits AWC, the sensory neuron responsible for detection of butanone (Dobosiewicz et al., 2019). While diacetyl and butanone are never tested together in this assay format, the potential effects of the counterbalance stimulus inhibiting neural activity in AWC prior to butanone exposure may alter learning results.

Based on this information regarding the counterbalance method with diacetyl, in future assays, I would recommend against using diacetyl to counterbalance butanone, and instead assess associative learning in the butanone enhancement assay without the additional variables that diacetyl provide. An alternative method to balance attraction to the testing solution of butanone such that naïve response will not present a high attraction baseline is to lower the testing concentration of butanone. Previous studies (Karen Tran, 2015) in the microfluidic format optimized the testing solution of 10 μM butanone based on its effects through a gradient assay. Animals in the gradient format are not exposed to the full concentration of your stimulus unless they are in the peak exposure y-axis position, so most movement decisions which are used to assess chemoattraction are done traversing an environment with a much lower stimulus concentration. In future assays, testing with more subtle butanone concentrations such as 1 μM may help differentiate learned behavior without the addition of a counterbalance stimulus.

Translating the butanone enhancement assay to the microfluidic format leads to a number of potential future works. The post structure, height, and overall design of microfluidic devices is highly customizable opening the door for studies of how learning changes as animals age. Establishing a platform for associative learning measurement makes it possible to understand how mutant animals may learn differently while exposing them to conditions identical to wildtype animals simultaneously. Previously, *olrn-1* mutants, shown to have defective in induction of the AWC^{ON} neuron required for butanone sensation (Bauer Huang et al., 2007), showed reduced associative learning in a butanone enhancement assay (Karen Tran, 2015) however results were variable. It is possible that variability in *olrn-1* chemotaxis in this assay was due to the increased handling effects and necessary acclimation time, delaying learned behavior assessment. Training and testing animals together in one microfluidic device allows greater understanding of the naïve behavior of mutant animals. It is likely that mutant strains like *olrn-1* carry variable behavior, changing the potential comparison between baseline levels. In the (Torayama et al., 2007) assay wildtype animals showed an high baseline CI to butanone (approximately +0.7), but if mutant strains with abnormal learning exhibit changes in behavior it will be much more difficult to associate chemotaxis differences between strains.

Translation of the butanone enhancement assay to the pulse format allowed for assessment of stimulus-evoked response changes between trained and untrained animals. We found that trained animals (to the pairing of butanone and food) showed stronger response at the sensory level to the removal of butanone, suggesting an

increased sensitivity to the odor. Future experimentation will explore whether learned behavior also has effects downstream at the interneuron levels, and if mutants incapable of associating butanone with unconditional stimuli, such as *olm-1*, have specific neural abnormalities when training is attempted.

The changes in ability for animals to move as they age (Hahm et al., 2015) also provides a source of improvement in this associative learning assay. Because the assay assesses instantaneous behavioral type and not an action that requires coordinated and directed taxis like chemotaxis across an agar dish, the assay is more translatable to study behavioral changes as an animal ages. Behavioral plasticity associated with neurodegenerative diseases like AD, PD, and ALS often are subtle at first but become more pronounced as patients age. It is expected that human disease models of neurodegenerative disorders effect learning and memory will also show age-dependent phenotypical changes that require a flexible assessment system to elucidate changes.

Methods and Materials

Strains and *C. elegans* culture

All *C. elegans* were maintained under standard conditions on NGM plates and fed OP50 *E. coli* bacteria seeded onto each plate. Wild-type animals were Bristol strain (N2). Neural imaging strain expressing GCaMP in AWC: CX14215, *kyEx4467* [*str-2::GCaMP5 D380Y*]. To synchronize for age, we picked L4 larval stage animals one day prior to experimentation such that all animals tested were at the young adult stage.

To prepare for an experiment, animals were isolated by genotype and/or arena placement and then transferred to an unseeded NGM plate immediately prior to experimentation. The plates were then flooded with S. medium buffer prior to their experiment. Animals were then collected into loading tubing using a 1 mL syringe prior to injection into the microfluidic arena.

Microfluidic device fabrication

All microfluidic devices were fabricated as previously described (Lagoy and Albrecht, 2015). Briefly, transparency photomasks were printed at 25,000 dpi from designs sketched using DraftSight CAD software. SU-8 mold masters were prepared on silicon wafers using standard photolithography techniques, and microfluidic devices were fabricated by pouring degassed PDMS (Sylgard 184, Dow Corning) onto the mold and heat curing. Individual devices were then cut out and punched to provide inlet and outlet flow. A hydrophobic glass substrate was created by vapor deposition of tridecafluoro-1,1,2,2-tetrahydrooctyl trichlorosilane (TFOCS, Gelest) and then sealed reversibly to the microfluidic channels. An upper glass slide, with holes drilled over inlet and outlet ports

with a diamond-coated drill bit, was sealed above the device, which was then placed into a metal clamp.

Stimulus preparation

All odor dilutions were freshly prepared on the day of experimentation. NA22 *E. coli* stock solutions were prepared using previously described methods (Keil et al., 2017). Briefly, NA22 *E. coli* was cultured, concentrated into pellet form, and suspended in S. medium buffer. A stock solution was diluted to an OD600 of 7.0, and 50 µg/ml of kanamycin was added to prevent bacteria from growing. Chemical solutions were prepared at a 1:20 dilution of stock solution and filtered through a 5 µm filter. Diacetyl (11 nM) was prepared from a 10⁻³ dilution (11 mM) stock solution immediately prior to experimentation as the counter buffer. Butanone (Sigma) was prepared fresh from pure stock to 1 mM for training and 10 µM for testing. Xylene cyanol dye (1x) was dissolved in the butanone testing solution to visualize odorant pulses.

Microfluidic device setup

Microfluidic devices were cleaned, assembled, and degassed in a vacuum desiccator for 30–60 min prior to experimentation. Degassing devices accelerates the absorption of air bubbles within the device. For behavioral experiments, devices were filled with 5% (w/v) Pluronic F127 through the outlet port to prevent bacterial and molecular absorption by passivation of the microfluidic surfaces and to minimize bubble entrapment via its surfactant properties. Reservoirs of loading solutions were prepared as previously described (Lagoy and Albrecht, 2015), purging the reservoir system of

bubbles and connecting the tubing into the inlets of the device. Once flow was properly established and tested for the testing phase, the testing solution was let run clear of the arena and animals were gently loaded into their respective arenas. Then, training solution was loaded into both top and both bottom arenas carefully through both upstream worm loading ports simultaneously, as to not cause overflow into the other half of the device through prior channels. Once training solution filled the device with animals in their respective arenas, flow was stopped for all channels and animals were left to the conditions of their training buffer for 1 hour. After 1 hour, a 30 second testing paradigm was started, delivering 30 s pulses of 10 μ M butanone once every 5 minutes.

Animal tracking systems

Videos of testing phase of learning were captured using a 6.6 MP PixelLink FireWire Camera at 2 fps for 30 minutes with an image resolution of \sim 30 pixels/mm. Videos were processed after experimentation as previously described using MATLAB to extract behavioral data (Albrecht and Bargmann, 2011) for all behavioral experiments, classifying forward behavioral probability for calculation of attraction index.

Neural calcium imaging and data analysis

Neural imaging videos and light assessment were acquired at 5x magnification (NA=0.25) with a Hamamatsu Orca-Flash 4.0 sCMOS camera using MicroManager/ImageJ software. The system has a Lumencor SOLA-LE solid-state lamp pulsed to excite GCaMP during fluorescence calcium imaging. To achieve autonomous experimentation, custom Arduino, MicroManager, and ImageJ scripts work together to

control illumination timing, image acquisition, and stimulus delivery. An Arduino Uno microcontroller was programmed to control fluidic valves through a ValveLink 8.2 (AutoMate Scientific) controller. A MicroManager script allows the user to configure all camera and illumination settings prior to experimentation.

Calcium imaging was performed on freely-moving animals as previously described (Larsch et al., 2013) using lines expressing GCaMP in selected neurons. Calcium imaging in AWC was performed at 10 fps, recording responses to 30 s chemical stimulation from 15–45 s within a 60 s trial. Videos were analyzed for neural fluorescence and locomotion using NeuroTracker software in ImageJ, which tracks the position of the neuron over time and integrates fluorescent intensity of the soma using a 4 x 4 pixel box. Fluorescence (F) was normalized by dividing by the initial baseline fluorescence in the first 4 s of each trial before stimulation (F_0), and the peak was collected for each stimulation.

Statistical analysis

Statistics were performed using one-way ANOVA with Bonferroni's correction for multiple comparisons or a paired two-tailed t-test when specified for 2 sample comparison, using the Statistics and Machine Learning Toolbox in MATLAB. Data represented as mean \pm s.e.m. or mean \pm s.d. and are consistent for each experiment.

Chapter 6: Future directions and conclusions

6.1: Furthering characterization and throughput of adult *C. elegans* sleep studies

6.1.1: Further investigation of the disconnect between sensory response during sleep and premotor neuron response related to arousal delay

One of the most exciting results coming from my thesis project was the discovery of modulation to sensory-evoked response in the premotor neuron AVA described in **Chapter 4**. In all other sensory and interneurons studied, the peak strength of sensory-evoked response remained consistent regardless of whether animals were asleep or awake, leading us to ask whether modulation that leads to arousal delay was happening directly at the motor neurons or muscles, or still somewhere upstream in interneuron circuits. We found that AVA responded reliably with reversal movement, rather than sensory stimulation (**Fig. 26i**).

Our next logical step would be to investigate additional aspects of the motor circuit to further probe how and why arousal response is delayed during adult sleep. One avenue would be to explore synaptic connectivity to AVA to measure where neural plasticity is being developed to lead to reduced arousal in AVA. AVA, an important hub of the motor circuit, is post-synaptic to 40 cells including a direct synaptic connection to ASH, but also 2nd degree connections through AIB, AVD, and RIC (**Fig. 27c**). We have seen that AIB responds in unison with ASH-evoked stimulus, but we have yet to measure response in AVD and RIC. Also, there are a plethora of potential neuropeptides that may be acting on AVA to mitigate response. FLP-11 (Turek et al., 2016), FLP-13, FLP-24, NLP-8 (Nath et

al., 2016), and NLP-22 (Nelson et al., 2013) provide logical starting points to assess neuropeptide related effects due to previous connections to sleep-like states in *C. elegans*, with the goal of understanding connection of adult sleep to previously observed DTS and SIS.

It has yet to be seen if similar motor circuits obey the same modulation paradigm observed with ASH-AIB-AVA. Delayed arousal has been shown in sleep states to attractive odors, mechanical stimulation, light stimulation, and many noxious cues. Investigating circuits using these stimulation pathways will elucidate if arousal threshold changes in sleep come from a common neural plasticity like global brain shifts (Kato et al., 2015; Nichols et al., 2017), or is compartmentally modulated in respect to stimulation type and animal development.

6.1.2: Use of optogenetic stimulation to further throughput of neural imaging during sleep and wake states

One of the main limitations of the current closed-loop sleep assessment system is throughput due to waiting for animals to observe desired state changes. This allows us to observe more natural phenotypes of sleep and wake associated neural activity, but the trade-off comes from a lack of data throughput. A single animal takes hours to study and depending on behavior exhibited may or may not provide suitable sleep and wake neural responses. Wildtype sleep activity is highly variable in the microfluidic device (**Fig. 19c**).

Recently, methods to initiate sleep using optogenetic stimulation have been developed (Steuer Costa et al., 2019; Urmersbach et al., 2016) that use channelrhodopsins expressed in the RIS neuron to activate RIS selectively, initiating a sleep-like state. While RIS is active at the onset of sleep, selective control of RIS is challenging and does not simply act as a ON/OFF switch to make *C. elegans* sleep. It is possible that optogenetic strategies to induce sleep rapidly with more control will require complex expression through many neurons, however with reagents available to us now we tried to use optogenetics to improve sleep throughput (**Fig. 31**). With use of standard optogenetic techniques, we did see that ATR treated animals showed more sleep upon red-light activation of the red-shifted channelrhodopsin ReaChR (Lin et al., 2013), which was sustained even after red light was turned off, but the behavioral effects were not as desirable. Red light activation initiated spontaneous avoidance responses most often before some animals would exhibit quiescence. We hypothesize two reasons behind this. First, AIB and RIS share a gap junction connection. It is possible that intense activation

of RIS through optogenetics will also create activity in AIB, an interneuron deeply tied to reversal circuits within *C. elegans*. Second, use of optogenetics with RIS has never quite shown what many would consider “sleep control” but rather stopping behavior (Steuer Costa et al., 2019). Recent publications have termed RIS a generic stop neuron, providing function outside of just sleep induction. It is likely that creating an optogenetic sleep control mechanism will require further exploration of how sleep is induced in *C. elegans*, and potentially development of new lines with more suitable approaches to induce sleep. Ideally, with a quick induction method to initiate natural sleep states we would be able to increase neural recording throughput dramatically. It would allow us to load many animals at once, assessing their response simultaneously, and increase the number of sleep events we could record from any given animal.

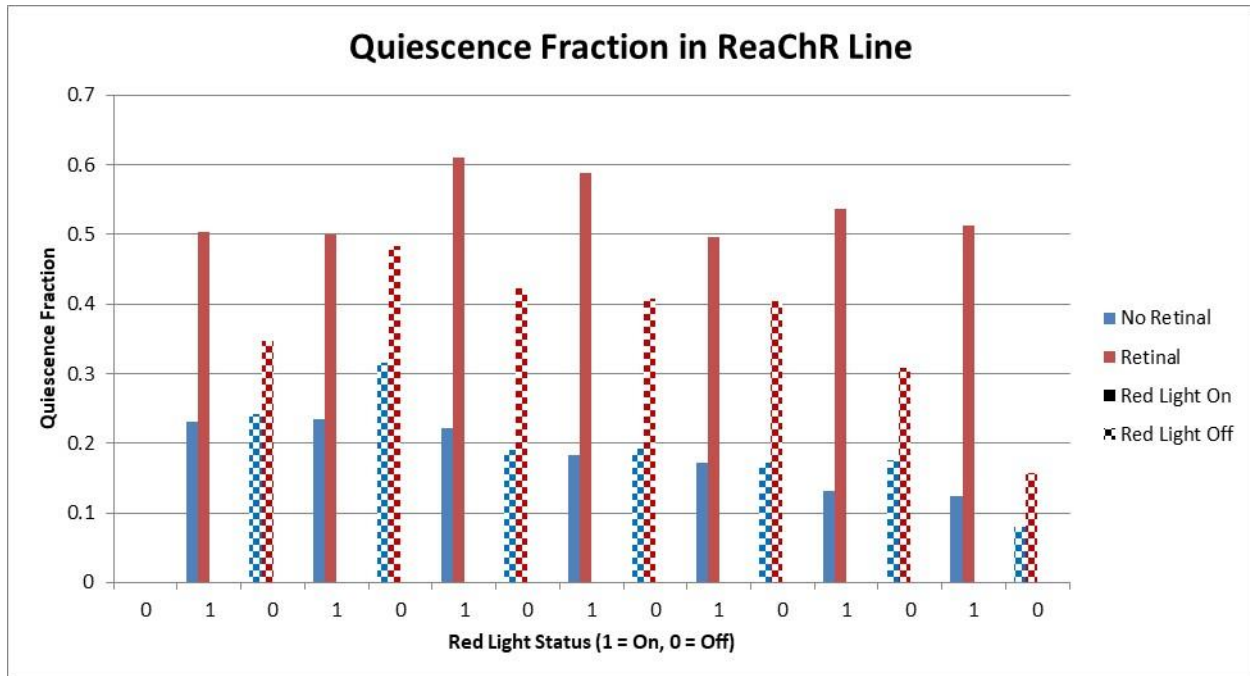


Figure 31. Control of sleep non-ideal with ReaChR optogenetic line

Strain used:

HBR1139: *unc-119(ed3) III, goels261[aptf-1-5'utr::ReaChR::mKate2-aptf-1-3'utr,unc-119(1)]*.

Provided by the Bringmann lab (Urmersbach et al., 2016).

6.1.3: Characterize disease-related mutants to study sleep disorders impacting humans

After using the sleep assessment systems discussed in **Chapters 3 and 4** to probe for behavioral features of sleep in *C. elegans*, the next step towards the long-term goal of this project is to use the system to classify sleep disorders, studying human disease models of sleep in *C. elegans* to understand how we can use the model organisms' many strengths to understand neurological function and disease. A potential avenue for translatable study involves restless leg syndrome (RLS). RLS affects nearly 20% of subjects surveyed in the US (Allen et al., 2011), leading to significant detriments towards overall health and workplace productivity because of sleep disturbance. Genome-wide association studies have revealed genes implicated in RLS, including MEIS1 (Winkelmann et al., 2007). MEIS1 shares orthologs in *C. elegans* with *unc-62*, which has been shown to be involved in neurogenesis and mutations in *unc-62* causes embryonic arrest or death (Arata et al., 2006; Van Auken et al., 2002). Additionally, reduced expression of *unc-62* resulted in increased ferritin expression (Catoire et al., 2011), establishing a link between RLS and iron metabolism. Study of *unc-62* mutants could elucidate how RIS-linked abnormalities manifest themselves in sleep especially in changes to sensory activity during sleep, and sensory-evoked response during sleep. Our system is ideally suited to study these phenomena.

6.2: Future work investigating butanone enhancement neurally and across ages

6.2.1: Investigation of butanone enhancement with older adults and L4s has so far been inconclusive

After establishing an all-microfluidic platform for the study of associative learning in *C. elegans* our next step was to create microfluidic devices for studying how learning capabilities change as animals age. Preliminary data by (Karen Tran, 2015) done with the help of a rotational student Jeremy Shui suggested that L4 animals showed an inability to learn association of butanone to OP50 *E. coli*. We designed microfluidic devices (**Fig. 32d,e**) with proportionally smaller (for L4) and larger (for day 5 older adults) spacing between posts to assess learning across ages. Early results have been inconclusive to this point (**Fig. 32**). Devices were not presenting smooth stimulus pulses across the arena to accurately assess temporal behavioral dynamics between tests or within one test, however animal movement was consistent with movement on the plate. So far, data suggests that L4 animals (**Fig. 32a**) showed butanone enhancement, but older adults (**Fig. 32b,c**) did not, however repeated measures will be necessary to make any conclusions.

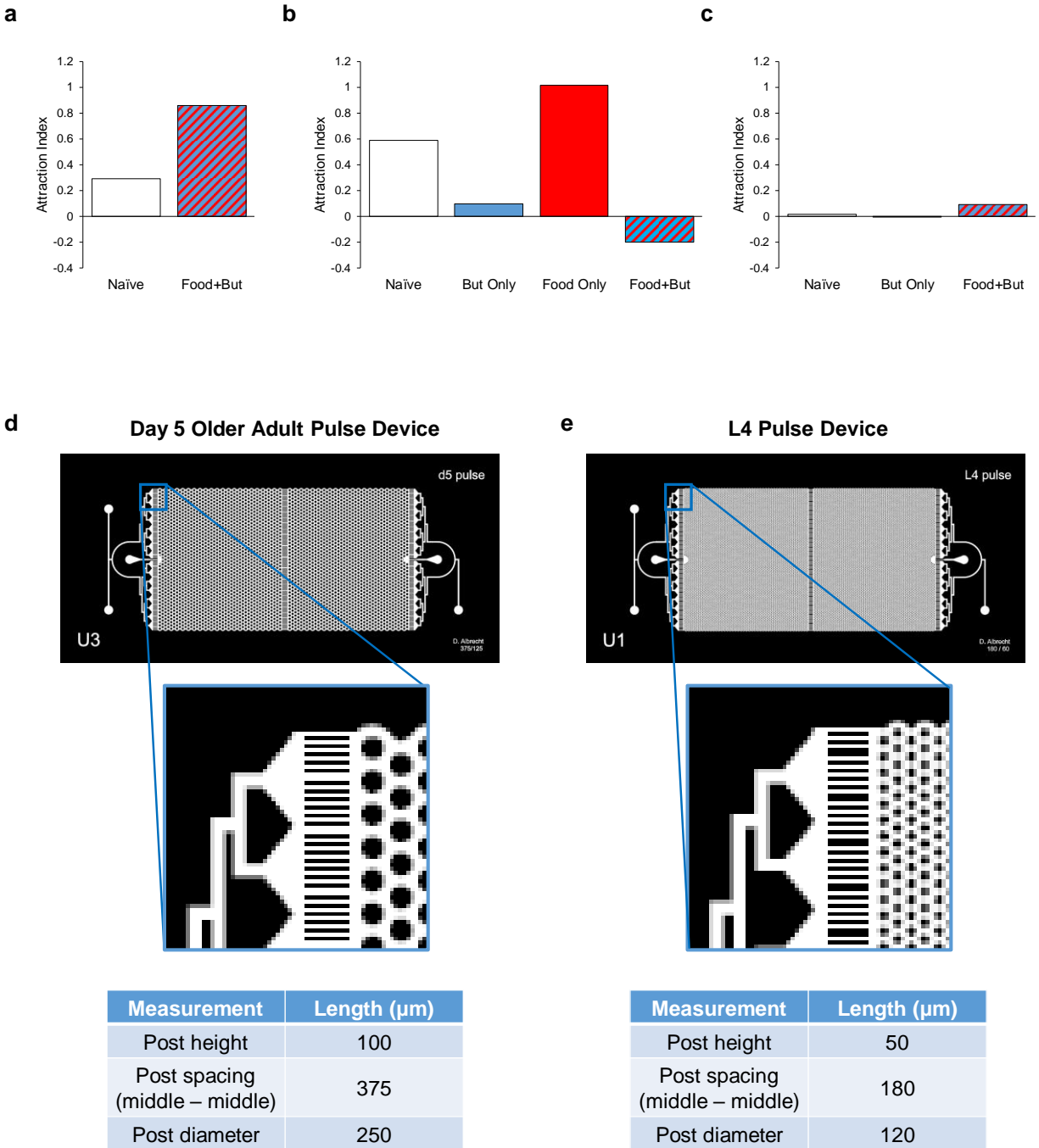


Figure 32. Assessment of associative learning as animals age

(a) Attraction index for L4 animals. Pulses of 10 μM Butanone assessed against a counter-stimulus of 10 nM Diacetyl. (b) Attraction index for day 5 adult animals. Pulses of 10 μM Butanone assessed against a counter-stimulus of 10 nM Diacetyl. (c) Attraction index for day 5 adult animals. Pulses of 10 μM Butanone assessed against a counter-stimulus of 100 nM Diacetyl. N = ~ 50 animals for each condition. (d) Device design for “U3” Day 5 Older Adult Pulse Device and associated dimensions. (e) Device design for “U1” L4 Pulse Device and associated dimensions.

6.2.2: Study neural activity changes in associative learning assay

Additionally, given the microfluidic platform to assess behavioral plasticity with associative learning the next development step will be to translate behavioral plasticity to measurements of neural plasticity: bridging the gap between neural and behavioral functions related to learning. Prior experiments have demonstrated how pulse-based assays can be translated to neural imaging readily (**Fig. 5**), so we will use the same systems to assess associative learning. Initial evaluation of the system will look at both the AWC^{ON} sensory neuron responsible for detecting butanone, but also interneurons AIB, AIA, and AIY which act downstream of AWC to initiate preferential behavior. One potentially challenging factor will be that we cannot use the same paralysis techniques used in previous pulse assay neural imaging experiments (**Fig. 5**) due to the necessity of animals to feed on the NA22 *E. coli* to learn to train the CS to the US in associative learning, as tetramisole paralyzes muscles in the pharynx preventing animals from feeding. We have preliminary data (**Fig. 30c,d**) which suggests that there may be modulation on the sensory level as a result of associative learning, however throughput of neural imaging is slow with the difficulties associated with tracking moving animals. To combat these issues, we will attempt to stage paralysis at the end of training as well as assessing neural activity without paralysis to gauge whether animals can be tested with a paralytic. If not, neural activity will still be measurable however we can use multi-trap devices to keep the head of the animal stationary for easier tracking (**Fig. 33a-c**) and high-throughput assessment.

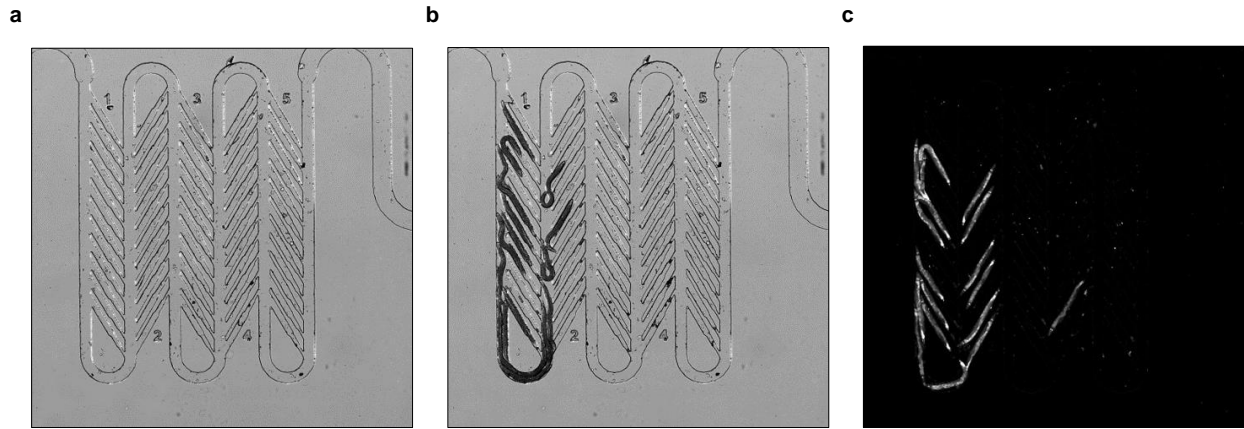


Figure 33. Neural imaging in associative learning assay

(a) View of Multi-trap device without animals. Larger channel spanning device facilitates fluid flow and animal loading. (b) Loading of animals into the trap device sequentially into nose traps. (c) Neural activity measurements with the multi-trap device.

6.3: Investigating functional properties of *C. elegans* sleep

6.3.1: Combining sleep and learning assessment to study functional memory consolidation in *C. elegans* using optogenetics

With development of assays to assess both sleep and learning, an exciting potential combination appears in assessing the role of memory consolidation during sleep in *C. elegans*. Memory consolidation has been shown consistently to be supported by sleep in humans (Albouy et al., 2008, 2013a, 2013b; Frank and Benington, 2006; Gais et al., 2007; Maquet, 2001; Rasch and Born, 2013; Rauchs et al., 2008; Sterpenich et al., 2009; Tononi and Cirelli, 2014) however it remains one of the functions of human sleep that has not yet been shown in *C. elegans* (Trojanowski and Raizen, 2015; Vorster and Born, 2015). Provided findings on functional behavioral and neural plasticity associated with learned behavior, and optogenetic systems for controlling sleep behavior, we will be able to combine these assays to assess whether sleep in *C. elegans* can lead to memory consolidation (**Fig. 34**). We have already developed standards for assessing behavioral plasticity of associative learning all within the microfluidic device, so with working optogenetic sleep initiation mechanism we would be able to control and/or measure how much sleep we can provide animals and assess how sleep effects their short- and long term memory. *C. elegans* have been shown to retain memories for 24 h after spaced training associative learning assays (Amano and Maruyama, 2011), providing ample time to either measure the amount of sleep animals exhibit and correlate sleep amount to strength of memory, or to control the amount of sleep and measure how sleep amount effects strength of memory.

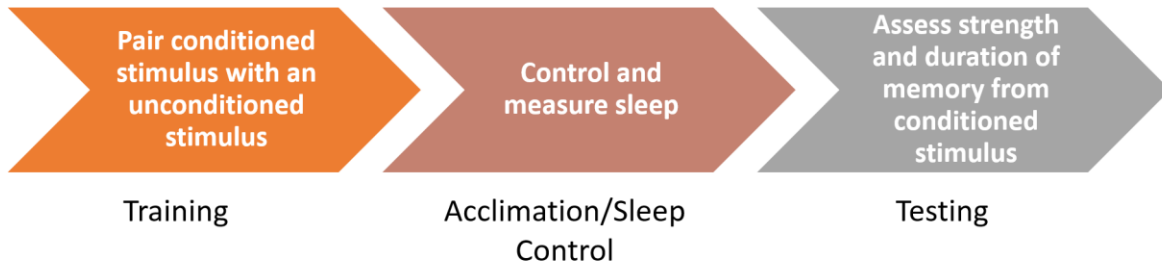


Figure 34. Memory Consolidation Schematic

6.4: Summary and major conclusions

The core objective of this project was to develop tools to assess behavioral and neural plasticity in a high-throughput manner, and through the project much has been learned about how *C. elegans* behave and adapt to the world around them. Tools for understanding both sleep and learning in *C. elegans* were developed that will be useful not just to the lab, but to the *C. elegans* community. In aim 1 I sought to develop new methods to measure sleep behavior that would improve the throughput and capabilities of studying *C. elegans* sleep. In developing this method, I discovered what is now believed to be a novel sleep-like state, that had previously been unreported in *C. elegans*. The microfluidic platform developed is capable of measuring sleep behavior of up to 100 animals simultaneously and elucidate the effects of genetics and environmental factors during sleep, characterizing what factors influence why *C. elegans* sleep.

In aim 2 I expanded the study of sleeping *C. elegans* to develop a method of assessing neural activity in an unbiased manner. To this point many of neural imaging experiments conducted in the field make use of predictable sleep timing to associate neural activity with states of lethargus associated with sleep. While researchers can try to control for recognizing sleep behavior, I sought to automate this process and developed a closed-loop system that both detects sleep states, and stimulates to assess neural responses. Through this system it was discovered that adult *C. elegans* sleep presents different state-dependence in neural activity than DTS, and sleep-dependent modulation varies depending on the specific subcircuit affected. Only a small percentage of the 302 neurons *C. elegans* possess have been specifically measured for effects during sleep, and

systems like this will open the door for much more exploration of how the brain adapts processing during sleep, and how this may be altered by sleep disorders. The structure of the closed-loop system also presents an exciting platform for linking behavior and neural activity across phenomena in *C. elegans*. At its core, the closed-loop system works to identify behavior using computer vision, and assess neural response, a paradigm that can easily be fitted to nearly any neurological phenomenon. Much potential exists to translate the closed-loop system to behaviors such as mating, feeding, learning, social behavior, and much more.

Finally, in aim 3 I sought to improve the butanone enhancement associative learning assay by translating assessment from less reproducible methods to a structure that facilitates high reproducibility and translatability to future measurements vital to understanding learning in *C. elegans*. I was able to translate the assay to a pulse microfluidic format and develop attraction metrics based on instantaneous behavior which confirm the association from the butanone enhancement assay demonstrated previously in plate-based methods. With a pulse microfluidic assay we now can more readily assess how learning changes as animals age and how learning is imprinted on the nervous system. Altogether, these tools and biological insights developed and discovered during this project will aid researchers in understanding the fundamental mechanisms behind sleep and learning, and work towards our long-term goal of understanding the molecular and neural circuitry changes that underlie neurological disorders.

Chapter 7: Bibliography

Adam, K., and Oswald, I. (1977). Sleep Is for Tissue Restoration. *J R Coll Physicians Lond* 11, 376–388.

Albouy, G., Sterpenich, V., Balteau, E., Vandewalle, G., Desseilles, M., Dang-Vu, T., Darsaud, A., Ruby, P., Luppi, P.-H., Degueldre, C., et al. (2008). Both the Hippocampus and Striatum Are Involved in Consolidation of Motor Sequence Memory. *Neuron* 58, 261–272.

Albouy, G., King, B.R., Maquet, P., and Doyon, J. (2013a). Hippocampus and striatum: Dynamics and interaction during acquisition and sleep-related motor sequence memory consolidation. *Hippocampus* 23, 985–1004.

Albouy, G., Sterpenich, V., Vandewalle, G., Darsaud, A., Gais, S., Rauchs, G., Desseilles, M., Boly, M., Dang-Vu, T., Balteau, E., et al. (2013b). Interaction between Hippocampal and Striatal Systems Predicts Subsequent Consolidation of Motor Sequence Memory. *PLOS ONE* 8, e59490.

Albrecht, D.R., and Bargmann, C.I. (2011). High-content behavioral analysis of *Caenorhabditis elegans* in precise spatiotemporal chemical environments. *Nat Meth* 8, 599–605.

Allen, R.P., Bharmal, M., and Calloway, M. (2011). Prevalence and disease burden of primary restless legs syndrome: results of a general population survey in the United States. *Mov. Disord.* 26, 114–120.

Alzheimer's Association (2013). Latest Alzheimer's Facts and Figures.

Amano, H., and Maruyama, I.N. (2011). Aversive olfactory learning and associative long-term memory in *Caenorhabditis elegans*. *Learn Mem* 18, 654–665.

Anderson, A., Chew, Y.L., Schafer, W., and McMullan, R. (2019). Identification of a Conserved, Orphan G Protein-Coupled Receptor Required for Efficient Pathogen Clearance in *Caenorhabditis elegans*. *Infection and Immunity* 87, e00034-19.

Ankeny, R.A., and Leonelli, S. (2011). What's so special about model organisms? *Studies in History and Philosophy of Science Part A* 42, 313–323.

Antoshechkin, I., and Sternberg, P.W. (2007). The versatile worm: genetic and genomic resources for *Caenorhabditis elegans* research. *Nat Rev Genet* 8, 518–532.

Arata, Y., Kouike, H., Zhang, Y., Herman, M.A., Okano, H., and Sawa, H. (2006). Wnt signaling and a Hox protein cooperatively regulate *psa-3/Meis* to determine daughter cell fate after asymmetric cell division in *C. elegans*. *Dev. Cell* 11, 105–115.

- Ardizzi, J.P., and Epstein, H.F. (1987). Immunochemical localization of myosin heavy chain isoforms and paramyosin in developmentally and structurally diverse muscle cell types of the nematode *Caenorhabditis elegans*. *J. Cell Biol.* 105, 2763–2770.
- Banks, S., and Dinges, D.F. (2007). Behavioral and Physiological Consequences of Sleep Restriction. *J Clin Sleep Med* 3, 519–528.
- Bargmann, C.I., and Horvitz, H.R. (1991). Chemosensory neurons with overlapping functions direct chemotaxis to multiple chemicals in *C. elegans*. *Neuron* 7, 729–742.
- Bauer Huang, S.L., Saheki, Y., VanHoven, M.K., Torayama, I., Ishihara, T., Katsura, I., van der Linden, A., Sengupta, P., and Bargmann, C.I. (2007). Left-right olfactory asymmetry results from antagonistic functions of voltage-activated calcium channels and the Raw repeat protein OLRN-1 in *C. elegans*. *Neural Development* 2, 24.
- Benington, J.H., and Craig Heller, H. (1995). Restoration of brain energy metabolism as the function of sleep. *Progress in Neurobiology* 45, 347–360.
- Bentley, B., Branicky, R., Barnes, C.L., Chew, Y.L., Yemini, E., Bullmore, E.T., Vértés, P.E., and Schafer, W.R. (2016). The Multilayer Connectome of *Caenorhabditis elegans*. *PLOS Computational Biology* 12, e1005283.
- Boelaert, M., and Consortium, T.N. (2016). Clinical Research on Neglected Tropical Diseases: Challenges and Solutions. *PLOS Neglected Tropical Diseases* 10, e0004853.
- Bono, M. de, and Bargmann, C.I. (1998). Natural Variation in a Neuropeptide Y Receptor Homolog Modifies Social Behavior and Food Response in *C. elegans*. *Cell* 94, 679–689.
- Bono, M. de, and Maricq, A.V. (2005). Neuronal Substrates of Complex Behaviors in *C. Elegans*. *Annual Review of Neuroscience* 28, 451–501.
- Boulin, T., and Hobert, O. (2012). From Genes to Function : The *C. elegans* Genetic Toolbox. *Wiley Interdiscip Rev Dev Biol* 1, 114–137.
- Bray, M.-A., Carpenter, A., and Imaging Platform, Broad Institute of MIT and Harvard (2004). Advanced Assay Development Guidelines for Image-Based High Content Screening and Analysis. In *Assay Guidance Manual*, G.S. Sittampalam, A. Grossman, K. Brimacombe, M. Arkin, D. Auld, C.P. Austin, J. Baell, B. Bejcek, J.M.M. Caaveiro, T.D.Y. Chung, et al., eds. (Bethesda (MD): Eli Lilly & Company and the National Center for Advancing Translational Sciences), p.
- Bredesen, D.E., Rao, R.V., and Mehlen, P. (2006). Cell death in the nervous system. *Nature* 443, 796–802.
- Brenner, S. (1974). The Genetics of *Caenorhabditis Elegans*. *Genetics* 77, 71–94.
- Brown, E.N., Lydic, R., and Schiff, N.D. (2010). General Anesthesia, Sleep, and Coma. *New England Journal of Medicine* 363, 2638–2650.

- Burns, A.R., Luciani, G.M., Musso, G., Bagg, R., Yeo, M., Zhang, Y., Rajendran, L., Glavin, J., Hunter, R., Redman, E., et al. (2015). *Caenorhabditis elegans* is a useful model for anthelmintic discovery. *Nat Commun* 6.
- Campbell, S.S., and Tobler, I. (1984). Animal sleep: A review of sleep duration across phylogeny. *Neuroscience & Biobehavioral Reviews* 8, 269–300.
- Cassada, R.C., and Russell, R.L. (1975). The dauerlarva, a post-embryonic developmental variant of the nematode *Caenorhabditis elegans*. *Developmental Biology* 46, 326–342.
- Catoire, H., Dion, P.A., Xiong, L., Amari, M., Gaudet, R., Girard, S.L., Noreau, A., Gaspar, C., Turecki, G., Montplaisir, J.Y., et al. (2011). Restless legs syndrome-associated MEIS1 risk variant influences iron homeostasis. *Ann Neurol.* 70, 170–175.
- Chao, M.Y., Komatsu, H., Fukuto, H.S., Dionne, H.M., and Hart, A.C. (2004). Feeding status and serotonin rapidly and reversibly modulate a *Caenorhabditis elegans* chemosensory circuit. *PNAS* 101, 15512–15517.
- Chew, Y.L., Tanizawa, Y., Cho, Y., Zhao, B., Yu, A.J., Ardiel, E.L., Rabinowitch, I., Bai, J., Rankin, C.H., Lu, H., et al. (2018). An Afferent Neuropeptide System Transmits Mechanosensory Signals Triggering Sensitization and Arousal in *C. elegans*. *Neuron* 99, 1233-1246.e6.
- Cho, J.Y., and Sternberg, P.W. (2014). Multilevel Modulation of a Sensory Motor Circuit during *C. elegans* Sleep and Arousal. *Cell* 156, 249–260.
- Chronis, N., Zimmer, M., and Bargmann, C.I. (2007). Microfluidics for in vivo imaging of neuronal and behavioral activity in *Caenorhabditis elegans*. *Nat Methods* 4, 727–731.
- Chuang, L.F., and Collins, E.B. (1968). Biosynthesis of Diacetyl in Bacteria and Yeast. *J Bacteriol* 95, 2083–2089.
- Churgin, M.A., Jung, S.-K., Yu, C.-C., Chen, X., Raizen, D.M., and Fang-Yen, C. (2017). Longitudinal imaging of *Caenorhabditis elegans* in a microfabricated device reveals variation in behavioral decline during aging. *Elife* 6.
- Colbert, H.A., and Bargmann, C.I. (1995). Odorant-specific adaptation pathways generate olfactory plasticity in *C. elegans*. *Neuron* 14, 803–812.
- Consortium*, T.C. *elegans* S. (1998). Genome Sequence of the Nematode *C. elegans*: A Platform for Investigating Biology. *Science* 282, 2012–2018.
- Coon, D.W., and Edgerly, E.S. (1999). The personal and social consequences of Alzheimer disease. *Genet. Test.* 3, 29–36.
- Crocker, A., and Sehgal, A. (2010). Genetic analysis of sleep. *Genes Dev.* 24, 1220–1235.

- Crompton, D.W.T., and Nesheim, M.C. (2002). Nutritional impact of intestinal helminthiasis during the human life cycle. *Annu. Rev. Nutr.* 22, 35–59.
- Cronin, C.J., Mendel, J.E., Mukhtar, S., Kim, Y.-M., Stirbl, R.C., Bruck, J., and Sternberg, P.W. (2005). An automated system for measuring parameters of nematode sinusoidal movement. *BMC Genetics* 6, 5.
- Dabbish, N.S., and Raizen, D.M. (2011). GABAergic Synaptic Plasticity during a Developmentally Regulated Sleep-Like State in *C. elegans*. *J. Neurosci.* 31, 15932–15943.
- Dobosiewicz, M., Liu, Q., and Bargmann, C.I. (2019). Reliability of an interneuron response depends on an integrated sensory state. *ELife* 8, e50566.
- Driscoll, M., and Chalfie, M. (1991). The *mec-4* gene is a member of a family of *Caenorhabditis elegans* genes that can mutate to induce neuronal degeneration. *Nature* 349, 588–593.
- Driver, R.J., Lamb, A.L., Wyner, A.J., and Raizen, D.M. (2013). DAF-16/FOXO Regulates Homeostasis of Essential Sleep-like Behavior during Larval Transitions in *C. elegans*. *Current Biology* 23, 501–506.
- Dusenbery, D.B. (1985). Using a microcomputer and video camera to simultaneously track 25 animals. *Computers in Biology and Medicine* 15, 169–175.
- Edwards, S.L., Charlie, N.K., Milfort, M.C., Brown, B.S., Gravlin, C.N., Knecht, J.E., and Miller, K.G. (2008). A Novel Molecular Solution for Ultraviolet Light Detection in *Caenorhabditis elegans*. *PLoS Biol* 6, e198.
- Ezcurra, M., Walker, D.S., Beets, I., Swoboda, P., and Schafer, W.R. (2016). Neuropeptidergic Signaling and Active Feeding State Inhibit Nociception in *Caenorhabditis elegans*. *J Neurosci* 36, 3157–3169.
- Flavell, S.W., Pokala, N., Macosko, E.Z., Albrecht, D.R., Larsch, J., and Bargmann, C.I. (2013). Serotonin and the Neuropeptide PDF Initiate and Extend Opposing Behavioral States in *C. elegans*. *Cell* 154, 1023–1035.
- Fox, R.M., Von Stetina, S.E., Barlow, S.J., Shaffer, C., Olszewski, K.L., Moore, J.H., Dupuy, D., Vidal, M., and Miller, D.M. (2005). A gene expression fingerprint of *C. elegans* embryonic motor neurons. *BMC Genomics* 6, 42.
- Frank, M.G., and Benington, J.H. (2006). The Role of Sleep in Memory Consolidation and Brain Plasticity: Dream or Reality? *Neuroscientist* 12, 477–488.
- Friedland, A.E., Tzur, Y.B., Esvelt, K.M., Colaiácovo, M.P., Church, G.M., and Calarco, J.A. (2013). Heritable genome editing in *C. elegans* via a CRISPR-Cas9 system. *Nature Methods* 10, 741–743.

Gais, S., Albouy, G., Boly, M., Dang-Vu, T.T., Darsaud, A., Desseilles, M., Rauchs, G., Schabus, M., Sterpenich, V., Vandewalle, G., et al. (2007). Sleep transforms the cerebral trace of declarative memories. *PNAS* *104*, 18778–18783.

Gallagher, T., and You, Y.-J. (2014). Falling asleep after a big meal: Neuronal regulation of satiety. *Worm* *3*, e27938.

Galván, A. (2010). Neural plasticity of development and learning. *Human Brain Mapping* *31*, 879–890.

Gami, M.S., and Wolkow, C.A. (2006). Studies of *Caenorhabditis elegans* DAF-2/insulin signaling reveal targets for pharmacological manipulation of lifespan. *Aging Cell* *5*, 31–37.

Ganguly, S., Coon, S.L., and Klein, D.C. (2014). Control of melatonin synthesis in the mammalian pineal gland: the critical role of serotonin acetylation. *Cell Tissue Res* *309*, 127–137.

Ghosh, R., and Emmons, S.W. (2008). Episodic swimming behavior in the nematode *C. elegans*. *Journal of Experimental Biology* *211*, 3703–3711.

Gonzales, D.L., Zhou, J., and Robinson, J.T. (2019). μ Sleep: A Spontaneous *C. elegans* Sleep State Regulated by Satiety, Thermosensation and Mechanosensation. *BioRxiv* 547075.

Gorgoni, M., D'Atri, A., Lauri, G., Rossini, P.M., Ferlazzo, F., and De Gennaro, L. (2013). Is Sleep Essential for Neural Plasticity in Humans, and How Does It Affect Motor and Cognitive Recovery?

Gottlieb, D.J., Punjabi, N.M., Newman, A.B., Resnick, H.E., Redline, S., Baldwin, C.M., and Nieto, F.J. (2005). Association of sleep time with diabetes mellitus and impaired glucose tolerance. *Arch. Intern. Med.* *165*, 863–867.

Gray, J.M., Hill, J.J., and Bargmann, C.I. (2005). A circuit for navigation in *Caenorhabditis elegans*. *Proc. Natl. Acad. Sci. U.S.A.* *102*, 3184–3191.

Hahm, J.-H., Kim, S., DiLoreto, R., Shi, C., Lee, S.-J.V., Murphy, C.T., and Nam, H.G. (2015). *C. elegans* maximum velocity correlates with healthspan and is maintained in worms with an insulin receptor mutation. *Nat Commun* *6*.

Hart, A.C., and Chao, M.Y. (2010). From Odors to Behaviors in *Caenorhabditis elegans*. In *The Neurobiology of Olfaction*, A. Menini, ed. (Boca Raton (FL): CRC Press/Taylor & Francis), p.

Hasler, G., Buysse, D.J., Klaghofer, R., Gamma, A., Ajdacic, V., Eich, D., Rössler, W., and Angst, J. (2004). The association between short sleep duration and obesity in young adults: a 13-year prospective study. *Sleep* *27*, 661–666.

- Hedgecock, E.M., and Russell, R.L. (1975). Normal and mutant thermotaxis in the nematode *Caenorhabditis elegans*. *Proc. Natl. Acad. Sci. U.S.A.* 72, 4061–4065.
- Hennevin, E., Huetz, C., and Edeline, J.-M. (2007). Neural representations during sleep: From sensory processing to memory traces. *Neurobiology of Learning and Memory* 87, 416–440.
- Hill, A.J., Mansfield, R., Lopez, J.M.N.G., Raizen, D.M., and Van Buskirk, C. (2014). Cellular Stress Induces a Protective Sleep-like State in *C. elegans*. *Current Biology* 24, 2399–2405.
- Hilliard, M.A., Bergamasco, C., Arbucci, S., Plasterk, R.H., and Bazzicalupo, P. (2004). Worms taste bitter: ASH neurons, QUI-1, GPA-3 and ODR-3 mediate quinine avoidance in *Caenorhabditis elegans*. *EMBO J* 23, 1101–1111.
- Hilliard, M.A., Apicella, A.J., Kerr, R., Suzuki, H., Bazzicalupo, P., and Schafer, W.R. (2005). In vivo imaging of *C. elegans* ASH neurons: cellular response and adaptation to chemical repellents. *The EMBO Journal* 24, 63–72.
- Horvitz, H.R., Chalfie, M., Trent, C., Sulston, J.E., and Evans, P.D. (1982). Serotonin and Octopamine in the Nematode *Caenorhabditis elegans*. *Science* 216, 1012–1014.
- Hotez, P.J., Brindley, P.J., Bethony, J.M., King, C.H., Pearce, E.J., and Jacobson, J. (2008). Helminth infections: the great neglected tropical diseases. *J Clin Invest* 118, 1311–1321.
- Huang, S.-H., and Lin, Y.-W. (2018). Bioenergetic Health Assessment of a Single *Caenorhabditis elegans* from Postembryonic Development to Aging Stages via Monitoring Changes in the Oxygen Consumption Rate within a Microfluidic Device. *Sensors (Basel)* 18.
- Huang, H., Singh, K., and Hart, A.C. (2017). Measuring *Caenorhabditis elegans* Sleep During the Transition to Adulthood Using a Microfluidics-based System. *Bio Protoc* 7.
- Husson, S.J. (2012). Keeping track of worm trackers. *WormBook* 1–17.
- Institute of Medicine (US) Committee on Sleep Medicine and Research (2006). *Sleep Disorders and Sleep Deprivation: An Unmet Public Health Problem* (Washington (DC): National Academies Press (US)).
- Iwanir, S., Tramm, N., Nagy, S., Wright, C., Ish, D., and Biron, D. (2013). The Microarchitecture of *C. elegans* Behavior during Lethargus: Homeostatic Bout Dynamics, a Typical Body Posture, and Regulation by a Central Neuron. *Sleep* 36, 385–395.
- Jansen, G., Weinkove, D., and Plasterk, R.H.A. (2002). The G-protein γ subunit *gpc-1* of the nematode *C.elegans* is involved in taste adaptation. *The EMBO Journal* 21, 986–994.

Jiang, B., Ren, C., Li, Y., Lu, Y., Li, W., Wu, Y., Gao, Y., Ratcliffe, P.J., Liu, H., and Zhang, C. (2011). Sodium sulfite is a potential hypoxia inducer that mimics hypoxic stress in *Caenorhabditis elegans*. *J Biol Inorg Chem* *16*, 267–274.

Johnston, C.J.C., Robertson, E., Harcus, Y., Grainger, J.R., Coakley, G., Smyth, D.J., McSorley, H.J., and Maizels, R. (2015). Cultivation of *Heligmosomoides Polygyrus*: An Immunomodulatory Nematode Parasite and its Secreted Products. *J Vis Exp*.

Kaminsky, R., Ducray, P., Jung, M., Clover, R., Rufener, L., Bouvier, J., Weber, S.S., Wenger, A., Wieland-Berghausen, S., Goebel, T., et al. (2008). A new class of anthelmintics effective against drug-resistant nematodes. *Nature* *452*, 176–180.

Karen Tran (2015). A Microfluidic Platform for Exploring Learning Behavior in *C. elegans*.

Karni, A., Tanne, D., Rubenstein, B.S., Askenasy, J.J., and Sagi, D. (1994). Dependence on REM sleep of overnight improvement of a perceptual skill. *Science* *265*, 679–682.

Kato, S., Kaplan, H.S., Schrödel, T., Skora, S., Lindsay, T.H., Yemini, E., Lockery, S., and Zimmer, M. (2015). Global Brain Dynamics Embed the Motor Command Sequence of *Caenorhabditis elegans*. *Cell* *163*, 656–669.

Keating, C.D., Kriek, N., Daniels, M., Ashcroft, N.R., Hopper, N.A., Siney, E.J., Holden-Dye, L., and Burke, J.F. (2003). Whole-Genome Analysis of 60 G Protein-Coupled Receptors in *Caenorhabditis elegans* by Gene Knockout with RNAi. *Current Biology* *13*, 1715–1720.

Keil, W., Kutscher, L.M., Shaham, S., and Siggia, E.D. (2017). Long-term high-resolution imaging of developing *C. elegans* larvae with microfluidics. *Dev Cell* *40*, 202–214.

Kim, K.W., and Jin, Y. (2015). Neuronal responses to stress and injury in *C. elegans*. *FEBS Lett* *589*, 1644–1652.

Komatsu, H., Mori, I., Rhee, J.-S., Akaike, N., and Ohshima, Y. (1996). Mutations in a Cyclic Nucleotide-Gated Channel Lead to Abnormal Thermosensation and Chemosensation in *C. elegans*. *Neuron* *17*, 707–718.

Kramer, A., Yang, F.-C., Snodgrass, P., Li, X., Scammell, T.E., Davis, F.C., and Weitz, C.J. (2001). Regulation of Daily Locomotor Activity and Sleep by Hypothalamic EGF Receptor Signaling. *Science* *294*, 2511–2515.

Kreutzmann, J.C., Havekes, R., Abel, T., and Meerlo, P. (2015). Sleep deprivation and hippocampal vulnerability: changes in neuronal plasticity, neurogenesis and cognitive function. *Neuroscience* *309*, 173–190.

Krzyzanowski, M.C., Brueggemann, C., Ezak, M.J., Wood, J.F., Michaels, K.L., Jackson, C.A., Juang, B.-T., Collins, K.D., Yu, M.C., L'etoile, N.D., et al. (2013). The *C. elegans* cGMP-dependent protein kinase EGL-4 regulates nociceptive behavioral sensitivity. *PLoS Genet.* *9*, e1003619.

- Lagoy, Ross C., and Albrecht, Dirk R. (2015). Microfluidic Devices for Behavioral Analysis, Microscopy, and Neuronal Imaging in *Caenorhabditis elegans*. In C. Elegans, D. Biron, and G. Haspel, eds. (Humana Press), pp. 159–179.
- Lai, C.-H., Chou, C.-Y., Ch'ang, L.-Y., Liu, C.-S., and Lin, W. (2000). Identification of Novel Human Genes Evolutionarily Conserved in *Caenorhabditis elegans* by Comparative Proteomics. *Genome Res.* *10*, 703–713.
- Lamitina, S.T., Morrison, R., Moeckel, G.W., and Strange, K. (2004). Adaptation of the nematode *Caenorhabditis elegans* to extreme osmotic stress. *Am. J. Physiol., Cell Physiol.* *286*, C785-791.
- Lamprecht, R., and LeDoux, J. (2004). Structural plasticity and memory. *Nat Rev Neurosci* *5*, 45–54.
- Larsch, J., Ventimiglia, D., Bargmann, C.I., and Albrecht, D.R. (2013). High-throughput imaging of neuronal activity in *Caenorhabditis elegans*. *PNAS* *110*, E4266–E4273.
- Larsch, J., Flavell, S.W., Liu, Q., Gordus, A., Albrecht, D.R., and Bargmann, C.I. (2015). A Circuit for Gradient Climbing in *C. elegans* Chemotaxis. *Cell Rep* *12*, 1748–1760.
- Laszy, J., and Sarkadi, A. (1990). Hypoxia-induced sleep disturbance in rats. *Sleep* *13*, 205–217.
- Lawler, D.E., Chew, Y.L., Hawk, J.D., Aljobeh, A., Schafer, W.R., and Albrecht, D.R. (2019). Automated analysis of sleep in adult *C. elegans* with closed-loop assessment of state-dependent neural activity. *BioRxiv* 791764.
- L'Etoile, N.D., Coburn, C.M., Eastham, J., Kistler, A., Gallegos, G., and Bargmann, C.I. (2002). The Cyclic GMP-Dependent Protein Kinase EGL-4 Regulates Olfactory Adaptation in *C. elegans*. *Neuron* *36*, 1079–1089.
- Lewis, J.A., Wu, C.-H., Levine, J.H., and Berg, H. (1980). Levamisole-resistant mutants of the nematode *Caenorhabditis elegans* appear to lack pharmacological acetylcholine receptors. *Neuroscience* *5*, 967–989.
- Li, C. (2008). Neuropeptides. *WormBook* 1–36.
- Lin, J.Y., Knutsen, P.M., Muller, A., Kleinfeld, D., and Tsien, R.Y. (2013). ReaChR: a red-shifted variant of channelrhodopsin enables deep transcranial optogenetic excitation. *Nat Neurosci* *16*, 1499–1508.
- Liu, Y., Tanaka, H., and Fukuoka Heart Study Group (2002). Overtime work, insufficient sleep, and risk of non-fatal acute myocardial infarction in Japanese men. *Occup Environ Med* *59*, 447–451.
- Lockery, S.R., Lawton, K.J., Doll, J.C., Faumont, S., Coulthard, S.M., Thiele, T.R., Chronis, N., McCormick, K.E., Goodman, M.B., and Pruitt, B.L. (2008). Artificial Dirt:

Microfluidic Substrates for Nematode Neurobiology and Behavior. *Journal of Neurophysiology* 99, 3136–3143.

Mackiewicz, M., Shockley, K.R., Romer, M.A., Galante, R.J., Zimmerman, J.E., Naidoo, N., Baldwin, D.A., Jensen, S.T., Churchill, G.A., and Pack, A.I. (2007). Macromolecule biosynthesis: a key function of sleep. *Physiological Genomics* 31, 441–457.

Maquet, P. (2001). The Role of Sleep in Learning and Memory. *Science* 294, 1048–1052.

Matsuura, T., Suzuki, S., Musashino, A., Kanno, R., and Ichinose, M. (2009). Retention time of attenuated response to diacetyl after pre-exposure to diacetyl in *Caenorhabditis elegans*. *Journal of Experimental Zoology Part A: Ecological Genetics and Physiology* 311A, 483–495.

McCloskey, R.J., Fouad, A.D., Churgin, M.A., and Fang-Yen, C. (2017). Food responsiveness regulates episodic behavioral states in *Caenorhabditis elegans*. *J. Neurophysiol.* 117, 1911–1934.

McGaugh, J.L. (2000). Memory--a Century of Consolidation. *Science* 287, 248–251.

Meldrum, D.R., and Holl, M.R. (2002). Microscale bioanalytical systems. *Science* 297, 1197–1198.

Miller, A.C., Thiele, T.R., Faumont, S., Moravec, M.L., and Lockery, S.R. (2005). Step-Response Analysis of Chemotaxis in *Caenorhabditis elegans*. *J. Neurosci.* 25, 3369–3378.

Mitchell, P. (2001). Microfluidics—downsizing large-scale biology. *Nat Biotech* 19, 717–721.

Molina-García, L., Kim, B., Cook, S.J., Bonnington, R., O’Shea, J.M., Sammut, M., Gilbert, S.P.R., Elliott, D.J., Hall, D.H., Emmons, S.W., et al. (2019). A direct glia-to-neuron natural transdifferentiation ensures nimble sensory-motor coordination of male mating behaviour. *BioRxiv* 285320.

Monsalve, G.C., Van Buskirk, C., and Frand, A.R. (2011). LIN-42/PERIOD Controls Cyclical and Developmental Progression of *C. elegans* Molts. *Current Biology* 21, 2033–2045.

Moy, K., Li, W., Tran, H.P., Simonis, V., Story, E., Brandon, C., Furst, J., Raicu, D., and Kim, H. (2015). Computational Methods for Tracking, Quantitative Assessment, and Visualization of *C. elegans* Locomotory Behavior. *PLoS One* 10.

Nagy, S., Tramm, N., Sanders, J., Iwanir, S., Shirley, I.A., Levine, E., and Biron, D. (2014a). Homeostasis in *C. elegans* sleep is characterized by two behaviorally and genetically distinct mechanisms. *ELife Sciences* 3, e04380.

Nagy, S., Raizen, D.M., and Biron, D. (2014b). Measurements of behavioral quiescence in *Caenorhabditis elegans*. *Methods* 68, 500–507.

Nakai, J., Ohkura, M., and Imoto, K. (2001). A high signal-to-noise Ca²⁺ probe composed of a single green fluorescent protein. *Nat Biotech* 19, 137–141.

Nath, R.D., Chow, E.S., Wang, H., Schwarz, E.M., and Sternberg, P.W. (2016). *C. elegans* Stress-Induced Sleep Emerges from the Collective Action of Multiple Neuropeptides. *Current Biology* 26, 2446–2455.

Nelson, M.D., Trojanowski, N.F., George-Raizen, J.B., Smith, C.J., Yu, C.-C., Fang-Yen, C., and Raizen, D.M. (2013). The neuropeptide NLP-22 regulates a sleep-like state in *Caenorhabditis elegans*. *Nat Commun* 4, 2846.

Newman, A.B., Spiekerman, C.F., Enright, P., Lefkowitz, D., Manolio, T., Reynolds, C.F., and Robbins, J. (2000). Daytime sleepiness predicts mortality and cardiovascular disease in older adults. The Cardiovascular Health Study Research Group. *J Am Geriatr Soc* 48, 115–123.

Nichols, A.L.A., Eichler, T., Latham, R., and Zimmer, M. (2017). A global brain state underlies *C. elegans* sleep behavior. *Science* 356, eaam6851.

NIMH NIMH » U.S. Leading Categories of Diseases/Disorders.

Panda, S., Hogenesch, J.B., and Kay, S.A. (2002). Circadian rhythms from flies to human. *Nature* 417, 329.

Partridge, F.A., Brown, A.E., Buckingham, S.D., Willis, N.J., Wynne, G.M., Forman, R., Else, K.J., Morrison, A.A., Matthews, J.B., Russell, A.J., et al. (2017). An automated high-throughput system for phenotypic screening of chemical libraries on *C. elegans* and parasitic nematodes. *Int J Parasitol Drugs Drug Resist* 8, 8–21.

Penchovsky, R., and Traykovska, M. (2015). Designing drugs that overcome antibacterial resistance: where do we stand and what should we do? *Expert Opinion on Drug Discovery* 10, 631–650.

Petersen, R.C., Roberts, R.O., Knopman, D.S., Boeve, B.F., Geda, Y.E., Ivnik, R.J., Smith, G.E., and Jack, C.R. (2009). Mild cognitive impairment: ten years later. *Arch. Neurol.* 66, 1447–1455.

Pierce-Shimomura, J.T., Morse, T.M., and Lockery, S.R. (1999). The fundamental role of pirouettes in *Caenorhabditis elegans* chemotaxis. *J. Neurosci.* 19, 9557–9569.

Piggott, B.J., Liu, J., Feng, Z., Wescott, S.A., and Xu, X.Z.S. (2011). The Neural Circuits and Synaptic Mechanisms Underlying Motor Initiation in *C. elegans*. *Cell* 147, 922–933.

- Raizen, D.M., Zimmerman, J.E., Maycock, M.H., Ta, U.D., You, Y., Sundaram, M.V., and Pack, A.I. (2008a). Lethargus is a *Caenorhabditis elegans* sleep-like state. *Nature* *451*, 569–572.
- Raizen, D.M., Zimmerman, J.E., Maycock, M.H., Ta, U.D., You, Y., Sundaram, M.V., and Pack, A.I. (2008b). Lethargus is a *Caenorhabditis elegans* sleep-like state. *Nature* *451*, 569–572.
- Rajaratnam, S.M.W., Howard, M.E., and Grunstein, R.R. (2013). Sleep loss and circadian disruption in shift work: health burden and management. *Med. J. Aust.* *199*, S11-15.
- Ramot, D., Johnson, B.E., Jr, T.L.B., Carnell, L., and Goodman, M.B. (2008). The Parallel Worm Tracker: A Platform for Measuring Average Speed and Drug-Induced Paralysis in Nematodes. *PLOS ONE* *3*, e2208.
- Rankin, C.H., Beck, C.D., and Chiba, C.M. (1990). *Caenorhabditis elegans*: a new model system for the study of learning and memory. *Behav. Brain Res.* *37*, 89–92.
- Rasch, B., and Born, J. (2013). About Sleep's Role in Memory. *Physiological Reviews* *93*, 681–766.
- Rauchs, G., Orban, P., Schmidt, C., Albouy, G., Balteau, E., Degueldre, C., Schnackers, C., Sterpenich, V., Tinguely, G., Luxen, A., et al. (2008). Sleep Modulates the Neural Substrates of Both Spatial and Contextual Memory Consolidation. *PLOS ONE* *3*, e2949.
- Reilly, D.K., Lawler, D.E., Albrecht, D.R., and Srinivasan, J. (2017). Using an Adapted Microfluidic Olfactory Chip for the Imaging of Neuronal Activity in Response to Pheromones in Male *C. Elegans* Head Neurons. *J Vis Exp*.
- Reppert, S.M., and Weaver, D.R. (2002). Coordination of circadian timing in mammals. *Nature* *418*, 935.
- Ritu Dhawan, P.L.W., David B. Dusenbery (1999). Comparison of Lethality, Reproduction, and Behavior as Toxicological Endpoints in the Nematode *Caenorhabditis Elegans*. *Journal of Toxicology and Environmental Health, Part A* *58*, 451–462.
- Sambongi, Y., Takeda, K., Wakabayashi, T., Ueda, I., Wada, Y., and Futai, M. (2000). *Caenorhabditis elegans* senses protons through amphid chemosensory neurons: proton signals elicit avoidance behavior. *Neuroreport* *11*, 2229–2232.
- Sanfilippo-Cohn, B., Lai, S., Zhan, G., Fenik, P., Pratico, D., Mazza, E., and Veasey, S.C. (2006). Sex differences in susceptibility to oxidative injury and sleepiness from intermittent hypoxia. *Sleep* *29*, 152–159.
- Saper, C.B., Scammell, T.E., and Lu, J. (2005). Hypothalamic regulation of sleep and circadian rhythms. *Nature* *437*, 1257.

Schafer, W.R., and Kenyon, C.J. (1995). A calcium-channel homologue required for adaptation to dopamine and serotonin in *Caenorhabditis elegans*. *Nature* 375, 73–78.

Schmidt, M.H. (2014). The energy allocation function of sleep: A unifying theory of sleep, torpor, and continuous wakefulness. *Neuroscience & Biobehavioral Reviews* 47, 122–153.

Schwartz, S.W., Cornoni-Huntley, J., Cole, S.R., Hays, J.C., Blazer, D.G., and Schocken, D.D. (1998). Are sleep complaints an independent risk factor for myocardial infarction? *Ann Epidemiol* 8, 384–392.

Schwarz, J., Spies, J.-P., and Bringmann, H. (2012). Reduced muscle contraction and a relaxed posture during sleep-like Lethargus. *Worm* 1, 12–14.

Sehgal, A., and Mignot, E. (2011). Genetics of Sleep and Sleep disorders. *Cell* 146, 194–207.

Sengupta, P., Colbert, H.A., and Bargmann, C.I. (1994). The *C. elegans* gene *odr-7* encodes an olfactory-specific member of the nuclear receptor superfamily. *Cell* 79, 971–980.

Sessle, B.J. (2016). Chapter 1 - The Biological Basis of a Functional Occlusion: The Neural Framework. In *Functional Occlusion in Restorative Dentistry and Prosthodontics*, I. Klineberg, and S.E. Eckert, eds. (Mosby), pp. 3–22.

Shamsuzzaman AM, Gersh BJ, and Somers VK (2003). Obstructive sleep apnea: Implications for cardiac and vascular disease. *JAMA* 290, 1906–1914.

Sharma, N., Classen, J., and Cohen, L.G. (2013). Neural plasticity and its contribution to functional recovery. *Handb Clin Neurol* 110, 3–12.

Sia, S.K., and Whitesides, G.M. (2003). Microfluidic devices fabricated in Poly(dimethylsiloxane) for biological studies. *ELECTROPHORESIS* 24, 3563–3576.

Siegel, J.M. (2004). The Neurotransmitters of Sleep. *J Clin Psychiatry* 65, 4–7.

Singh, K., Chao, M.Y., Somers, G.A., Komatsu, H., Corkins, M.E., Larkins-Ford, J., Tucey, T., Dionne, H.M., Walsh, M.B., Beaumont, E.K., et al. (2011). *C. elegans* Notch Signaling Regulates Adult Chemosensory Response and Larval Molting Quiescence. *Current Biology* 21, 825–834.

Singh, K., Huang, H., and Hart, A.C. (2013). Do *C. elegans* Sleep? A Closer Look. *Sleep* 36, 307–308.

Skora, S., Mende, F., and Zimmer, M. (2018). Energy Scarcity Promotes a Brain-wide Sleep State Modulated by Insulin Signaling in *C. elegans*. *Cell Rep* 22, 953–966.

- Spies, J., and Bringmann, H. (2018). Automated detection and manipulation of sleep in *C. elegans* reveals depolarization of a sleep-active neuron during mechanical stimulation-induced sleep deprivation. *Scientific Reports* 8, 9732.
- Sterpenich, V., Albouy, G., Darsaud, A., Schmidt, C., Vandewalle, G., Vu, T.T.D., Desseilles, M., Phillips, C., Degueldre, C., Balteau, E., et al. (2009). Sleep Promotes the Neural Reorganization of Remote Emotional Memory. *J. Neurosci.* 29, 5143–5152.
- Stetak, A., Hörndli, F., Maricq, A.V., van den Heuvel, S., and Hajnal, A. (2009). Neuron-Specific Regulation of Associative Learning and Memory by MAGI-1 in *C. elegans*. *PLoS ONE* 4.
- Steuer Costa, W., Van der Auwera, P., Glock, C., Liewald, J.F., Bach, M., Schüler, C., Wabnig, S., Oranth, A., Masurat, F., Bringmann, H., et al. (2019). A GABAergic and peptidergic sleep neuron as a locomotion stop neuron with compartmentalized Ca²⁺ dynamics. *Nat Commun* 10, 4095.
- Suda, H., Shouyama, T., Yasuda, K., and Ishii, N. (2005). Direct measurement of oxygen consumption rate on the nematode *Caenorhabditis elegans* by using an optical technique. *Biochemical and Biophysical Research Communications* 330, 839–843.
- Tajima, T., Watanabe, N., Kogawa, Y., Takiguchi, N., Kato, J., Ikeda, T., Kuroda, A., and Ohtake, H. (2001). Chemotaxis of the nematode *Caenorhabditis elegans* toward cycloheximide and quinine hydrochloride. *J. Biosci. Bioeng.* 91, 322–324.
- Tanaka, D., Furusawa, K., Kameyama, K., Okamoto, H., and Doi, M. (2007). Melatonin signaling regulates locomotion behavior and homeostatic states through distinct receptor pathways in *Caenorhabditis elegans*. *Neuropharmacology* 53, 157–168.
- Taylor, A.M., and Jeon, N.L. (2010). Micro-scale and microfluidic devices for neurobiology. *Current Opinion in Neurobiology* 20, 640–647.
- Tian, L., Hires, S.A., Mao, T., Huber, D., Chiappe, M.E., Chalasani, S.H., Petreanu, L., Akerboom, J., McKinney, S.A., Schreiter, E.R., et al. (2009). Imaging neural activity in worms, flies and mice with improved GCaMP calcium indicators. *Nature Methods* 6, 875–881.
- Tononi, G., and Cirelli, C. (2014). Sleep and the Price of Plasticity: From Synaptic and Cellular Homeostasis to Memory Consolidation and Integration. *Neuron* 81, 12–34.
- Torayama, I., Ishihara, T., and Katsura, I. (2007). *Caenorhabditis elegans* Integrates the Signals of Butanone and Food to Enhance Chemotaxis to Butanone. *J. Neurosci.* 27, 741–750.
- Toth, L.A., and Bhargava, P. (2013). Animal Models of Sleep Disorders. *Comp Med* 63, 91–104.

- Tramm, N., Oppenheimer, N., Nagy, S., Efrati, E., and Biron, D. (2014). Why Do Sleeping Nematodes Adopt a Hockey-Stick-Like Posture? *PLoS ONE* 9, e101162.
- Troemel, E.R. (1999). Chemosensory signaling in *C. elegans*. *Bioessays* 21, 1011–1020.
- Trojanowski, N.F., and Raizen, D.M. (2015). Call it Worm Sleep. *Trends in Neurosciences*.
- Trojanowski, N.F., Nelson, M.D., Flavell, S.W., Fang-Yen, C., and Raizen, D.M. (2015). Distinct Mechanisms Underlie Quiescence during Two *Caenorhabditis elegans* Sleep-Like States. *J. Neurosci.* 35, 14571–14584.
- Tsunematsu, T., Kilduff, T.S., Boyden, E.S., Takahashi, S., Tominaga, M., and Yamanaka, A. (2011). Acute Optogenetic Silencing of Orexin/Hypocretin Neurons Induces Slow-Wave Sleep in Mice. *J. Neurosci.* 31, 10529–10539.
- Turek, M., Lewandrowski, I., and Bringmann, H. (2013). An AP2 transcription factor is required for a sleep-active neuron to induce sleep-like quiescence in *C. elegans*. *Curr. Biol.* 23, 2215–2223.
- Turek, M., Besseling, J., and Bringmann, H. (2015). Agarose Microchambers for Long-term Calcium Imaging of *Caenorhabditis elegans*. *J Vis Exp*.
- Turek, M., Besseling, J., Spies, J.-P., König, S., and Bringmann, H. (2016). Sleep-active neuron specification and sleep induction require FLP-11 neuropeptides to systemically induce sleep. *ELife* 5, e12499.
- Urmersbach, B., Besseling, J., Spies, J.-P., and Bringmann, H. (2016). Automated analysis of sleep control via a single neuron active at sleep onset in *C. elegans*. *Genesis* n/a-n/a.
- Van Auken, K., Weaver, D., Robertson, B., Sundaram, M., Saldi, T., Edgar, L., Elling, U., Lee, M., Boese, Q., and Wood, W.B. (2002). Roles of the Homothorax/Meis/Prep homolog UNC-62 and the Exd/Pbx homologs CEH-20 and CEH-40 in *C. elegans* embryogenesis. *Development* 129, 5255–5268.
- Van Buskirk, C., and Sternberg, P.W. (2007). Epidermal growth factor signaling induces behavioral quiescence in *Caenorhabditis elegans*. *Nat Neurosci* 10, 1300–1307.
- Veitinger, S. (2011). The Patch-Clamp Technique.
- Velluti, R. (1997). Interactions between sleep and sensory physiology. *Journal of Sleep Research* 6, 61–77.
- Viscomi, M.T., and D’Amelio, M. (2012). The “Janus-faced role” of autophagy in neuronal sickness: focus on neurodegeneration. *Mol. Neurobiol.* 46, 513–521.

Vorster, A.P., and Born, J. (2015). Sleep and memory in mammals, birds and invertebrates. *Neuroscience & Biobehavioral Reviews* 50, 103–119.

Waggoner, L.E., Zhou, G.T., Schafer, R.W., and Schafer, W.R. (1998). Control of Alternative Behavioral States by Serotonin in *Caenorhabditis elegans*. *Neuron* 21, 203–214.

Walker, M.P., and Stickgold, R. (2006). Sleep, Memory, and Plasticity. *Annual Review of Psychology* 57, 139–166.

Walker, M.P., Stickgold, R., Alsop, D., Gaab, N., and Schlaug, G. (2005). Sleep-dependent motor memory plasticity in the human brain. *Neuroscience* 133, 911–917.

Ward, S. (1973). Chemotaxis by the Nematode *Caenorhabditis elegans*: Identification of Attractants and Analysis of the Response by Use of Mutants. *Proc Natl Acad Sci U S A* 70, 817–821.

Weber, F., Chung, S., Beier, K.T., Xu, M., Luo, L., and Dan, Y. (2015). Control of REM sleep by ventral medulla GABAergic neurons. *Nature* 526, 435–438.

Weeks, J.C., Roberts, W.M., Robinson, K.J., Keaney, M., Vermeire, J.J., Urban, J.F., Lockery, S.R., and Hawdon, J.M. (2016). Microfluidic platform for electrophysiological recordings from host-stage hookworm and *Ascaris suum* larvae: A new tool for anthelmintic research. *Int J Parasitol Drugs Drug Resist* 6, 314–328.

White, J.G., Southgate, E., Thomson, J.N., and Brenner, S. (1986). The structure of the nervous system of the nematode *Caenorhabditis elegans*. *Phil. Trans. R. Soc. Lond. B* 314, 1–340.

WHO Soil-transmitted helminth infections.

Winkelmann, J., Schormair, B., Lichtner, P., Ripke, S., Xiong, L., Jalilzadeh, S., Fulda, S., Pütz, B., Eckstein, G., Hauk, S., et al. (2007). Genome-wide association study of restless legs syndrome identifies common variants in three genomic regions. *Nat. Genet.* 39, 1000–1006.

Xu, X., Warrington, A.E., Bieber, A.J., and Rodriguez, M. (2011). Enhancing CNS repair in neurological disease: challenges arising from neurodegeneration and rewiring of the network. *CNS Drugs* 25, 555–573.

Yamuy, J., Fung, S.J., Xi, M., Morales, F.R., and Chase, M.H. (1999). Hypoglossal motoneurons are postsynaptically inhibited during carbachol-induced rapid eye movement sleep. *Neuroscience* 94, 11–15.

You, Y., Kim, J., Raizen, D.M., and Avery, L. (2008). Insulin, cGMP, and TGF- β Signals Regulate Food Intake and Quiescence in *C. elegans*: A Model for Satiety. *Cell Metabolism* 7, 249–257.

Zhang, J.-H., Chung, T.D.Y., and Oldenburg, K.R. (1999). A Simple Statistical Parameter for Use in Evaluation and Validation of High Throughput Screening Assays. *J Biomol Screen* 4, 67–73.

Zheng, Y., Brockie, P.J., Mellem, J.E., Madsen, D.M., and Maricq, A.V. (1999). Neuronal Control of Locomotion in *C. elegans* Is Modified by a Dominant Mutation in the GLR-1 Ionotropic Glutamate Receptor. *Neuron* 24, 347–361.

Chapter 8: Appendix

Appendix 1

Movement detection protocol for 384-well plate

Overall Outline:

- 1) Input Video File
 - a. Dialog box opens. Requests location of the avi file and the number of frames to analyze
- 2) Correct Image for Shifting/Rotation of Plate
 - a. Asks user to select control well points to correct for plate rotation
 - b. Corrects image for motion
 - i. Use threshold to set all gray values under 120 to 0 (black)
 - ii. Create binary image using default ImageJ auto-thresholding for each frame
 - iii. Find center of mass for both left and right control well for each frame
 - iv. Move entire frame of video by average X and Y displacement for two control wells for that corresponding video frame compared to first frame
- 3) Calculate Movement Based on Subtraction of Adjacent Frames
 - a. Find difference between each adjacent frame (i.e. 1 to 2 is #1, 2 to 3 is #2, etc.)
 - b. Create binary image using default ImageJ auto-thresholding for each frame
- 4) Center Around Well Area and Calculate Moved Pixels for each Frame
 - a. Create boxes dividing 396 well plate into equal boxes. For each box on each frame calculate center of mass and select 25% of the surrounding width and height for analysis (this area roughly corresponds to the entire visible well)
 - b. Measure and save pixel intensity inside of the selected are for each frame for collection
- 5) Save Data and Post Processing
 - a. Note: Saved as comma separated TXT file. First row provides title for x and y position columns. Each row is organized as:
 - i. Column 1: X Position of the well
 - ii. Column 2: Y Position of the well
 - iii. Columns 3-(number of frames+1): Average pixel intensity of calculated difference from part 3a organized by frame. Intensity is based on grayscale (0-255). 255 (white) would represent every pixel having moved. 0 (black) represents no pixel movement.
 - b. Data can be read in to Excel as follows: (instructions based on Excel 2016)

- i. "Data" -> "Get External Data" -> "From Text"
- ii. Select TXT file that was outputted
- iii. Make sure "Delimited" is selected and click "Next >"
- iv. Click box to the left of "Comma" and click "Finish"
- v. Put data where desired ("Existing worksheet" if you selected a blank space where you can place the data, but a "New worksheet" is fine)

Detailed Outline:

1) Input Video File

- a. Dialog box opens. Requests location of the avi file and the number of frames to analyze

```
DIALOG.CREATE("SPECIFICATIONS");

//CREATION OF FILE : INPUT FULL LOCATION OF THE FILE (INCLUDING ROOT DIRECTORY)

FILELOCATION="E:\\[FILENAME].AVI";
DIALOG.ADDSTRING("FILE LOCATION:",FILELOCATION);

//SPECIFICATIONS FOR IMAGE PROCESSING : INPUT THE NUMBER OF IMAGES TO ANALYZE
DIALOG.ADDNUMBER("IMAGES:", 0);
DIALOG.SHOW();
FILELOCATION = DIALOG.GETSTRING();
IMAGES = DIALOG.GETNUMBER();
```

2) Correct Image for Shifting/Rotation of Plate

- a. Asks user to select control well points to correct for plate rotation

```
// CORRECT FOR IMAGE SHIFTING
RUN("AVI...", "SELECT="+FILELOCATION+" FIRST=1 LAST="+IMAGES+" CONVERT");
RENAME("ORIGINAL");
RUN("DUPLICATE...", "TITLE=FIRST DUPLICATE RANGE 1-1");
SETTOOL("LINE");
WAITFORUSER("FINDING ROTATION ANGLE","THIS WILL CORRECT FOR ROTATION OF THE
PLATE:\NDRAW A LINE FROM CENTER OF LEFT CONTROL WELL TO THE CENTER OF THE RIGHT
CONTROL WELL\NWHEN YOU ARE HAPPY WITH THE LINE CLICK OK");
RUN("CLEAR RESULTS");
RUN("MEASURE");
SELECTWINDOW("FIRST");
CLOSE();
SELECTWINDOW("ORIGINAL");
RUN("ROTATE... ", "ANGLE="+GETRESULT("ANGLE",0)+" GRID=1 INTERPOLATION=BILINEAR
STACK");
```

b. Corrects image for motion

- i. Use threshold to set all gray values under 120 to 0 (black)

```
SETMINANDMAX(120, 256);  
RUN("APPLY LUT", "STACK");
```

- ii. Create binary image using default ImageJ auto-thresholding for each frame

```
SELECTWINDOW("ORIGINAL");  
RUN("DUPLICATE...", "TITLE=THRESHOLD DUPLICATE RANGE=1-NSLICES");  
SELECTWINDOW("THRESHOLD");  
RUN("MAKE BINARY", "METHOD=DEFAULT BACKGROUND=DEFAULT CALCULATE");  
RUN("SET MEASUREMENTS...", "AREA MEAN MIN CENTER MEDIAN STACK REDIRECT=NONE  
DECIMAL=3");
```

- iii. Find center of mass for both left and right control well for each frame

```
SELECTWINDOW("ORIGINAL");  
RUN("DUPLICATE...", "TITLE=THRESHOLD DUPLICATE RANGE=1-NSLICES");  
SELECTWINDOW("THRESHOLD");  
RUN("MAKE BINARY", "METHOD=DEFAULT BACKGROUND=DEFAULT CALCULATE");  
RUN("SET MEASUREMENTS...", "AREA MEAN MIN CENTER MEDIAN STACK REDIRECT=NONE  
DECIMAL=3");  
  
ALLX=0;  
ALLY=0;  
FOR (x=0; x<6000; x=x+5750){  
    Y=1750;  
    RUN("CLEAR RESULTS");  
    MAKERECTANGLE(x,Y, 250, 250);  
    RUN("MEASURE");  
    ALLX=ALLX+GETRESULT("XM",0);  
    ALLY=ALLY+GETRESULT("YM",0);  
}  
  
ALLX=ALLX/2;  
ALLY=ALLY/2;
```

- iv. Move entire frame of video by average X and Y displacement for two control wells for that corresponding video frame compared to first frame

```
FOR (i=2; i<NSLICES+1; i++){  
    SELECTWINDOW("THRESHOLD");  
    SETSLICE(i);
```

```

NEWX=0;
NEWY=0;
FOR(X=0; X<6000; X=X+5750){
    Y=1750;
    RUN("CLEAR RESULTS");
    MAKERECTANGLE(X,Y, 250, 250);
    RUN("MEASURE");
    NEWX=NEWX+GETRESULT("XM",0);
    NEWY=NEWY+GETRESULT("YM",0);
}
NEWX=NEWX/2;
NEWY=NEWY/2;

SELECTWINDOW("ORIGINAL");
SETSLICE(1);
RUN("SELECT ALL");
RUN("COPY");
ROI.MOVE(ROUND(ALLX-NEWX),ROUND(ALLY-NEWY));
RUN("PASTE");
}

```

3) Calculate Movement Based on Subtraction of Adjacent Frames

- a. Find difference between each adjacent frame (i.e. 1 to 2 is #1, 2 to 3 is #2, etc.)

```

// FIND MOVEMENT BY ADJACENT FRAME SUBTRACTION
SELECTWINDOW("THRESHOLD");
RUN("SELECT ALL");
RUN("DUPLICATE...", "TITLE=THRESH DPLICATE RANGE=1-1");
SELECTWINDOW("THRESHOLD");
CLOSE();
SELECTWINDOW("THRESH");
RENAME("THRESHOLD");
SELECTWINDOW("ORIGINAL");
RUN("DUPLICATE...", "TITLE=BACKEND DPLICATE RANGE=2-"+NSLICES);
SELECTWINDOW("ORIGINAL");
SETSLICE(NSLICES);
RUN("DELETE SLICE");
IMAGECALCULATOR("DIFFERENCE CREATE STACK", "ORIGINAL", "BACKEND");
RENAME("DIFF");

```

- b. Create binary image using default ImageJ auto-thresholding for each frame

```

SETOPTION("BLACKBACKGROUND", FALSE);
RUN("MAKE BINARY", "METHOD=DEFAULT BACKGROUND=DEFAULT CALCULATE BLACK");

```

4) Center Around Well Area and Calculate Moved Pixels for each Frame

- a. Create boxes dividing 396 well plate into equal boxes. For each box on each frame calculate center of mass and select 25% of the surrounding width and height for analysis (this area roughly corresponds to the entire visible well)

```
// FIND AVERAGE INTENSITY OF SUBTRACTED FRAMES
SELECTWINDOW("ORIGINAL");
CLOSE();
SELECTWINDOW("BACKEND");
CLOSE();
F = FILE.OPEN("E:\\NEW\\TESTDATA.TXT");
PRINT(F,"X POS,Y POS");

// FIND MOVEMENT FOR EACH WELL CENTERED AROUND PROPER AREA
FOR (XSTART=0; XSTART<6000; XSTART=XSTART+250){
  FOR (YSTART=0; YSTART<4000; YSTART=YSTART+250){
    A="";
    SELECTWINDOW("THRESHOLD");
    RUN("CLEAR RESULTS");
    MAKERECTANGLE(XSTART,YSTART,250,250);
    RUN("MEASURE");
    CENTERX=GETRESULT("XM",0);
    CENTERY=GETRESULT("YM",0);
    NEWX=ROUND(CENTERX-62.5);
    NEWY=ROUND(CENTERY-62.5);
    SELECTWINDOW("DIFF");
    A=A+(XSTART/250+1)+","+(YSTART/250+1);
    FOR (I=1; I<NSLICES+1; I++){
      SETSLICE(I);
      MAKERECTANGLE(NEWX,NEWY,125,125);
      RUN("CLEAR RESULTS");
```

- b. Measure and save pixel intensity inside of the selected are for each frame for collection

```
      RUN("MEASURE");
      A=A+"," +GETRESULT("MEAN",0);
    }
  }
```

5) Save Data and Post Processing

```
    PRINT(F,A);
  }
}
```

- a. Note: Saved as comma separated TXT file. First row provides title for x and y position columns. Each row is organized as:
 - vi. Column 1: X Position of the well
 - vii. Column 2: Y Position of the well
 - viii. Columns 3-(number of frames+1): Average pixel intensity of calculated difference from part 3a organized by frame. Intensity is based on grayscale (0-255). 255 (white) would represent every pixel having moved. 0 (black) represents no pixel movement.
- b. Data can be read in to Excel as follows: (instructions based on Excel 2016)
 - ix. "Data" -> "Get External Data" -> "From Text"
 - x. Select TXT file that was outputted
 - xi. Make sure "Delimited" is selected and click "Next >"
 - xii. Click box to the left of "Comma" and click "Finish"
 - xiii. Put data where desired ("Existing worksheet" if you selected a blank space where you can place the data, but a "New worksheet" is fine)

Adult sleep project scripts

Code for the adult sleep project detailed in Chapters 2-4 uploaded at:

<https://github.com/dlawler12/AdultSleep>